

NASA Contractor Report 165405

Deposit Formation in Hydrocarbon Rocket Fuels

(NASA-CR-165405) DEPOSIT FORMATION IN HYDRCCARECN ROCKET FUELS Final Progress Report, Apr. 1980 - May 1981 (United Technologies Research Center) 138 p HC A07/ME A01	N81-30280
	Unclas 27230

CSCL 211 G3/28

Richard Roback
Eugene J. Szetela
Louis J. Spadaccini

UNITED TECHNOLOGIES RESEARCH CENTER
East Hartford, CT 06108

August 1981



National Aeronautics and
Space Administration

Lewis Research Center

Cleveland, Ohio 44135



1. Report No. NASA CR-165405	2. Government Accession No.	3. Recipient's Catalog No.	
4. Title and Subtitle Deposit Formation in Hydrocarbon Rocket Fuels		5. Report Date August 1981	
		6. Performing Organization Code	
7. Author(s) Richard Roback, Eugene J. Szetela, Louis J. Spadaccini		8. Performing Organization Report No. R81-915216-1	
		10. Work Unit No.	
9. Performing Organization Name and Address United Technologies Research Center Silver Lane East Hartford, CT 06108		11. Contract or Grant No. NAS3-22277	
		13. Type of Report and Period Covered Final Progress Report 4/80-5/81	
12. Sponsoring Agency Name and Address National Aeronautics and Space Administration Washington, D.C. 20546		14. Sponsoring Agency Code YOS8912	
		15. Supplementary Notes NASA-Lewis Research Center, Cleveland, OH 44135 Project Manager, Philip A. Masters	
16. Abstract <p>An experimental program was conducted to study deposit formation in hydrocarbon fuels under flow conditions that exist in high-pressure, rocket engine cooling systems. A high pressure fuel coking test apparatus was designed and developed and was used to evaluate thermal decomposition (coking) limits and carbon deposition rates in heated copper tubes for two hydrocarbon rocket fuels, RP-1 and commercial-grade propane. Tests were also conducted using JP-7 and chemically-pure propane as being representative of more refined cuts of the baseline fuels. A parametric evaluation of fuel thermal stability was performed at pressures of 136 atm to 340 atm, bulk fuel velocities in the range 6 to 30 m/sec, and tube wall temperatures in the range 422 to 811K. In addition, the effect of the inside wall material on deposit formation was evaluated in selected tests which were conducted using nickel-plated tubes.</p> <p>The results of the tests indicated that substantial deposit formation occurs with RP-1 fuel at wall temperatures between 600 and 800K, with peak deposit formation occurring near 700K. No improvements were obtained when de-oxygenated JP-7 fuel was substituted for RP-1. The carbon deposition rates for the propane fuels were generally higher than those obtained for either of the kerosene fuels at any given wall temperature. There appeared to be little difference between commercial-grade and chemically-pure propane with regard to type and quantity of deposit. The results of tests conducted with RP-1 indicated that the rate of deposit formation increased slightly with pressure over the range 136 atm to 340 atm. Finally, plating the inside wall of the tubes with nickel was found to significantly reduce carbon deposition rates for RP-1 fuel.</p>			
17. Key Words (Suggested by Author(s)) Thrust chamber cooling; hydrocarbon rocket coolants; hydrocarbon fuel thermal decomposition; hydrocarbon rocket fuel stability; deposit formation; carbon formation rates.		18. Distribution Statement Unclassified - Unlimited	
19. Security Classif. (of this report) Unclassified	20. Security Classif. (of this page) Unclassified	21. No. of Pages 160	22. Price*

* For sale by the National Technical Information Service, Springfield, Virginia 22161

Deposit Formation in Hydrocarbon Rocket Fuels

TABLE OF CONTENTS

	<u>Page</u>
SUMMARY	1
INTRODUCTION	2
TECHNICAL APPROACH	4
Fuels Characterization	4
Test Facility and Test Hardware	5
Test Matrix and Operating Procedures	9
Data Analysis.	11
EXPERIMENTAL RESULTS AND DISCUSSION	14
Calibration Tests.	14
RP-1 Tests	17
JP-7 Tests	21
Propane Tests	24
High Pressure Tests	27
Tests With Nickel-Plated Tubes	28
Deposit Morphology	29
CONCLUDING REMARKS	34
REFERENCES	37
TABLES	
FIGURES	
APPENDIX A - TABULATED TEST DATA	A-1

Deposit Formation in Hydrocarbon Rocket Fuels

Richard Roback
Eugene J. Szetela
Louis J. Spadaccini

SUMMARY

An experimental research program was undertaken to evaluate the thermal stability characteristics of hydrocarbon rocket fuels under conditions that simulate high-pressure, hydrocarbon-fueled rocket cooling systems. The thermal decomposition (coking) limits and rates of deposition in heated copper tubes for two hydrocarbon fuels, RP-1 and propane, were determined using a continuous flow test apparatus which permitted independent variation and evaluation of the effect of wall temperature, pressure, and fluid velocity on fuel thermal stability. In addition, tests were conducted to investigate the effects of further refining of these fuels, to reduce the concentration levels of deposit forming precursors, on improving their thermal stability.

Parametric tests to map the thermal stability characteristics of RP-1 and commercial-grade propane, were conducted at pressures of 136 atm to 340 atm, bulk fluid velocities in the range 6 to 30 m/sec, and tube wall temperatures in the range 422 to 811K. Selected tests were also performed using de-oxygenated JP-7 and chemically-pure propane as being representative of more refined cuts of the standard rocket fuels. In addition, the effect of the inside wall material on deposit formation was evaluated in selected comparative tests which were conducted using nickel-plated tubes.

The results of the tests indicated that substantial deposit formation occurs with RP-1 fuel at wall temperatures between 600 and 800K, with peak deposit formation occurring near 700K. No improvements were obtained when de-oxygenated JP-7 fuel was substituted for RP-1. For both fuels, carbon deposition rates ranged from approximately 400 to 600 $\mu\text{g}/\text{cm}^2\text{-hr}$ at wall temperatures of 500 to 800K. Examination of deposits obtained with propane fuels indicated heavier, blacker and more uniform deposits than those observed with the kerosene-type fuels and there appeared to be little difference between commercial-grade and chemically-pure propane with regard to type and quantity of deposit. The carbon deposition rates for the propane fuels were generally higher than those obtained for either of the kerosene fuels at any given wall temperature and ranged from 400 to 600 $\mu\text{g}/\text{cm}^2\text{-hr}$ at wall temperatures as low as 400 to 500K. The results of tests conducted with RP-1 at pressures of 136 atm to 340 atm indicated that the rate of deposit formation increased slightly with pressure over the range tested. Finally, plating the inside wall of the tubes with nickel was found to significantly reduce carbon deposition rates for RP-1 fuel.

INTRODUCTION

In an effort to increase the performance of hydrocarbon/LOX rocket engines for space booster or orbit transportation systems, i.e. to reduce weight and increase specific impulse, combustion pressures as high as practical are desirable. However, increased combustion pressure leads to a nearly proportionate increase in wall heat flux in the thrust chamber, and therefore, greater stress is placed on the design of the regenerative cooling system. To some extent, the increased heat fluxes can be accommodated by increasing coolant-side heat transfer rates by the expedients of reducing coolant channel flow area, and/or increasing coolant flow velocity, etc., but the implementation of these expedients is not without cost. Therefore, it is desirable to establish upper wall temperature limits to maximize the heat flux into the propellant coolant. Regenerative cooling with hydrocarbon fuels is feasible up to a point where the coolant wall temperature reaches a limit defined by a thermal decomposition or "coking" temperature. Deposit formation on the coolant wall surface, which usually occurs when the thermal decomposition temperature is reached, causes an increased thermal resistance, a progressively increasing wall temperature and, ultimately, failure. Therefore, the rocket engine designer needs to know what maximum heat fluxes can be accommodated under a variety of coolant flow conditions and, especially in the case of the reusable engines, when fuel deposits will be incurred, their nature, (as it affects heat transfer limits) and what rates of formation will prevail.

Hydrocarbon fuel stability and deposit formation (coking) has been the subject of investigation for many years (Refs. 1 to 19). Although the exact mechanism of deposit formation has not been clearly defined, it usually results from the pyrolysis of organic molecules which make up the fuel. Free radicals are generated thermally and, because of their affinity for atoms such as nitrogen, oxygen, and sulfur which might be in the fuel, stable complex solids are formed (Refs. 20 to 25). Studies have shown that additional processing of the fuel to remove these deposit forming precursors has improved fuel thermal stability and decreased deposit formation (Refs. 26 to 31). Fuel decomposition rates and subsequent deposit formation rates have been found to be a function of temperature, pressure, velocity and the composition and physical state of the fuel.

Because of its superior thermal conductivity, copper has been the preferred material for forming the regenerative cooling passages in the high-heat-flux regions of high-pressure rocket thrust chambers. However, studies of the effect of wall materials on deposit formation, Refs. 6, 10 and 32, indicated that deposit rates on copper can be very high. No data was available with regard to deposit formation of rocket fuels such as RP-1 and propane at conditions simulating high-pressure rocket operation. Results deduced from low-pressure coking tests for jet fuels on stainless steel indicated that a coolant-side wall temperature limit in the range 600 to 700K may exist for typical kerosene-type fuels.

However, the effects of the use of copper as a wall material and the effects of fuel pressure and velocity were not determined in the previous investigations. Therefore, to permit more accurate determinations of the maximum allowable coolant-side wall temperatures, a fuel coking test apparatus was designed and developed and was used for parametric evaluation of fuel thermal stability under conditions that simulate high-pressure, hydrocarbon-fueled rocket cooling systems. Using the apparatus developed, experiments were directed toward (1) evaluating the thermal decomposition (coking) limits and rates of deposition in heated copper tubes for two hydrocarbon fuels, RP-1 and propane, and (2) investigating the effect of further refining of these fuels, to reduce the concentration levels of deposit-forming precursors, on improving their thermal stability. Tests were conducted using RP-1 and commercial-grade propane as the standard hydrocarbon rocket fuels and de-oxygenated JP-7 and chemically-pure propane as being representative of more refined cuts of these fuels. A parametric evaluation of fuel thermal stability was performed at pressures of 136 atm to 340 atm, bulk fuel velocities in the range 6 to 30 m/sec, and tube wall temperatures in the range 422 to 811K. In addition, the effect of the inside wall material on deposit formation was evaluated in selected comparative tests which were conducted using nickel-plated tubes.

TECHNICAL APPROACH

As stated above, the objective of the present investigation was to determine the character and rate of formation of fuel deposits under conditions representative of advanced hydrocarbon/oxygen rocket engine cooling systems, and to investigate the effect of increased fuel purity on mitigating deposit formation rates. The overall approach adopted to accomplish these objectives consisted of: characterizing the test fuels as to their chemical composition and physical properties, designing and fabricating appropriate test apparatus, and utilizing this equipment in an experimental study of deposit formation in electrically-heated copper tubes. The fuel properties, test equipment and operating procedures are discussed in detail in the following sections.

Fuels Characterization

The standard fuels which were tested during this program were RP-1 rocket fuel (MIL-P-25576), supplied by the Government, and a commercial-grade propane, purchased from a local supplier. In addition to the primary objectives of this program, to determine the coking temperature limit and rate of carbon deposition for the as-delivered fuels, the merits of further refining of these fuels relative to improving their thermal stabilities were also investigated. To this end, additional quantities of refined quality fuels, which met the specifications listed in Table I, were obtained. Since refinement of a relatively small quantity of the RP-1 fuel was neither practical nor cost effective, it was decided, with NASA approval, to utilize JP-7 (MIL-T-38219) fuel to simulate refined quality RP-1 fuel. Because JP-7 fuel is severely hydrotreated to meet a thermal stability specification, it generally has an order of magnitude less sulfur than RP-1 fuel. In all other respects, the JP-7 fuel tested met the RP-1 specification. Additional on-line treatment of the JP-7 by filtration through a molecular sieve to remove water and by nitrogen sparging to reduce the dissolved oxygen content was required to provide a fuel of sufficiently refined quality to meet the specifications listed in Table I and to adequately establish the effect of fuel refinement on deposit formation. The use of chemically pure propane (minimum 99% pure in liquid phase), purchased directly, was determined to be the most cost effective way to obtain refined-quality propane.

Each fuel chosen for testing was characterized as to selected chemical and physical properties. These properties determinations were obtained utilizing a combination of in-house, Government and independent analytical laboratory facilities; API and ASTM standard correlational procedures (Refs. 33 and 34); supplier's certified analyses (Refs. 35 and 36); and published data (Refs. 37 to 43). Typical physical properties of the test fuels are shown in Table II, while the variation of selected physical properties with temperature is shown in Table III for RP-1 and JP-7 fuels and in Table IV for the propane fuels. Certificates of analysis for the RP-1 and JP-7 fuels used in this program were

provided by the fuel suppliers. Selected chemical analyses of constituents not generally included in the military specifications were performed either in-house or by an independent testing laboratory. A summary of these analyses is shown in Table V.

Since commercial-grade propane is distributed in bulk, a certificate of analysis is not normally available. However, the commercial-grade propane used in this test program was certified by the supplier as meeting the ASTM standard for motor-grade propane. This fuel contains a minimum of 90% propane, a maximum of 5 percent propylene and the remainder comprises a mixture of other hydrocarbons such as butane, butylene, and ethane. The chemically-pure propane was certified as being 99% propane. Typical analyses of the commercial-grade propane and the chemically-pure propane utilized in this test program are shown in Table VI.

Test Facility and Test Hardware

Description of Apparatus

The test program was conducted in a self-contained combustion test facility which consists of a concrete test cell and a separate control room for operating personnel. The test facility is capable of continuous operation with fuel flowing at a velocity up to 36.5 m/sec and at pressures as high as 340 atm. An electrical power supply, which is capable of providing 40 KVA AC and 4000 amps, was used to provide power for electrically heating the copper test tube up to the maximum temperature of 866K specified for the test program.

The test apparatus, shown schematically in Fig. 1, consisted of the following major components: (1) a fuel supply tank, (2) a run tank to which is connected a zeolite-type molecular sieve water-absorber and a porous metal sparging element for reducing water and dissolved oxygen concentrations to the levels specified for the refined fuels, (3) a fuel delivery system consisting of two piston-type accumulators which are pressurized and used to drive fuel through the test section, (4) a venturi flowmeter, (5) a resistance-heated test tube connected to a 40 KVA high-amperage power supply, (6) an in-line filter for collecting any solid particles which might form in the bulk flow or breakoff from the test tube wall during test, (7) a fuel cooler, (8) an electrically-driven metering valve which was used to control the fuel flow through the test section, (9) a turbine-type flowmeter, and (10) a fuel dump tank.

The original design of the test apparatus included a high-pressure (340 atm), variable displacement axial piston pump, which was to be used to raise the pressure

of the test fuel to the desired level and pump it through the test section. However, after several pump failures occurred, it was concluded that the pump was not compatible with low viscosity fluids, such as RP-1 and propane, and therefore, the fuel delivery system was modified to utilize two high-pressure piston type accumulators as fluid transfer barriers. For the low-pressure tests (136 atm) the accumulators were installed in parallel (as shown in the inset in Fig. 1), and one side of each accumulator was precharged with test fuel while the opposite side was pressurized with 156 atm nitrogen which actuated the pistons and forced the test fuel through the test section. A dome-loaded pressure regulator was used to regulate the nitrogen driver gas pressure. With this configuration, a total of approximately 48 gallons of fuel could be expended before the system had to be refilled.

Because the facility was not capable of supplying a high flow rate of nitrogen at pressures in excess of 156 atm, this configuration could not be used for higher pressure tests and therefore, additional modifications were made to the fuel delivery system to permit the use of high-viscosity hydraulic fluid, pumped by the existing high-pressure piston pump, as the accumulator driver fluid. This system, also shown in the Fig. 1 inset, consists of two piston accumulators in series; the first accumulator contained hydraulic fluid on one side of piston and test fuel on the other side, and the second accumulator (which empties through the test section) contained test fuel on both sides of the piston. With this arrangement, the hydraulic fluid and test fuel are separated by a relatively large volume of contained fuel, thus eliminating the potential for contamination of the test fuel by hydraulic fluid left on the wall of the accumulator or by hydraulic fluid leaking across the piston seals. However, this arrangement limited the fuel capacity to 23 gallons and it was therefore necessary to refill more frequently between tests.

Test Tube Fabrication and Characteristics

Since test data at pressures up to 340 atm was desired, all tube test elements were designed to withstand this pressure at tube wall temperatures up to 1000K. A duplex tube wall configuration was selected to meet this requirement and to also provide a better match of the specific electrical resistance of the tube elements to the capabilities of the electric power supply. In the duplex tube configuration, an inner wall of an oxygen free-high conductivity copper (No. 102; 99.95% pure; electrical conductivity = 0.586 Megmho-cm) provided the desired test surface for studying the rates of deposit formation on copper while an outer wall of Inconel 600 provided the necessary high-temperature tensile strength.

The individual test tube elements comprised an inner 0.254-cm ID x 0.366-cm OD copper tube surrounded by a 0.366-cm ID x 0.478-cm OD Inconel tube. This configuration had the advantage that, while the structural load was carried by the outer sheath, the majority of the power (~ 95%) was generated in the copper and, as a result, the tube radial temperature gradient was small. The duplex tube was manufactured by threading the 0.254-cm ID x 0.366-cm OD copper tube into an

oversized Inconel outer sheath, and subsequently drawing the Inconel tube through a die to obtain the proper sheath thickness and OD of the duplex tube. This process ensured a good bond, i.e., intimate wall contact between the Inconel and copper surfaces which was subsequently verified by various tests described later in this subsection.

To preclude any significant electrical or thermal resistance at the interface of the two metals, stemming from oxidation, contamination or local separation, the tubes were cleaned and inspected before and after fabrication. Tests to evaluate the effectiveness of several candidate procedures for cleaning the copper and Inconel tubing prior to fabricating the duplex test tubes indicated that a thorough degreasing was sufficient for the Inconel tube, since Inconel is relatively corrosion resistant and is not easily oxidized. A 10 percent nitric acid solution appeared to clean the copper surface adequately; however, a water slurry of a commercially-available powdered copper cleaner containing oxalic acid was just as effective and easier to use. Based on the results of these tests, the cleaning procedure adopted consisted of (a) immersion of both the copper and Inconel tubing in a hot degreasing solution, followed by a thorough water rinse; and (b) application of the commercial copper cleaner to the outer surface of the copper tubing with a fine brush, removal with a clean sponge and water, followed by a final water-rinse and degreasing. Handling of all materials was done with lint-free gloves.

Prior to fabricating the required quantity of tubing, a sample length was manufactured according to the procedure described above, and the sample was subjected to several tests and examinations to evaluate the quality of the mechanical bond between the Inconel and copper tubes. The test procedures included metallographic examination, shear tests, and thermal cycling in a high-temperature oven followed by sectioning and microscopic examination.

Metallographic examination of tube samples, including scanning electron-microprobe analysis at the Inconel/copper interface, indicated that the copper closely followed the contour of the Inconel surface and the interface was free of contamination (i.e., no oxides or elements other than the parent metals were present) and/or air gaps. A maximum separation of approximately 0.00025-cm was observed between the copper and Inconel surfaces, which was attributed primarily to the sample preparation procedures (i.e., cutting, mounting and polishing).

The shear test was performed in an experiment in which an axial load was applied to the inner copper tube in an attempt to push the copper out of the Inconel sheath. Several tube samples having different lengths (0.2, 0.51 and 0.64 cm) were tested and it was found that an average shear load of 57 atm on the Inconel/copper interface was required for initial movement of the copper; an average shear load of 516 atm was required to extrude the copper through the Inconel tube.

A thermal cycling test was performed in which a sample tube was heated to 811K in an oven, air cooled to room temperature and then reheated and re-cooled. This test was designed to aggravate any tendency to separate at the bond surface because of the difference in thermal expansion between copper and Inconel and evaluate any possible separation on cooling, which, if encountered, would preclude reuse of tubes in which no deposits were formed. The sample tube was sectioned and microscopic examination indicated that no apparent separation of the copper from the Inconel had occurred.

The results of the various tests indicated that the mechanical bond between the Inconel and copper sections of the duplex tube was of very high quality, and that any tendency for separation at the Inconel/copper interface would be opposed during testing by the combined action of internal pressure forces and the higher rate of thermal expansion of copper relative to Inconel. Therefore, having validated the manufacturing process, the entire length of tubing required for all tests was manufactured in a single run.

The test tube assembly is shown schematically in Fig. 2 and by the photograph in Fig. 3. The test tube was silver soldered to a copper bus ring which in turn was bolted to copper ring adaptors. A high temperature silver solder (890K) was used during fabrication of the initial set of test tube assemblies to insure that no problems with tube attachment would occur during testing at the highest wall temperature. These tubes had to be discarded because longitudinal cracks developed in the Inconel outer sheath at the points of attachment to the copper bus rings, apparently as the result of excessive thermal stressing of the tube which occurred during the application of the high temperature silver solder. A detailed heat transfer analysis of the test tube assembly, which will be described in a later section, indicated that the temperature of the bus ring and adapter would not exceed 425K for the highest test tube temperature; therefore, a lower melting temperature silver solder (650K) was used for subsequent tubes and the problem was eliminated.

Ten thermocouples were spotwelded to the outer tube wall of each assembled test piece to monitor the outside tube wall temperature during a test. These thermocouples were placed at equal spacings of 2.54-cm starting at a location of 1.27-cm from the bus rings. The placement of the thermocouples was also determined from the heat transfer analysis which will be discussed later. The surface of the tube was coated with Sauereisen at the thermocouple junctions, to electrically insulate the thermocouple wire from the tube, and the wire was wrapped once around the tube and coated with additional Sauereisen cement to insure good thermal contact. By use of an AC power supply, thermocouple errors resulting from a voltage drop across the thermocouple bead were minimized.

The test section mounting arrangement is shown in the schematic of Fig. 4 and the photograph in Fig. 5. The test tube assembly is supported on teflon-lined cradles that were designed to accommodate the bus rings and to permit thermal expansion by providing a low coefficient of sliding friction. The teflon also acts as an electrical insulator and prevents grounding of the test tube. In

addition, non-conductive flexible hose was installed at the entrance and exit of the test tube assembly to allow thermal expansion and to electrically isolate the tube from the other components of the test apparatus. Connections to the power supply were made using a solid connector and a flexible water-cooled cable. Adjustable wall anchors and transformer connections were provided to assist in aligning the tube assembly prior to testing.

Data Acquisition and Control System

All test data were recorded utilizing a microprocessor-controlled, data acquisition/reduction system. The data system converted outputs from thermocouples, current transmitters, pressure transducers, etc., to precisely scaled DC voltages for measurement, and displayed the data in engineering units. The reduced data was logged on paper tape via a programmed logging format or through demand logging by push-button control. Specific groups of data channels were scanned and/or logged at specific intervals, or continuously. The system enabled scanning up to 70 channels at a scan rate of 35 channels per second on standard resolution, and 10 channels per second on high resolution. Data was logged on paper tape at the rate of 6 lines per second.

A built-in cathode ray tube (CRT) was used to display key operating parameters such as fuel pressure, temperature and flow rate; tube wall temperatures; and input voltage and current. The display provided a continuous visual check of the thermocouple outputs and test control parameters. An alarm function is also included and was utilized to provide a continuous check of each thermocouple output to ascertain that prescribed maximum temperature limits were not exceeded during a test run.

The primary fuel flow measurement was made with a turbine-type flow meter which was located downstream of the test section. In addition, a redundant fuel flow measurement system, consisting of a venturi-type flow meter and a differential pressure transducer, was installed upstream of the test section. Pressures were measured both with strain-gauge type pressure transducers and conventional Bourdon type pressure gauges. All instrumentation received frequent routine calibrations against laboratory standards.

Test Matrix and Operating Procedures

The experimental program began with a sequence of shakedown tests to verify the structural integrity of the system and to optimize procedures for testing and data acquisition. The shakedown period also included tests directed toward verifying the absence of a significant thermal resistance at the copper-Inconel interface, resulting from poor metal-to-metal contact or from impurities at the Inconel/copper interface. For this purpose, special tests were conducted (a) using high-pressure water in place of fuel, and (b) using a specially instrumented

test tube which allowed direct temperature measurement at the Inconel/copper interface as well as at the Inconel outer wall. After qualification of the experimental hardware and test procedures, a series of parametric tests was conducted to document the coking limits and decomposition rates of RP-1, JP-7, commercial-grade propane and chemically-pure propane. The full matrix of test conditions included fluid inlet velocities of 6.1, 12.2, 18.3, 24.4, 30.5 m/sec; tube entrance static pressures from 136 to 340 atm; and tube wall temperatures of 422, 589, 700 and 811K. The duration of each test was to be ten minutes; unless, during a test any tube wall temperature exceeded the maximum allowable limit of 866K, in which case the test was terminated.

Fuels testing at a pressure of 136 atm was started with standard, as-delivered RP-1 fuel and then proceeded to JP-7 fuel. Appropriate changes were made to the test apparatus to accommodate liquid propane and testing was continued with commercial-grade propane and, finally, chemically-pure propane. A limited number of tests were then performed with RP-1 fuel at pressures up to 340 atm to determine the effect of increased pressure on deposit formation. Finally the effect of inside wall material on deposit formation was evaluated in selected tests which were conducted using nickel-plated tubes.

Prior to each test the inside of the test tube was cleaned with a degreasing solution and a water slurry of commercial powdered copper cleaner, rinsed with water and dried with nitrogen, and then installed in the test apparatus. In addition, the in-line fuel filter located downstream of the test tube was replaced. If tests using kerosene fuel of refined quality were conducted, sparging and water filtration of the fuel were performed to reduce the oxygen and water concentrations to the desired levels. The piston type accumulators were then charged with the appropriate fuel and pressurized with nitrogen driver gas for the 136 atm tests, or with hydraulic fluid supplied by the high pressure pump for the higher pressure tests.

The test was initiated by opening the accumulator valve and then adjusting the downstream metering valve until the desired flow rate was obtained. The electrical powerstats were activated and set for a low power level at which a relatively flat wall temperature distribution was obtained (e.g., at wall temperatures of approximately 350 to 450K). Data was recorded at this initial power setting; any deviation from a flat temperature profile was noted as being indicative of improper thermocouple attachment.

The electrical powerstats were then advanced to a predetermined position to achieve the desired wall temperature (transient time was usually less than 6 seconds) and the corresponding input power was maintained as the test was continued for ten minutes or until a maximum wall temperature of 866K was reached. The data logger continuously monitored and recorded test data at one minute intervals, or more frequently if large variations in data were occurring. After the test was completed, the test tube was removed and set aside for sectioning and deposit analysis. The fuel filter was also removed and set aside for post-test examination.

Data Analysis

During testing, coking was detected by a change in the tube axial wall temperature distribution when the system pressure, fluid velocity, and tube heating rate were held constant. After each test in which there was a positive indication of coking, qualitative and quantitative analysis of the deposits formed was performed and the results were correlated with the initial wall temperature and test operating parameters.

Calculation of Inner Wall Temperature

The test tube inner wall temperatures were calculated from the measured outer wall temperatures using a computerized heat transfer analysis. In this analysis (TCAL), a finite difference representation of the heat conduction equation (a time-dependent version of Laplace's equation) is solved by a relaxation technique. This solution is applied to any one-, two-, or three-dimensional model in order to calculate the steady-state or transient temperature distribution for all elements of the model. The required inputs to the computer program included a geometric description of the test tube assembly, the physical properties of the duplex tube and bus ring materials, the transport properties of the test fuels and the ambient environment, and the heat generated (electrically) within the apparatus. Material and fluid properties are permitted to vary with temperature. A preprocessor was used to convert coarse dimensions of two-dimensional or axisymmetric models into TCAL input. The output is the steady-state (or transient) temperature of the elements, including the local temperature of the fluid.

A 152 element model was utilized to describe the tube/bus ring configuration used in the tests and to calculate the axial and radial wall temperature gradients for RP-1 fuel flowing at a velocity of 30.5 m/sec through a tube having a maximum inner wall temperature of 811K. This was the most severe test condition with respect to the radial temperature gradient. The fuel inlet temperature was assumed to be 311K. The elemental description of the tube/bus ring configuration and the calculated local wall and bulk fuel temperatures are shown in Fig. 6. It should be noted that the TCAL analysis indicated that less than 1 percent of the electrical energy dissipated in the tube wall was lost to the surroundings, and that the balance of the electrical energy input to the system (more than 99 percent) appeared as heat conducted into the test fluid. Therefore, knowing the radial origin of the electrical energy input (from the relative electrical resistance of the Inconel and copper wall materials), the wall temperature drop (from the external point of temperature measurement to the inside copper wall) and the fluid temperature rise was calculated using the TCAL computer program. It can be seen from the figure, that the bulk temperature of the fuel was increased by 71K as it flowed through the heated tube and that the maximum

temperature difference between the outer and inner walls is 15K. Because the relatively massive bus-ring/connector assembly remained essentially at ambient temperature during a test, significant local cooling and steep temperature gradients occurred at the ends of the tube. Therefore, to avoid placement of thermocouples at locations which could be affected by tube end cooling, the grid elements adjacent to either bus ring were subdivided into smaller elements (not shown in Fig. 6) and a more accurate calculation of the local temperature distribution in this region was performed. This calculation indicated that placement of the thermocouples at least 1.27-cm from the bus ring would avoid the tube end effects.

The results of the TCAL calculation are also shown graphically in Fig. 7, along with the axial variation of heat transfer coefficient. The equation used for calculating the local heat transfer coefficients was obtained from Ref. 44. It will be shown later that this equation matches measured data with reasonable accuracy. An unanticipated result of the calculation was the prediction that the maximum wall temperature would occur near the inlet of the tube and not at the exit where intuitively it would be expected. This seemingly anomalous behavior can be explained by examining the axial variation of the heat transfer coefficient along the inner wall. The variation of bulk fuel properties with temperature results in a local heat transfer coefficient which is lowest at the tube entrance, where the fuel is cold, and increases as the fuel is heated. As a result, in the case of the kerosene type fuels, the highest wall temperatures occur near the tube entrance and the wall temperature decreases along the length of the tube.

These calculations, which were performed for one extreme in the matrix of test conditions (i.e., the highest wall temperature and highest velocity), indicated a temperature difference between the outer and inner walls of only 13 to 15K. The TCAL results were used to predict the wall temperature difference (inner vs outer) over the entire range of test conditions, see Fig. 8. The differences ranged from approximately 3 to 13K at the highest wall temperature of 811K and 1 to 3K at the lowest wall temperature of 422K. These temperature differences were, for the most part, within the expected experimental accuracy of the temperature measurement and, therefore, the measured outer (Inconel) wall temperature was considered representative of the inner (copper) wall temperature.

Deposit Characterization

After each test in which there was a positive indication of coking, the tube was sectioned. As shown in Fig. 9, five 1.27-cm long sections were cut from the 25-cm length of tubing and from each of these sections, a longitudinal and transverse section was prepared for microscopic examination. The transverse

sections were mounted in plastic, metallographically polished, and photomicrographs were taken to estimate deposit thickness. The longitudinal sections were used for qualitative analysis of the deposits, in terms of type and uniformity. The remaining four sections, each approximately 3.8-cm long, were used in burnoff tests where a quantitative estimate of the total carbon deposit was made by determining the quantity of CO_2 evolved.

Depending upon the type and amount of deposit present, several methods were considered to determine the quantity of deposit on the tube surface. These procedures included (1) direct measurement of deposit thickness, (2) tube weighing before and after deposit burnoff, (3) deposit burnoff in air with analysis of evolved gases and (4) surface analysis using ion spectroscopy. Examination of the deposits obtained early in the tests with RP-1 indicated that the deposits were of sufficient quantity, i.e., > 0.1 mg, to permit the determination of deposit rates by burnoff in air with analysis of the evolved CO_2 . Tube weighing before and after deposit burnoff was not performed because of anticipated inaccuracy in weighing such small quantities and because the weighing procedure would be complicated by the fact that the copper surface could be oxidized during burnoff. The direct measurement of the deposit thickness from photomicrographs of transverse sections of the tube was also undertaken but the results were inconclusive because of the non-uniform deposition of material along the tube.

EXPERIMENTAL RESULTS AND DISCUSSION

The experimental test program comprised (a) two special calibration tests to verify that there was no significant thermal resistance at the Inconel/copper tube interface; (b) an extensive series of tests designed to investigate the deposit formation tendencies of RP-1, JP-7, commercial-grade propane and chemically pure propane at a pressure of 136 atm and over a range of velocities and wall temperatures; (c) tests to determine the effect of pressure on deposit formation; and (d) a short series of tests to evaluate the effect of the tube inside wall material on deposit formation. A discussion of the results of these experiments is included in the following sections. A tabulation of all the test data, including calculated parameters (e.g., velocity, Reynolds No., discharge coefficient and deposit thermal resistance), is presented in Appendix A.

Calibration Tests

A special calibration test using high-pressure water in place of fuel was conducted to determine if there was any significant thermal resistance at the Inconel/copper interface which could result from poor metal-to-metal contact or from impurities at the interface. If a significant interfacial resistance was present, the theoretical heat transfer prediction would have to be modified and the input power and output wall temperature settings revised. Water was used for these tests, since its thermal properties are known with greater accuracy than any other candidate test fluid. Testing with water ensured that the contribution of uncertainties in the basic fluid transport characteristics to any differences between the TCAL predictions and the actual temperature measurements would be minimized. Therefore, if the measured wall temperature profile closely matched the TCAL temperature profile predictions for water, the absence of a significant thermal resistance at the Inconel/copper tube interface would be verified.

Three well-known heat transfer correlations described in Ref. 45, (i.e., the classical Dittus-Boelter equation, the Sieder-Tate equation and the Colburn equation) were used to predict the axial temperature distribution along the outer wall of the heated tube. These equations were chosen because they appeared to be best suited for experiments conducted with high-pressure water. The Dittus-Boelter and Sieder-Tate equations utilize fluid bulk properties and/or corrections for wall to bulk temperature differences. With the exception of specific heat, film properties are used in the Colburn equation. For water flowing at a pressure of 64 atm and a velocity of 7.5 m/sec, through a tube heated with 17.6 kW of electrical power, the three equations predicted temperatures which were higher than the experimental values. The Colburn equation gave the best correlation, perhaps because the conditions of the experiment better matched the conditions for which the equation was derived. A comparison between the Colburn prediction and the experimental results is shown in Fig. 10. The shaded area represents a ± 5 percent difference in power input, and reflects the differences in the heat balance obtained when the measured input power was compared with the measured sensible heat added to the water. Since

no Inconel-copper interfacial resistance was assumed in the theoretical analysis and since, as stated above, the predicted temperatures were higher than the measured wall temperatures, (the converse would be expected if a significant interfacial thermal resistance were present) the absence of any significant resistance present at the Inconel/copper interface of the tube was inferred.

A test was also performed using a special tube which was instrumented with thermocouples attached to the copper tube outer wall through holes drilled in the Inconel sheath. This tube had been prepared by NASA/LeRC to aid in correlating experimental data with the theoretical heat transfer predictions, and to verify the integrity of the mechanical bond at the Inconel/copper interface. Pretest inspection of the tube revealed that there were very fine cracks in the Inconel sheath, close to the copper bus rings. These cracks were similar to ones observed previously at UTRC, stemming from overheating of the tube during application of the high-temperature silver solder for attaching the bus rings to the tubing. This special tube was instrumented with additional thermocouples on the outside Inconel wall and then tested at operating conditions of reduced severity. This was done because the results of earlier experiments had shown that regions of locally high temperatures would develop around the cracks and, thereby, limit the maximum allowable power input to the tube.

Tests were performed with RP-1 fuel at a pressure of approximately 136 atm, fluid velocity of 6.1 m/sec and wall temperatures ranging from 350 to 750K. At the highest wall temperature, a leak developed around one of the thermocouples attached to the copper and therefore, the test was terminated and no additional testing with the tube was attempted. A comparison of the temperature distributions measured along the outer walls of the copper and Inconel sections of the tube is shown in Fig. 11. It can be seen that there is excellent agreement between the two wall temperature distributions, (except at the peak temperature where the largest difference is only 10K), thereby verifying, in a general sense, the TCAL temperature predictions as well as confirming the absence of a significant resistance at the interface between the two metals. The relatively high temperature reading of the thermocouple located at the tube exit (i.e., the 23-cm station) was attributed to cracks in the outer tube.

Special tests were also conducted with RP-1 in which the fluid velocity was fixed and the power level into a single tube was varied sequentially to produce peak wall temperatures within the range 400 to 900K. Operating conditions were held constant only momentarily, so that data could be recorded at each power setting and in the absence of significant deposit formation. The tests were repeated for the full range of fluid velocities. The temperature distributions obtained at the maximum and minimum test velocities (i.e., 7.1 and 30.5 m/sec) are shown in Fig. 12. These results indicated that substantial changes in the heat transfer processes were incurred as the flow, power and wall temperature were varied. At low velocity conditions, and particularly at high power, the wall temperature increased with length near the tube entrance,

reached a maximum value at approximately 20-30 percent of the tube length, and thereafter decreased continuously to the end of the tube. In contrast, at high fluid velocity the wall temperature distribution did not show a peak; instead the wall temperatures gradually decreased from the tube entrance to the tube exit.

The wall temperature distribution noted at low velocity appears to indicate laminar-like flow at the tube entrance, followed by a transition to turbulent flow. In laminar flow, an initial high heat transfer coefficient is expected until an appreciable thermal boundary layer thickness has accumulated. Thereafter, the heat transfer coefficient diminishes rapidly to a minimum value as the thermal boundary layer grows and then it rises again as transition to a fully-developed turbulent flow condition ensues. This entrance effect could be expected to be minimized at the higher Reynolds numbers associated with the higher flow rates. The inlet Reynolds number at the low velocity condition is approximately 7000 and, therefore, turbulent flow would be expected to exist in the tube. However, there is theoretical and experimental evidence (Ref. 46) which indicates that in the case of liquid flow in smooth pipes, heating tends to stabilize a laminar boundary layer and to lower the liquid viscosity and thus delay the transition to fully developed turbulent flow. At 20 to 30 percent of the tube length, the Reynolds number has apparently increased sufficiently to permit the transition to turbulent flow.

Wall temperatures measured in the special tests described above were used to calculate experimental heat transfer coefficients which were compared with theoretical heat transfer coefficients calculated from the following correlations:

Dittus-Boelter:
$$Nu = 0.023 Re^{0.8} Pr^{0.4} \quad (\text{Ref. 45})$$

Sieder-Tate
$$Nu = 0.023 Re^{0.8} Pr^{0.4} \left(\frac{\mu_B}{\mu_W} \right)^{0.14} \quad (\text{Ref. 45})$$

Rocketdyne:
$$Nu = 0.0056 Re^{0.95} Pr^{0.4} \quad (\text{Ref. 44})$$

Where Nu, Re, Pr are the Nusselt, Reynolds and Prandlt numbers, respectively, and μ_B and μ_W are viscosities at the bulk and wall temperatures, respectively.

The experimentally-determined heat transfer coefficients calculated for a flow velocity of 18.3 m/sec are compared with the theoretical heat transfer coefficients in Fig. 13. It can be seen that all the experimental data fall slightly above the theoretical predictions. Since the test conditions were held constant only momentarily, so that no significant deposit formation would occur, the differences between the experimental data and the theoretical curves cannot be attributed to carbon formation. Furthermore, at the velocity of 18.3 m/sec, the tube entrance effects were

not appreciable and should not have had a significant effect on the heat transfer. However, it is possible that the higher experimental heat transfer coefficients noted could have been caused by a slightly higher than usual tube roughness which resulted during tube fabrication.

RP-1 Tests

Since the special calibration tests corroborated the results of the physical tests performed on the tubing, it was concluded that a good mechanical bond, free of contamination existed at the metal interface and that the radial temperature gradient across the tube was negligible for the purposes of the intended tests. Therefore, more detailed testing with RP-1 fuel was initiated; a summary of the tests performed is shown in Table VII. RP-1 testing began at a fluid velocity of 6.1 m/sec and a wall temperature of 422K. However, no significant temperature rise was observed along the tube during the ten minute test duration, suggesting the absence of significant deposit formation. The tube used in this test was sectioned and microscopic inspection of the inner copper surface confirmed that deposits had not been formed. In appearance, the surface was only slightly stained with no evidence of black, carbon-like deposits which were subsequently obtained at higher temperatures. Based on these results, no additional testing was done at a wall temperature of 422K.

Outer tube wall temperatures were measured in tests within a range of fluid velocities from 6.1 to 30.5 m/sec. The input heat flux to the tube was varied between 173 and 1460 Watt/cm² so that wall temperatures in the desired range from 583 to 811K could be achieved. The wall temperature distributions are shown in Figs. 14 through 16 where each condition shown is a composite of data obtained from a different test. The results shown in Figs. 14 through 16 indicate that the temperature rise that was obtained during the ten-minute duration was lowest at the lowest wall temperature, increased with increasing wall temperature and reached a maximum value at locations which were initially at temperatures between 700 and 750K. Since it was expected that a wall temperature rise indicated deposit formation, this behavior suggested that the rate of deposit formation increased with increasing temperature, reached a maximum at a temperature of 700 to 750K and fell off thereafter. Also, the first indication of a significant local temperature rise generally occurred at the tube entrance (region of highest wall temperature) and eventually spread to other locations all along the tube.

The effect of the initial wall temperature on temperature rise with time is shown more clearly in Fig. 17, where the tube temperature rise data are plotted against the initial wall temperature. It can be seen that a maximum temperature rise of approximately 80K occurred at a location on the tube where the initial wall temperature was between 700 and 750K. There appears to be no appreciable effect of fluid velocity, except possibly to produce a slight shift in the location of the peak temperature rise.

Heat transfer across a deposit layer formed and the wall is governed by the following:

$$Q/A = \frac{k}{\tau} \Delta T_w$$

where Q/A is the heat flux, k is the thermal conductivity of the deposit, τ is the deposit thickness and ΔT_w is the wall temperature rise. If the thermal conductivity of the deposit is assumed to be constant and the deposit thickness increases during the test, then for the constant heating rate, maintained during the test, the tube wall temperature would be expected to increase in proportion to accumulated deposit thickness. Similarly, if the deposit rate is assumed to be independent of fluid velocity (as a first order assumption), but the power input to the tube is increased to maintain a given initial wall temperature when the fuel flow rate (and therefore velocity) is increased, then the wall temperature rise observed should be higher at the higher velocities (i.e., equal deposit thickness, but proportionately increased heat flux). However, since the wall temperature rise was observed to be essentially independent of velocity for the RP-1 tests (see Fig. 17), either the rate of deposit formation decreases with increased fluid velocity, or other factors, such as a synergistic effect of deposit roughness may contribute to an enhanced local heat transfer coefficient.

For each test which gave a positive indication of deposit formation, i.e., a significant local wall temperature rise with time, the test tube was sectioned and the tube sections were prepared for microscopic examination and deposit burn-off. Microscopic examination of the inside surfaces of longitudinal sections of the tubes revealed that the deposit coverage was generally very non-uniform and ranged from specks, to connected islands of deposits, to essentially full coverage. No particular pattern could be established with test conditions and the non-uniform deposit coverage made a determination of the point of incipient deposit formation impossible.

Also, the deposits observed were multi-colored and took on various shades of red, black and sometimes gray. All three colors could sometimes be observed on samples taken from a single tube; however, it was difficult to associate color with a particular run condition or wall temperature. The deposits appeared to vary in degree of roughness but were generally hard and did not break loose from the tube surface very easily. From the general appearance of the surfaces of the tubes, it was concluded that the formation of deposits on copper is a very complex process leading to various intermediate compounds which can take on various colors and textures.

Transverse cross sections of the tubes were also taken at approximately the same location as the longitudinal sections. These cross-sections were potted in plastic and polished to produce a flat surface for subsequent microscopic examination. Photomicrographs of these surfaces were taken and an attempt was made

to determine the deposit thickness. The deposits observed in these photomicrographs were usually not of constant thickness and, because of the non-uniformity of the deposit formation, covered only a small portion of the surface. However, on the average, they ranged from 0.0002 to 0.001-cm in thickness.

Because of the high magnification of the small surface area which is observed in the transverse sections, the photomicrographs of the tube transverse sections appeared to indicate even greater non-uniformity of deposit formation than the longitudinal sections had shown. In fact, in many cases, the transverse sections showed little or no deposit formation whereas the longitudinal sections taken from approximately the same locations on the tube and viewed at lower magnification indicated significant deposit coverage. For these reasons, deposit rate estimates obtained from the photomicrographs were not used as the primary measurement of deposition rate. These data were instead inferred from the results of the burnoff tests to be discussed below.

A typical photomicrograph of a tube cross-section (with deposits) corresponding to a test with RP-1 is shown in Fig. 18. The dark area shown in the photomicrographs is the plastic potting material and the bright area is the copper. The thin line of material between the dark and bright areas is deposit. From this figure, there appears to be an indication that the deposit is thicker for the low velocity condition. The particular sections shown represent some of the more uniform deposits; however, many of the samples revealed deposits having a much more irregular pattern, from which consistent trends in either deposit nature or thickness with test conditions could not be derived.

The primary measure of the deposit formation rate with the various test operating conditions was made by burning off the tube deposits and measuring the quantity of CO_2 evolved. A special laboratory bench-type apparatus was employed for this task, wherein a metered flow of air was passed at a constant rate through heated sections of the test tube. The product gases resulting from the burnoff were subsequently passed through a nondispersive infrared analyzer which measured the concentration of CO_2 in the effluent gas. This instrument was calibrated before each series of burnoff tests using air for setting the instrument zero level and a N_2/CO_2 gas mixture of certified CO_2 concentration for establishing the scale factor. Also, prior to initiating the tube deposit burnoff tests, a special calibration run was made in which pre-weighed samples of instrument grade graphite were burned off. Agreement between the weight of carbon calculated from the CO_2 evolved and the actual weight of graphite was within two percent. No special post-test procedures were employed prior to deposit burnoff to remove any residual fuel which might remain in the tubes. It was felt that since several days elapsed between testing, tube sectioning, and deposit burnoff, there was adequate time for the tubes to dry. Furthermore, since the burnoff procedure involved a gradual heating of the tube sections, there should have been sufficient time for vaporization of any residual liquid fuel prior to oxidation of carbonaceous deposits. However, in order

to check if significant residual fuel remained in the tubes, alternate sections of several tubes were washed in solvent, blown dry with nitrogen, and heated in a vacuum oven to remove any traces of residual fuel. Comparison of rate data determined for these specially treated sections with that determined for adjacent untreated sections indicated that any effect of residual fuel was insignificant.

Output from the meter was continuously recorded to give a time trace of percentage CO_2 evolved during burnoff of the deposit. Integration of the data over the total burnoff time gave the total volume of CO_2 evolved, from which a carbon weight and deposition rate were calculated. As shown in Fig. 9, four equally-spaced sections (each approximately 4-cm long) were cut from each test tube and used for the burnoff tests. The four tube sections represented approximately 60 percent of the total surface area of the tube; the remainder of the tube was used for the longitudinal and transverse sections. The results of the burnoff tests for RP-1 are shown in Table VIII.

The data listed in Table VIII are presented graphically in Fig. 19, in the form of plots of the rates of carbon deposition as a function of the average initial wall temperatures. The open symbols represent the data obtained from individual tube sections (i.e., 15 percent of the total tube length) while the closed symbols represent an average of the four sections of the tube (60 percent of the total tube length). It can be seen that there is considerable scatter in the data; however, some general trends can be observed. The data scatter is believed to result from the combined effects of experimental error and the non-uniformity of the deposits on the tubes. The deposit rate data appear to substantiate the conclusions drawn previously from the wall temperature distributions (see Fig. 17); i.e., the rate of carbon increases with increasing temperature, reaches a maximum and then falls off as temperature is increased further. This maximum deposition rate occurs at a wall temperature of approximately 600K at the lowest fluid velocity and appears to shift to higher temperatures (700 to 750K) as the fluid velocity is increased. For each velocity, the maximum deposition rate occurred at a lower temperature than was inferred from the temperature rise data shown in Fig. 17.

The rate of carbon deposition also appears to decrease as the fluid velocity increases. In order to explore this apparent trend, data was taken from Fig. 19 and replotted in Fig. 20 to illustrate the dependency of the rate of carbon deposition on velocity. It can be seen that the rate of deposit formation decreases as the fluid velocity is increased up to a wall temperature of 700K; whereupon, the rate of carbon deposition appears to reverse trend and increase with flow velocity.

Another measure of the rate of carbon deposition which occurred during a test is the deposit thermal resistance build up rate (R_c), which is defined as:

$$R_c = \frac{\Delta T_w}{(Q/A)(t)}$$

where ΔT_w is the wall temperature rise (deg K) observed during the test, Q/A is the heat flux (Watt/cm²), and t is the test duration (min.). The thermal resistance growth rates calculated for tube sections which exhibited temperature rises during testing with RP-1 fuel are shown in Fig. 21. These rates were calculated for the full test duration of 10 minutes. It should be noted that the thermal resistance buildup rates generally decreased with time as shown in the data tabulations for RP-1 in Appendix A. The data presented in Fig. 21 indicates that the resistance buildup rate reached a maximum at tube locations where the initial wall temperature was approximately 700K. In addition, the magnitude of the peak appears to decrease as the fluid velocity is increased, a trend which is in agreement with the deposit burnoff data discussed above. Also, as the fluid velocity is increased, the initial wall temperature at which the maximum rate occurs appears to shift to a lower value. The deposit thermal resistance data were also plotted against the reciprocal of the initial wall temperature (i.e., the Arrhenius form) and are shown in Fig. 22. Straight lines were fit through the data on either side of the peak buildup rates and are also shown in the figure. A comparison of the thermal resistance buildup rate data obtained for the highest fluid velocity considered in this program ($V = 30.5$ m/sec) with experimental data for RP-1 (Ref. 49.) obtained at velocities in the range 46-76 m/sec is also shown. It can be seen that there is good agreement in the magnitude of the rates over the temperature range indicated.

As indicated previously in the description of the test apparatus, a 0.45 μm nylon-membrane filter was placed downstream of the test section to collect any particles which might form in the fuel or break off from the test tube wall during testing. Post-test examination of the filters indicated that varying amounts of grey-to-black material was collected from test to test. No particular pattern was evident either in the amount of deposit or the visual appearance of the filter paper as test conditions were varied. However, there was some indication that more material was collected at the higher test velocities, which would be consistent with increased deposit erosion which might be expected at higher velocities. This conclusion is complicated, however, by the fact that deposit was also found to collect on the inside surface of the flexible hose and intermediate tubing downstream of the test section. Since it was not possible to determine how much of this material was carried over from a previous test, no attempt was made to analyze the material collected on the filter for subsequent correlation with test conditions.

JP-7 Tests

Since significant deposit formation was obtained in the tests with RP-1 fuels, testing proceeded to JP-7 fuel to investigate the effect of utilizing lower sulfur

content fuel on deposit formation rates. A summary of the actual tests which were performed with JP-7 fuel is also shown in Table VII. Prior to each test, the JP-7 fuel was sparged with nitrogen in order to reduce the dissolved oxygen content to less than 10 ppm. Measurements of the dissolved oxygen content were made with a Beckman dissolved oxygen analyzer. It was found that the JP-7 fuel in the as-delivered condition generally contained less than 20 ppm oxygen and that a 30 minute sparging of the fuel was sufficient to reduce the oxygen content to less than 5 ppm. Axial wall temperature distributions obtained with the JP-7 are shown in Fig. 23. In this figure, data are presented for tests at fluid velocities of 6.1, 18.3 and 30.5 m/sec, all with an initial wall temperature of approximately 700K. The temperature distributions obtained with JP-7 are similar to those obtained with RP-1, in that the peak temperature occurs near the tube inlet, and entrance effects which are apparent at the low velocity, disappear as the fluid velocity is increased. One significant difference in these distributions is that the magnitude of the temperature rise noted during the test appears to increase with velocity, whereas it appeared to be independent of velocity for RP-1 fuel (see Fig. 17). Also shown in Fig. 23 is the wall temperature distribution obtained when the test duration was extended to 20 minutes. It can be seen that the increase in temperature observed during the last ten minutes of the test is not appreciably different from that observed after the first ten minutes. If the rate of deposition had remained constant as the test progressed, the deposit thickness would have increased with time and the magnitude of the temperature rise over the last ten minutes would have also increased as the run progressed, suggesting that the rates of deposit formation for JP-7 fuel are not constant with time. The implied decrease in deposit formation rate may also be attributed to deposits breaking off the wall surface after reaching a critical thickness or to passivation of the copper surface as the test proceeded.

The axial temperature distributions obtained as the wall temperature was increased for a fixed fluid velocity of 18.3 m/sec are shown in Fig. 24. Although the results are similar to those obtained with RP-1 fuel; (i.e., significant deposit formation, as evidenced by a wall temperature rise, occurs only after the initial wall temperature was increased to approximately 700K) the magnitude of the temperature rise was appreciably less than that with RP-1. This trend is also shown in the next two figures, Figs. 25 and 26, wherein the axial wall temperature distributions obtained with JP-7 are compared directly to those obtained with RP-1 for the same run conditions. The temperature rises obtained with JP-7 fuel are generally less than those obtained with RP-1 fuel for most of the conditions shown. However, at a fluid velocity of 30.5 m/sec and tube wall temperature of approximately 700K there appeared to be more deposit formation with the JP-7 fuel than with RP-1, as indicated by a general temperature rise along the entire length of tube.

Since the temperature rises obtained during the tests with JP-7 were generally much lower than those obtained with RP-1, it was expected that less deposit would be found with JP-7. When the tubes were sectioned, microscopic examination revealed that there was significant deposit formation with JP-7 and that the deposits appeared darker and more uniform than the RP-1 deposits. This apparent anomaly of the lower temperature rise with test time (inconsistent with the observation of increased deposit rates) may be due to a different character of the deposits formed with the JP-7 fuel. Relatively heavy deposits with JP-7 were not anticipated, due to the reduced sulfur content, and it was hypothesized that the presence of antioxidant and lubricity improving additives, in the absence of dissolved oxygen in the fuel, might have promoted higher rates of deposit formation. Therefore, a test was conducted with unsparged JP-7 fuel (Run No. 32) to determine if dissolved oxygen might affect deposit formation. When the results of this test also indicated heavy deposit formation, additional testing with JP-7 was suspended because the JP-7 did not appear to offer any benefit in terms of increased thermal stability.

Since JP-7 fuel must satisfy a special thermal stability requirement, which is not included in the RP-1 specification, it was assumed that JP-7 would have better thermal stability and; therefore, lower deposit formation at a given test condition than RP-1 fuel. Also, the severe hydrotreatment required to produce JP-7 fuel of sufficient quality to meet the thermal stability specification usually results in production of a fuel containing very low concentrations of sulfur compounds, which are known to promote deposit formation. Examination of previous certificates of analysis for typical batches of the two fuels indicated that the total sulfur content of JP-7 was generally an order of magnitude less than that for RP-1. However, comparison of the certificates of analysis of the RP-1 and JP-7 fuels (Table V) actually tested in this program revealed that the difference in sulfur content between the two fuels was only a factor of 2.3, and not the order of magnitude expected. This smaller difference in sulfur content could contribute to the unexpectedly small difference in deposit rates observed in the experiments.

Furthermore, in order to characterize the actual difference in thermal stability between the two fuels, samples were sent to an industrial laboratory where high-temperature stability of the two fuels was measured with a Jet Fuel Thermal Oxidation Tester (JFTOT) according to ASTM procedure D3241, (Ref. 48). The results of these evaluations, which are shown in Table IX, indicate that not only do the RP-1 and JP-7 both meet the thermal stability specification for JP-7, but that the RP-1 is even more stable than the nominally higher quality JP-7 fuel. For JP-7, the wall temperature that caused deposits which exceeded the thermal stability specification (the breakpoint temperature) was 638K. On the other hand, RP-1 was heated to 653K, the temperature limit for the test apparatus, and the deposits observed were still within the specification limit. Therefore, based on this result, it can be concluded that the particular batches of RP-1 and JP-7 fuels tested in this program were not significantly different, and that there probably would be a slightly lower rate of carbon deposition for RP-1.

Photomicrographs of transverse sections of tubes tested with RP-1 and JP-7 at a fluid velocity of 6.1 m/sec and a wall temperature of approximately 811K are compared in Fig. 27. It can be seen that for this test condition, the deposits obtained with JP-7 appear to be more uniform and heavier than those shown for RP-1 fuel.

Deposit burnoff tests were also conducted on the tube sections obtained from the JP-7 tests. A summary of the results of these tests is given in Table X. Since only a limited number of tests were performed with JP-7, not enough test data was available to graphically indicate the trends with test conditions. However, the tabular data do indicate that the deposit formation rates are generally of the same magnitude as was determined for RP-1. However, unlike the results obtained with the RP-1 fuel there does not appear to be a significant effect of fluid velocity on the deposit rate. This result is also in agreement with the temperature rise indications noted previously in the discussion of the JP-7 tests.

Propane Tests

All deposit formation tests with propane were conducted at a pressure of 136 atm. For commercial-grade propane, test data was obtained for fluid velocities ranging from 6.1 to 36.6 m/sec and for wall temperatures ranging from 422 to 811K. Most of the tests using commercial-grade propane at the higher temperatures (700-811K) had to be terminated prematurely; i.e., before the full ten minute test time was achieved because the wall temperatures near the fluid exit end of the tube fluctuated excessively and eventually exceeded the maximum allowable level (866K). Since this behavior, which will be discussed in detail below, was expected to also occur with chemically-pure propane, subsequent tests with chemically-pure propane were limited to wall temperatures between 422 and 589K. A summary of run conditions for both commercial-grade propane and chemically-pure propane is shown in Table XI.

The tube outer wall temperature distributions at the start of test that were obtained for propane and RP-1 over a range of electrical power input levels are compared in Fig. 28. It can be seen that unlike the results obtained for the distillate fuels RP-1 and JP-7, the wall temperatures observed in the propane tests at the start of the test run exhibited a more or less monotonic increase in temperature from the inlet end to the exit end of the heated tube. This behavior would be expected from a fluid whose local heat transfer coefficient was nearly constant over the range of bulk temperatures from tube inlet to exit. All the required transport properties data for propane are not available at the temperature and pressure of the tests, and therefore, a detailed heat transfer analysis (TCAL) of the variation of wall temperature and heat transfer coefficient along the tube length could not be made. However, low-temperature property data for propane indicates that the expected variation of heat transfer coefficient at higher temperatures would be much less than that shown for RP-1

in Fig. 7, and therefore, the wall temperature distributions obtained with propane are not unexpected. Also the entrance effect which was observed in the RP-1 and JP-7 wall temperature distributions is not apparent in the propane distributions shown in Fig. 28. This result is not surprising since even at the lowest flow velocity of 6.1 m/sec, the flow Reynolds number for propane was substantially higher than that for the RP-1 and JP-7 fuels.

An anomaly which can be seen in Fig. 28, is a sharp increase in wall temperature near the tube exit at the highest power setting ($T_{\text{wall}} \approx 700\text{K}$). Further, at the higher power settings, the wall temperature readings were observed to be very unsteady with increasing test time. An example of this behavior is shown in Fig. 29, where even though the variation of test conditions with time was small (i.e., < 2 percent) the wall temperature at the tube exit fluctuated over a 200K temperature range. This behavior was consistent and was observed in the majority of tests where the initial wall temperature was set at 700 or 811K. One explanation could be the formation and breakoff of flake-like deposit accumulations. However, this character of deposits is not consistent with the physical nature of the deposits observed on the tube surfaces when the relevant tubes were sectioned and examined. Also, the amount and appearance of the material trapped in the downstream fuel filter was not significantly different from that observed after the low temperature tests or after tests with RP-1 and JP-7. Of the eleven propane tests that were conducted at wall temperatures of 700K and above, ten had to be terminated before the full ten minute test duration was reached because the wall temperature oscillations became so severe that the maximum over-temperature condition of 866K was exceeded. Fluctuations in wall temperature were also observed during many of the tests which were conducted at temperatures of 589K, although they generally were not as severe and did not lead to premature shutdown.

It should be noted that when the test tube wall reaches 589K, the bulk temperature of the propane exceeds the critical point (366K), suggesting that perhaps the temperature fluctuations may be due to a change in character of the propane when the critical temperature is exceeded. Moreover, when the wall temperature exceeded 700K, and severe temperature instabilities were observed, the measured bulk fluid temperature was generally in the range 400 to 500K. In this temperature range, the specific heat of propane at a pressure of 136 atm changes very rapidly with temperature and passes through a maximum at 440K (Ref. 43). Therefore, it would appear likely that other properties of propane such as density, viscosity, and thermal conductivity may also be changing very rapidly and that these properties changes could lead to the unusual heat transfer characteristics that were observed for propane. Instabilities have been observed in other experiments in which propane was flowed through heated tubes, particularly at higher wall temperatures (Ref. 50).

The wall temperature distributions obtained for both grades of propane are not appreciably different and are compared in Figs. 30 and 31. Data obtained for a maximum wall temperature of approximately 422K (Fig. 30) indicate that wall temperature increased from the tube entrance to the exit and the local

temperature measurements were essentially constant over the ten minute test duration. At a maximum wall temperature of 589K (Fig. 31), the wall temperature again increased along the length of the tube, but the local wall temperature varied with time as the test proceeded. In contrast to the test runs conducted with the kerosene fuels, a continuous drop in local wall temperature with increasing test time was frequently noted with the propane fuels, suggesting that deposit formation may have occurred but that the deposits were rough enough to significantly increase the turbulence level in the flow, and thereby, increase the heat transfer to the fuel. The drop in temperature appears to decrease as the velocity increases, or consistent with the hypothesis above, the "rough wall" augmentation in local heat transfer characteristics diminished at the higher Reynolds numbers.

The deposit burnoff data for the propane fuels are tabulated in Table XII. Since most of the high-wall temperature ($> 589\text{K}$) tests with propane were terminated prematurely, the burnoff data could not be used in a graphical presentation of the dependence of the rates of carbon deposition on wall temperature. The rate data shown in Table XII for wall temperatures of 422 and 589K indicate that the deposit rates for both grades of propane fall in the range 400 to 600 $\mu\text{g}/\text{cm}^2\text{-hr}$, and generally overlap. Therefore, the rate data for the two fuels were combined to correlate the rates of deposit formation with fluid velocity. The average rate of deposit formation calculated for each test tube at wall temperatures of 422 and 589K is shown in Fig. 32. Although there is some scatter in the data, the carbon deposition rate for propane fuel appears to decrease slightly with increasing fluid velocity for each wall temperature condition. As is shown in the figure, at low velocities, the deposit rates for a wall temperature of 589K are higher than the deposit rates for a wall temperature of 422K; however, at the higher fluid velocities, no significant difference in the deposit rates is discernible.

Microscopic examination of the deposits obtained with both types of propane indicated heavier, blacker and more uniform deposits than those observed with the kerosene-type fuels, especially at the higher tube temperatures. The carbon deposition rates determined for propane in the burnoff tests confirmed this observation, and the deposit levels are generally higher than those obtained for either of the kerosene fuels at any given tube wall temperature. The carbon deposition rate for propane generally ranged from 400 to 600 $\mu\text{g}/\text{cm}^2\text{-hr}$ over wall temperatures as low as 394 to 533K; whereas comparable rates were not observed for the kerosene fuels until the wall temperatures reached 589 to 700K.

One test with chemically-pure propane, (Run No. 53), was repeated (Run No. 60) but purposely terminated after a duration of 3 minutes to determine the effect of test time on deposition rate. The average deposit rate for the short test was 918 $\mu\text{g}/\text{cm}^2\text{-hr}$ whereas the rate calculated for the full ten minute run was 352 $\mu\text{g}/\text{cm}^2\text{-hr}$; a decrease in deposition rate by a factor of 2.6. Also, two tests with commercial-grade propane (Run Nos. 33 and 34) were conducted at essentially identical test conditions but for different test durations, i.e., 2 and 5 minutes,

respectively. The burnoff data also indicated a decrease in the deposition rate with time by a factor of 2.7 (i.e., 2021 $\mu\text{g}/\text{cm}^2\text{-hr}$ for the 2 minute test vs. 738 $\mu\text{g}/\text{cm}^2\text{-hr}$ for the 5 minute test). For the limited number of results obtained it appears that there may be a nearly linear decrease of deposition rate with time and therefore, test duration may be an important factor to consider in deposit rate correlations.

Photomicrographs of representative transverse sections of tubes which were tested with the propane fuels at a velocity of 30.5 m/sec and wall temperatures of 589K are shown in Fig. 33. It can be seen that the deposits are generally thicker and more uniform than those obtained with the kerosene fuels (cf., Fig. 27). Also, it appears that for this test condition, there may be less deposit for chemically-pure propane than for commercial-grade propane.

An interesting phenomenon that was observed in many of the higher wall temperature propane deposits was the appearance of dendritic or tree-like formations in which the deposits appeared to grow out from the copper surface as filaments. This structure is apparent in Fig. 34. Scanning electron microprobe analysis, discussed in a later section, revealed that the filament composition was primarily copper, with some carbon concentrated at the base of the tree-like structure. The dendrites were quite tenacious and although they could be removed by hard scraping, they could not easily be brushed or blown from the copper surface.

Filament deposits have been observed in various studies of carbon deposition on metal surfaces and several mechanisms have been proposed to explain filamentary carbon growth (Ref. 51). One explanation is that after a carbon particle is deposited on metallic surface, it diffuses into the bulk metal, either by dissolving in the metal or by diffusion through the surface and grain boundaries, and aggregates at some active sites along grain boundaries to form carbon nuclei. These nuclei grow to microscopic carbon through the continued supply of carbon atoms and push the metal grains out of the substrate. Copper does not dissolve carbon to any extent, but it does form filamentary deposits from acetylene (Ref. 52). These filamentary deposits on copper are quite different from carbon filaments. They grow erratically and once formed, the filaments appear to be reactive toward one another, and sometimes fuse together to form a solid mass in which the original filaments are indistinguishable.

High Pressure Tests

A limited number of tests were conducted with RP-1 fuel at pressures above 136 atm using the modified fuel delivery system described previously. Briefly, this system consisted of two piston type accumulators in series; the first accumulator contained hydraulic fluid on one side of the piston and test fuel on the other side, and the second accumulator (which emptied through the test section) contained test fuel on both sides of the piston (see Fig. 1). With this arrangement, the hydraulic fluid and the test fuel were separated by a fluid volume, thus eliminating possible contamination of the test fuel by any hydraulic fluid left on the wall of the accumulator or by leaking across the piston seals. A high-pressure piston pump was used to supply the accumulator

with hydraulic fluid. A handwheel located on the pump controlled the flow rate of hydraulic fluid through the pump and was set at the appropriate rate prior to initiation of the test. Pressure was regulated by bypassing excess hydraulic fluid through a pressure-relief bypass. During testing with this high-pressure system, it was found that the flow rate of hydraulic fluid through the pump tended to drift during the test. Therefore, compared to the low-pressure system, more frequent adjustment of the flow rate through the test section and the electrical power into the test tube was required to maintain the desired fuel velocity and wall temperature.

A summary of the run conditions for the high-pressure tests is shown in Table XIII. The tube wall temperature distributions obtained at pressures of 136, 204, and 340 atm are presented in Fig. 35. As can be seen in the figure, there are some differences in the wall temperature distributions and temperature rises obtained at each pressure. Much of these differences can be attributed to the variations in the test conditions, noted on the figure, which occurred because of the difficulties discussed above. Therefore, it would appear that there is no significant change in the wall temperatures as a consequence of increasing pressure, suggesting that the rate of deposit formation is relatively independent of pressure over the pressure range of 136 to 340 atm. Microscopic examination of the deposits obtained from these tests also revealed that there was no substantial difference in deposit appearance over the range of pressures tested; that is, the deposits were generally brownish-red in color, occasionally intermixed with black and/or grey-metallic streaks or specks.

A summary of the deposit burnoff data for the high-pressure tests is presented in Table XIV, and the overall rates of carbon deposition which are plotted in Fig. 36 fall within a relatively narrow band. A least squares fit of this data produced the straight line shown in the figure and indicates that the deposit formation rate increases slightly with pressure.

Tests With Nickel-Plated Tubes

Copper is prevalent in rocket engine cooling systems because of its superior thermal conductivity. However, previous experimental studies of the effect of wall materials on deposit formation, Refs. 6, 10, and 32, have indicated that carbon deposit rates on copper can be very high. Also, the results of the present experiments for kerosene fuels and propane fuels discussed in the previous sections appear to corroborate and extend the findings of the earlier experimental studies. It would appear that the copper surface probably promotes deposit formation to as great an extent as any deposit forming precursor contained in the fuels tested. Therefore, in order to obtain an indication of the importance of the tube wall material on deposit formation, five tests were conducted using tubes in which the inside (copper) surface had been plated with nickel by means of an electroless process. All of the tests were run using RP-1 fuel at a pressure of 136 atm. A summary of the test conditions is shown in Table XIII. The tube wall temperature distributions obtained with the nickel-plated tubes are compared with those obtained with the

copper tubes in Fig. 37. It can be seen from the figure that the temperature distributions are very similar and that the temperature rise obtained with the nickel-plated tube is significantly less than that obtained with copper, suggesting a substantial decrease in deposit formation.

The tubes used in the nickel-plated tube tests were sectioned and subjected to microscopic examination and deposit burnoff measurements. Initial microscopic examination of the virgin tubing indicated that the appearance of the nickel surface varied from rough granular to smooth fine-grained, perhaps due to variations in plating solution concentrations stemming from lack of solution agitation/circulation or solution instability. However, because of the differences in grain size and color as viewed through the microscope, (varied from black to metallic grey), it was difficult to distinguish black carbon deposits. Photomicrographs of transverse sections of the test tubes are shown in Fig. 38. They indicate that the nickel coating was generally of good quality and of uniform thickness (.0002-.0005 cm). These photomicrographs (at 500X magnification) do not indicate any significant deposit formation.

A scanning electron microprobe analysis was made of the five sections taken from the tube which was tested at a wall temperature of 700K and fluid velocity of 6.1 m/sec (the test condition which gave the highest deposition rate on copper). Photomicrographs taken at a magnification of 1600X revealed no deposits, and an elemental analysis indicated the presence of nickel and phosphorus (the major constituents in the electroless plating solution) but no copper, carbon, oxygen or sulfur. Also, the results of the burnoff tests of the sectioned nickel-plated tubes, presented in Table XV, indicate that very little material was deposited on the nickel surface during testing. Since the average rates of deposition ranged from 40 to 80 $\mu\text{g}/\text{cm}^2\text{-hr}$, it can be concluded that a substantial decrease in deposit formation occurred when the copper tubes were replaced with nickel-plated tubes.

Deposit Morphology

In order to characterize the complex structure of the deposits observed during this program, a scanning-electron microscope (SEM) was used to study the deposits. The SEM is particularly useful for examining solid specimens whose surface structures are rough, because it has considerably greater depth of focus than a conventional reflected-light microscope. As an aid in interpreting the SEM photomicrographs obtained in this program, a brief discussion of the morphology of the carbonaceous material (Ref. 53) is useful. Carbon lends itself to the formation of stable complex solids because of its chemical valance of four and its readiness to combine with itself and with other atoms such as hydrogen, nitrogen, oxygen, and sulfur. In such carbonaceous materials, the carbon atoms are bound together by strong covalent bonds to form the main units of molecular structure which can consist of chains or rings or both. Molecules with random three-dimensional networks and no particular microstructure may also be formed.

When viewed with a SEM, amorphous materials, such as asphalt, show no particular form because the molecular structure lack any order. On the other hand, crystalline materials, such as graphite have sharp geometric outlines because both atoms and molecules are arranged in a very high degree of three-dimensional order. Carbonized materials such as coke, however, are distinctly different from other carbonaceous materials. While they are neither amorphous or crystalline, these carbon residues do have a limited organization and orientation which gives them characteristic features. Generally, the carbon atoms tend to group together in tightly packed aggregates of spherical particles.

A SEM analysis was performed on four samples of deposit, one for each fuel, which were obtained in tests conducted with copper tubes (Run No. 3, 29, 40, and 55). SEM photomicrographs of the inside wall of a test tube at locations near the tube entrance (1.9 cm), in the middle (12.1 cm) and near the exit end (21.2 cm) are shown in Figs. 39 through 42. For reference, a photomicrograph of the surface of an unused tube is shown to the left in each figure.

The microstructure of RP-1 deposits (tube wall temperature of 700K, velocity of 7.2 m/sec-Run No. 3) is shown in Fig. 39. Near the entrance of the tube (1.9 cm), there appears to be a continuous film of deposit on the surface of the copper substrate. At higher magnification, it can be seen that the deposit is made up of agglomerated particles, which are very small ($\sim 0.5 \mu\text{m}$) and spherical in shape. In the photomicrographs taken at the 12.1 cm location, the microstructure of tightly packed aggregate of spherical particles is more evident. It appears that the top film of deposit fractured, exposing a highly-fused substrate which has been overlaid with the tightly packed spherical agglomerates. The photomicrograph taken at a location near the exit of the tube reveals another type of microstructure that has a more vitreous and amorphous appearance. Again, it appears that fracture of the deposit had taken place and the fused substrate is evident.

SEM photographs of JP-7 fuel deposits (tube wall temperature of 700K, velocity of 17.3 m/sec-Run No. 29) are shown in Fig. 40. Again, the microstructure of tightly packed spherical agglomerates typical of coke deposits is evident. In the photograph taken near the entrance of the tube, there are areas where the deposits appear to be more flocculent and porous. The photograph taken of the section from the middle of the tube shows a knobby surface which appears to have been formed by fusion of the spherical particles. The photograph taken at the end of the tube indicates a deposit which is vitreous in appearance. Not as much deposit fracturing is evident as was observed in the SEM analysis of the RP-1 deposits. The JP-7 deposits also appear to be generally more uniform than the RP-1 deposits.

The microstructure of commercial-grade propane deposits (wall temperature of 700K, velocity of 30.5 m/sec-Run No. 40) is shown in the SEM photomicrograph presented in Fig. 41. The sections near the entrance and at the middle of the tube show the typical dendritic formation. The dendrites were dispersed randomly along the entire length of the tube. Close-ups of these

areas do not show the aggregates of spherical particles that were observed with the kerosene type fuels and that are characteristic of coke formation; The highly-magnified photos of the dendrites show a distinctly smooth, finger-like structure. The microstructure of the deposits at the exit of the tube where the temperature was highest, is more dendritic in appearance and the finger-like deposits are more uniform and cover larger areas of the tube rather than being randomly clustered.

The microstructure of deposits obtained with chemically-pure propane (wall temperature of 589K, velocity of 18.3 m/sec-Run No. 55) is shown in Fig. 42. It can be seen that the dendritic formation is not as obvious at this wall temperature condition and that clusters of packed particles are spread across the length of the tube. These clusters appear to overlay a fused layer of deposits and are made up of packed spherical particles similar to the microstructure of the deposits obtained with the kerosene fuels. A SEM analysis was not made of deposits obtained in tests with commercial-grade propane at low wall temperatures. However, samples of deposits from tests with both grades of propane at various test conditions were examined microscopically at magnifications up to 400X and no apparent differences in deposit appearance was discerned.

These photomicrographs, shown in Figs. 39 through 42, indicate that the deposits accumulated during the heated tube tests are generally not formed on the tube surfaces as smooth, continuous films of uniform structure and composition. Instead, they indicate that discrete particles, spherical or dendritic in shape, accumulate over a fused substrate to produce a highly variable three-dimensional structure. The deposit surface appears to be sufficiently rough to significantly increase turbulence and thereby affect heat transfer. However, there also appears to be areas of the tube in which the surface has become smoother during deposit formation. From the SEM photomicrographs, it is obvious that surface roughness and deposit homogeneity can be expected to change along the length of a test tube and may significantly affect the local heat transfer characteristics.

As indicated in the discussion of the results obtained in tests with nickel-plated tubes, it was difficult to visually identify any deposits on the nickel surface using the relatively low-magnification reflected-light microscopes. A SEM analysis was made of a nickel-plate tube which has been tested with RP-1 fuel at conditions which gave substantial deposits in copper tubes (wall temperature of 700K, velocity of 6.1 m/sec-Run No. 70). The SEM photomicrographs of the surface of this tube are shown in Fig. 43. The photomicrograph shown at the extreme left shows the microstructure of a virgin tube and indicates a corn-cob appearance which is typical of an electroless-plated surface. The photomicrograph taken of the surface of the test tube near the fluid entrance end (1.9 cm) shows no appreciable difference in appearance from the unused tube. There is evidence of some deposit-like structure at the middle (12.1 cm) and near the end (21.2 cm) of the test tube, but they appear to be more random and widely dispersed than the deposits obtained in the kerosene fuel and propane tests.

A limited qualitative elemental analysis of the deposits was made utilizing a Scanning Electron Microprobe (SEMP). The SEMP incorporates an x-ray energy-dispersive spectrometer (EDS) which produces a qualitative scan of elements which are present in the deposit within a detectability limit of approximately 200 ppm. Because of poor sensitivity for elements with atomic numbers less than twelve, the EDS scan excludes likely constituents of deposits such as hydrogen, carbon, oxygen, and nitrogen. Also, x-ray emission from a thin conducting layer of gold, which coats the specimen to prevent charging, may mask the emission from elements such as sulfur. However, a selective wavelength spectrometer can be used with the SEMP which will allow characteristic x-ray mapping of selected elements. An image of the x-ray emission for the selected element is produced and matches exactly the standard photomicrograph of the sample. The presence of the element is indicated by clusters of white dots on a dark background to allow easy identification of the areas of local concentration of the particular element.

A SEMP analysis was made of samples from the same five test tubes which had undergone SEM analysis. The EDS scans of these samples indicated that besides the gold overlay and the parent materials in the inner tube surface; i.e., copper and nickel/phosphorus, other elements such as silicon, aluminum, potassium, calcium, and chlorine were present. It is believed that these materials were introduced during the cleaning and polishing required in the sample preparation for the SEMP analysis.

The results of the selected-wavelength analysis made with the SEMP are shown in Fig. 44. In the figure, the upper series of photographs correspond to a tube deposit obtained with JP-7 fuel. The first photograph shows a SEM photomicrograph of the deposit sample. This region was selectively scanned for the presence of copper, carbon, oxygen and sulfur and, if present, these elements would be indicated by an agglomeration of white dots against the dark background. It can be seen that the copper surface of the tube is clearly outlined but that no significant copper is contained in the area occupied by the deposit. The deposit, however, contains a heavy concentration of carbon and a smaller concentration of sulfur. The SEMP analysis of RP-1 fuel deposits gave essentially the same result as the JP-7 analysis except that a small concentration of oxygen was also present.

The bottom set of photographs represent a SEMP analysis of the microstructure of deposits obtained with propane at a high tube wall temperature ($\sim 700\text{K}$) condition and shows a typical dendrite formation. It can be seen that the dendrite contains a high concentration of copper, suggesting that tube material was forced up and away from the surface. Most of the carbon image results from that contained in the potting material but some carbon is also evident at the base of the tree-like structure. A very small concentration of sulfur is also indicated but no oxygen was observed. A less detailed SEMP analysis of a tube deposit obtained with

chemically-pure propane at a lower wall temperature ($\sim 589\text{K}$) was also performed (not shown in the figure). No obvious dendritic formations were observed in this particular sample although the deposit material contained significant amounts of copper, the presence of which may account for the observed decrease in wall temperature with increasing test time (see Fig. 31). However, the carbon content of the deposit was substantially more than that observed in the dendritic structure.

A SEMP analysis was also performed on five separate areas along the length of a nickel-plated tube which was tested at a wall temperature of 700K with RP-1 flowing at a velocity of 6.1 m/sec (the test condition which gave the highest deposition rate with copper). Photomicrographs at a magnification of $1600\times$ revealed no deposits and an elemental analysis indicated the presence of nickel and phosphorus (the major constituents in the electroless plating solution) but no copper, carbon, oxygen, or sulfur.

CONCLUDING REMARKS

The thermal decomposition (coking) limits and rates of deposition in heated copper tubes for two standard hydrocarbon rocket fuels, RP-1 and commercial-grade propane, have been investigated. In addition, tests were conducted using de-oxygenated JP-7 and chemically-pure propane as representative of more refined cuts of the standard fuels to determine the effect of improving thermal stability by reducing the concentration levels of deposit-forming precursors. The apparatus developed for these tests permitted independent variation and control of tube wall temperature, fluid pressure, and fluid velocity in order that the effects of each parameter could be investigated independently.

The results of the experiments with RP-1 fuel were as expected, in that there was previous evidence that copper promotes deposit formation in kerosene-type fuels. However, the relatively high deposition rates of between 400 and 600 $\mu\text{g}/\text{cm}^2\text{-hr}$ at temperatures of 500 to 800K for only a ten minute test duration were not anticipated. Peak deposit formation occurred near 700K, which is consistent with results obtained with kerosene-type aviation fuels. The deposit coverage was generally non-uniform and ranged from specks, to connected islands of deposits, to essentially full coverage. No particular pattern could be established with test conditions and the non-uniformity of deposit coverage made a determination of the point of incipient deposit formation impossible.

It was believed that JP-7, with a lower sulfur content (typically an order of magnitude lower) and a stringent thermal stability specification, would be a good simulator of refined quality RP-1 and demonstrate improved thermal stability. However, no benefit in terms of increased stability was realized with JP-7, since the results of tests indicated heavier deposit formation even though lower tube temperature rises were observed. Subsequent evaluation of the actual difference in the thermal stability between the two fuels was made in a series of tests using a Jet Fuel Thermal Oxidation Testor (JFTOT) to determine the breakpoint temperature. The results of this evaluation revealed that both the JP-7 and the RP-1 met the thermal stability specification for JP-7, and the RP-1 was even more stable than the normally high quality JP-7 fuel. Also, certified analyses of the two fuels indicated that the actual difference in sulfur contents was only a factor of two, and not the order of magnitude expected. Therefore, it can be concluded that there is little difference in carbon deposition rates and probably no particular advantage in using JP-7.

Another unexpected result of the study was that deposits obtained with propane fuels were heavier, blacker and more uniform than those observed with the kerosene-type fuels and there appeared to be little difference between commercial-grade and chemically-pure propane with regard to type and quantity of deposit. The carbon deposition rates for the propane fuels were generally higher than those obtained for either of the kerosene fuels at any given wall temperature. Two interesting phenomena were observed during testing with propane. The first phenomenon consisted of

unusual wall temperature instabilities whenever the bulk fluid temperature exceeded the critical temperature of propane. These temperature fluctuations were especially severe at wall temperature of 700K and above. For those wall temperatures, the bulk fluid temperature was in the range of 400 to 500K and corresponded to a temperature regime in which the specific heat of propane is known to vary rapidly with small changes in temperature. It is likely that other properties of propane, such as density, viscosity, thermal conductivity, etc. may also be changing rapidly and that these properties changes lead to unusual heat transfer characteristics above the critical temperature. The second phenomenon was observed in most of the deposits recovered from tests conducted with propane at the higher wall temperatures. These deposits contained dendritic or tree-like formations which appeared to grow out from the copper surface as filaments. The filament composition was primarily copper, with some carbon concentrated at the base of the tree-like structure.

Results of tests with RP-1 over a range of pressures from 136 to 340 atm revealed that there was no substantial difference in deposit appearance; that is, the deposits were generally brownish-red in color, occasionally intermixed with black and/or gray-metallic streaks or specks. Also, there was only a very slight increase in deposit formation rate with pressure. For both RP-1 and propane fuels, the rate of deposition appeared to decrease with increasing fluid velocity. However, for RP-1, wall temperatures above 700K, the rate of carbon deposition appeared to reverse trend and increased with increasing flow velocity.

Copper was specified for the tube inner surface in this experimental program because of its superior thermal conductivity, even though previous experimental studies had shown that deposit rates on copper can be very high. On the other hand, nickel, which has good thermal conductivity, did not appear to promote deposit formation with kerosene-type jet fuels. This conclusion was corroborated by the results of tests conducted in this experimental program which indicated a substantial reduction in deposit-formation when copper tubes were replaced with nickel-plated tubes.

Another observation made during the performance of this test program was that the deposition rate appeared to change with time and, therefore, test duration is an important factor to consider in deposit rate correlations. Also, post-test photomicrographic examination of the tube surfaces indicated that the deposits were generally not formed as smooth, continuous films of uniform structure and composition. Discrete particles, spherical or dendritic in shape, accumulated over a fused substrate to produce a highly variable three-dimensional microstructure. The deposit surface appeared to be sufficiently rough to significantly increase turbulence and thereby affect heat transfer. However, there were instances where the surface became smoother

during deposit formation. It was obvious from the photomicrographic analysis of the deposits that surface roughness and deposit homogeneity can be expected to change along the length of a test tube and may significantly affect the local heat transfer characteristics.

The results obtained in this experimental study suggest areas in which further work may be desirable to more firmly establish the trends observed. The result of the JFTOT analysis indicated that RP-1 fuel is very stable relative to standard jet fuels. Since it is known that deoxygenation of fuel significantly improves its thermal stability, additional parametric tests for de-oxygenated RP-1 are desirable to determine the minimum coking limits and deposition rates on copper. Also, since the substitution of the copper tubes with the nickel-plated tubes resulted in a substantial reduction in deposit formation, several different candidate high-thermal-conductivity tube materials (e.g., nickel, gold or silver platings, copper/nickel alloys, etc) should be investigated to determine their effect on deposit formation with RP-1 fuel. Furthermore, because the different techniques employed in manufacturing the regenerative cooling passages of high-pressure rocket thrust chambers result in surfaces of varying degrees of roughness, tests should be conducted to determine if there is an effect of surface roughness on deposit formation.

Finally, some of the trends observed in the present experimental study were not conclusive and therefore the range of test conditions should be extended to permit evaluation of the effects of run time, periodicity, and increased velocity.

REFERENCES

1. Szetela, E. J. and A. Vranos: Deposits from Heated Fuel - An Information Study. UTRC Report R75-214388-1. December 1975.
2. Szetela, E. J.: Deposits from Heated Gas Turbine Fuels. ASME 76-GT-9. 1976.
3. Szetela, E. J.: External Fuel Vaporization Study. Summary of Literature Survey. United Technologies Research Center Report R79-914607-5. July 1979.
4. CRC Literature Survey. Thermal Oxidation Stability of Jet Fuels. R. N. Hazlett, Ed., CRC Report 50-9. April 1979.
5. Watt, J. J., A. Evans and R. R. Hibbard: Fouling Characteristics of ASTM Jet-A Fuel When Heated to 700 F in a Simulated Heat Exchanger Tube. NASA TN D-4958. December 1968.
6. Faith, L. E., G. H. Ackerman, and H. T. Henderson: Heat Sink Capability of Jet A Fuel: Heat Transfer and Coking Studies. NASA CR-72951. July 1971.
7. Lohmann, R. P., E. J. Szetela and A. Vranos: Analytical Evaluation of the Impact of Broad Specification Fuels in High Bypass Turbofan Engine Combustors. NASA CR-159454. December 1978.
8. Taylor, W. F. and J. W. Frankenfeld: Development of High Stability Fuel, Exxon Report GRV. 12GAHF.75. January 1975.
9. Spadaccini, L. J. and E. J. Szetela: Approaches to the Prevaporized-Premixed Combustor Concept for Gas Turbines. ASME GT-85. 1975.
10. Taylor, W. F.: The Study of Hydrocarbon Fuel Vapor Deposits, AFAPL-TR-69-77. September 1969.
11. Emanuel, N. M., Editor: The Oxidation of Hydrocarbons in the Liquid Phase. Pergamon Press, p. 140. 1965.
12. Mayo, F. R., N. A. Kirshen, H. Richardson and R. S. Stringham: The Chemistry of Fuel Deposits and Their Precursors. Stanford Research Inst., AD754459. December 1972.
13. Mayo, F. R.: Accounts of Chemical Research 1. No. 7, p. 193. July 1968.
14. Nixon, A. C. and H. B. Minor: Effect of Additives on Jet Fuel Stability and Filterability. I&EC Vol. 48, No. 10. October 1956.

15. Nixon, A. C.: Auto-oxidation and Antioxidants, Lundberg, W. O., Ed., Vol. II, Chapter 17, Interscience Publishers. 1961.
16. McKeown, A. B. and R. R. Hibbard: Effect of Dissolved Oxygen on the Filterability of Jet Fuels for Temperatures Between 300 F and 400 F, NACA RM 55128. December 1955.
17. Hatcher, J. B.: High-Flux Heat Transfer and Coke Deposition of JP3 Fuel Mixture, JPL CIT Progress Report No. 20-157. February 1952.
18. Kennerly, G. W. and W. L. Patterson: Kinetic Studies of Petroleum Antioxidants. I&EC Vol. 48, No. 10. October 1956.
19. Norton, C. T. and D. E. Drayer: Oxidation of Organic Compounds. Vol. 1, Advances in Chemistry Series No. 75, ACS. 1968.
20. Taylor, W. F.: Development of High Stability Fuel, Exxon Report GRUS. 11GAHF.73. July 1973.
21. Taylor, W. F.: Mechanism of Deposit Formation in Wing Tanks, SAE Paper 680733. October 1968.
22. Taylor, W. F.: Development of High Stability Fuel. Exxon Report GRX. 6GAHF.72. April 1972.
23. Taylor, W. F. and J. W. Frankenfeld: Deposit Formation from Deoxygenated Hydrocarbons. Effect of Trace Nitrogen and Oxygen Compounds. Ind. Eng. Chem. Prod. Res. Dev. V17, No. 1, p. 86. November 1978.
24. Bachman, K. C.: Heat Transfer Unit Evaluates Performance of Jet Fuels for Supersonic Aircraft, SAE 650803. October 1965.
25. Smith, J. O., B. M. Faubuss, and L. I. Belenyessy: Evaluation of Hydrocarbons for High Temperature Fuels. Part II Fuel Evaluation and Property Correlation. Vol. I Correlation Studies, Thermal Stability, and Containment Effects. WADC TR 59-327, Pt. II., Vol. 1. February 1962.
26. Lander, H. R. and C. R. Martel: Jet Fuel Thermal Stability Improvements through Fuel Processing, AFAPL-TR-74-35. 1974.
27. U.S. Patent 3,666,656: Method for Inhibiting Fouling in a Refinery Process.
28. U.S. Patent 3,533,763: Process for Drying, Clarifying and Stabilizing Hydrocarbon Liquids.
29. U.S. Patent 3,509,040: Process for Producing Jet Fuel.

30. Johnston, R. K. and E. L. Anderson: Review of Literature on Storage and Thermal Stability of Jet Fuels. Southwest Research Institute, RTD-TDR-63-4270. January 1964.
31. Bradley, R., R. Bankhead and W. Bucher: High Temperature Hydrocarbon Fuels Research in an Advanced Aircraft Fuel System Simulator. AFFB-14-70, AFAPL-TR-73-95. April 1974.
32. Smith, J. D.: Fuel for the Supersonic Transport. I&EC Process Design and Development, Vol. 8, No. 3. July 1969.
33. ANON: Technical Data Book - Petroleum Refining. American Petroleum Institute, Division of Refining, Port City Press, Inc., Baltimore, MD. 1971.
34. ANON: Annual Book of ASTM Standards. American Society for Testing and Materials Part 25 - Petroleum Products and Lubricants. 1978.
35. James, F. W.: Certificate of Analysis of JP-7 Fuel (MIL-T-38219), Batch 6-80-CBG Manufactured by the Ashland Oil Co., Catlettsburg, KY. September 24, 1980.
36. Clink, W. E.: Certificate of Analysis of RP-1 Fuel (MIL-P-25576), Aerospace Fuels Laboratory, Mukilteo, WA. April 28, 1980.
37. Braker, W. and A. L. Mossman: Matheson Gas Data Book, Fifth Edition. Matheson Gas Products, E. Rutherford, NJ. September 1971.
38. Segeler, C. G., et. al: Gas Engineer's Handbook - American Gas Association Inc. The Industrial Press, New York, NY. 1965.
39. Segalman, I., P. Goldberg and J. J. Nolan: Hydrocarbon-Fueled Scramjet - Volume V - Cooling Investigation. United Aircraft Research Laboratories Technical Report, AFAPL-TR-68-146. June 1969.
40. Yesavage, V. F., D. L. Katz and J. E. Powers: Thermal Properties of Propane. Journal of Chemical and Engineering Data, Vol. 14, No. 2. April 1969.
41. Holland, P. M., et. al: A Correlation of the Viscosity and Thermal Conductivity Data of Gaseous and Liquid Propane. J. Phys. Chem. Ref. Data, Vol. 8, No. 2, 1979.
42. Stearns, W. V. and E. J. George: Thermodynamic Properties of Propane. Industrial and Engineering Chemistry, Vol. 35, No. 5. May 1943.
43. ANON: Provisional Thermodynamic Functions of Propane from 85 to 700K at Pressures to 700 Bar. National Bureau of Standards, Boulder, CO, Cryogenics Div. NTIS PB-272355. July 1977.

44. ANON: Investigation of Cooling Problems at High Chamber Pressures. Rocketdyne Report R6529. 1966.
45. McAdams, W. H.: Heat Transmission, Third Ed. McGraw-Hill Inc. New York, p. 219, 1954.
46. Schlichting, H.: Boundary Layer Theory, 4th Edition. McGraw Hill Book Co., Inc. New York. 1960.
47. Cook, R.: Advanced Cooling Techniques for High-Pressure Hydrocarbon-Fueled Engines. Rocketdyne Report RI/R079-310. October 1979.
48. ANON: ASTM D3241-77. Standard Test Method for Thermal Oxidation Stability of Aviation Turbine Fuel (JFTOT Procedure). 1980 Annual Book of ASTM Standards. Part 25 - Petroleum Products and Lubricants. American Society of Testing and Materials, Philadelphia, PA. 1980.
49. Wagner, W. R. and J. M. Shoji: Advanced Regenerative Cooling Techniques for Future Space Transportation Systems. AIAA Paper No. 75-1247. AIAA/SAE 11th Propulsion Conference. Anaheim, California. September 29-October 1, 1975.
50. Gross, R. S.: Combustion Performance and Heat Transfer Characterization of LOX/Hydrocarbon Type Propellants. Task I, Data Dump. Contract NAS 9-15158. Aerojet Liquid Rocket Co. August, 1980.
51. Walker, P. L. and P. A. Thrower: Chemistry and Physics of Carbon - A Series of Advances. Vol. 14. Marcel Dekker, Inc., New York. 1978.
52. Amelin, A. G. Kolloid. Zh. 29 (1), 16 (1967).
53. Schirmer, R. M. and H. T. Quigg: Aviation Turbine Fuels - Part I. Morphology of Deposits in Aircraft and Engine Fuel Systems. Phillips Petroleum Company Research and Development Report 54050-69. October 1969.

TABLE I

Fuels Contaminant Specification

	<u>RP-1</u>		<u>Propane</u>
Oxygen	5 ppm by wt.	Oxygen	5 ppm by wt.
Sulfur	report	Sulfur	report
Sulfur Compounds	report	Sulfur Compounds	report
Nitrogen	0.30 wt%	Carbon Dioxide	0.10 vol%
Water	10 ppm by wt.	Ethane	0.30 vol%
		Nitrogen	0.30 wt%
		Water	10 ppm by wt.

TABLE II

Typical Physical Properties of Test Fuels

	<u>RP-1</u>	<u>JP-7</u>	<u>Chemically Pure Propane</u>	<u>Commercial Propane</u>
Molecular weight	167	175	44.1	44.7
Freezing point, deg K	< 235	250	85	< 135
Mean boiling point (MBP), deg K	484	490	231	233
ASTM distillation, deg K				
IBP	459	461	--	--
10%	469	476	--	--
50%	484	489	--	--
90%	508	513	--	--
FBP	529	534	--	--
Specific gravity @ 289K	0.801	0.803	0.508	0.513
Critical temperature, deg K	666	670	370	370
Critical pressure, atm	21.7	20.8	42.0	41.9
Critical volume, cm ³ /gm	2.06	4.18	4.62	4.24
Heat of vaporization @ MBP, cal/gm	56.5	62.1	102	102
Heat of fusion, cal/gm	--	--	19.2	--
Heat of formation, cal/gm	-440	-430	-664	-620
Heat of combustion, cal/gm	10457	10486	11054	11045
Autoignition temperature, deg K	523	--	741	--
Flammability limits in air, vol. %	--	--	2.2-9.5	2.2-9.5
Flash point, deg K	337	336	--	--
Specific heat @ 298K, cal/gm-k	.477	.484	0.785	0.780
Thermal conductivity @ 298K, milliwatts/cm ² -k/cm	0.880	0.770	0.090	0.093
Viscosity @ 298K, centipoise	1.56	1.47	0.12	0.13
Vapor pressure @ 311K, atm	4.1x10 ⁻⁴	3.4x10 ⁻⁴	12.6	12.3

TABLE III

Temperature Dependence of Selected Physical Properties of RP-1 and JP-7

Temperature Deg K	RP-1					JP-7				
	Specific Heat Cal/gm-K	Density gm/cc	Vapor Pressure atm	Viscosity Centipoise	Thermal Conductivity mW/cm ² -K per cm	Specific Heat Cal/gm-K	Density gm/cc	Vapor Pressure atm	Viscosity Centipoise	Thermal Conductivity mW/cm ² -K per cm
300	0.477	0.801	1.00×10^{-4}	1.563	0.885	0.484	0.803	8.85×10^{-5}	1.468	0.777
325	0.503	0.782	9.66×10^{-4}	1.087	0.911	0.510	0.786	8.51×10^{-4}	1.091	0.800
350	0.527	0.763	5.87×10^{-3}	0.752	0.942	0.534	0.769	5.17×10^{-3}	0.798	0.827
375	0.563	0.744	0.016	0.542	0.967	0.560	0.750	0.014	0.579	0.848
400	0.577	0.724	0.048	0.426	0.974	0.586	0.727	0.042	0.442	0.855
425	0.603	0.704	0.127	0.351	0.982	0.612	0.702	0.112	0.355	0.862
450	0.628	0.682	0.297	0.298	0.971	0.637	0.681	0.262	0.285	0.853
475	0.653	0.660	0.653	0.256	0.958	0.663	0.655	0.575	0.235	0.841
500	0.679	0.637	1.251	0.223	0.942	0.687	0.631	1.102	0.199	0.827
525	0.705	0.612	2.124	0.190	0.922	0.717	0.606	1.871	0.167	0.810
550	0.732	0.583	3.330	0.174	0.898	0.740	0.577	2.934	0.142	0.788
575	0.758	0.552	5.261	0.157	0.871	0.767	0.551	4.635	0.121	0.765
600	0.784	0.515	7.963	0.136	0.837	0.793	0.513	7.016	0.101	0.735
625	0.812	0.472	11.59	0.121	0.798	0.822	0.468	10.21	0.086	0.701
650	0.837	0.405	16.61	0.104	0.730	0.848	0.404	14.63	0.069	0.641

TABLE IV
Selected Physical Properties of Propane at Saturation

Temperature	Commercial						Chemically-Pure					
	Specific Heat	Density	Vapor Pressure	Viscosity	Thermal Conductivity		Specific Heat	Density	Vapor Pressure	Viscosity	Thermal Conductivity	
Deg K	Cal/gm-K	gm/cc	atm	Centipoise	mW/cm ² -K per cm		Cal/gm-K	gm/cc	atm	Centipoise	mW/cm ² -K per cm	
100	0.462	0.751	2.00 x 10 ⁻⁷	6.00	2.47		0.460	0.745	2.36 x 10 ⁻⁷	3.60	2.45	
120	0.467	0.707	2.52 x 10 ⁻⁵	1.810	2.21		0.466	0.701	2.95 x 10 ⁻⁵	1.48	2.19	
140	0.474	0.684	6.51 x 10 ⁻⁴	0.860	2.03		0.474	0.678	7.60 x 10 ⁻⁴	0.841	1.98	
160	0.482	0.664	7.00 x 10 ⁻³	0.549	1.86		0.482	0.658	8.14 x 10 ⁻³	0.532	1.83	
180	0.492	0.644	4.26 x 10 ⁻²	0.387	1.68		0.493	0.637	4.88 x 10 ⁻²	0.374	1.66	
200	0.504	0.622	0.174	0.290	1.53		0.506	0.615	0.197	0.281	1.50	
220	0.520	0.602	0.536	0.225	1.39		0.522	0.593	0.595	0.219	1.36	
240	0.575	0.578	1.337	0.180	1.25		0.572	0.570	1.461	0.176	1.23	
260	0.630	0.552	2.854	0.145	1.13		0.632	0.546	3.071	0.143	1.11	
280	0.702	0.527	5.390	0.119	1.02		0.705	0.519	5.752	0.117	1.00	
300	0.789	0.497	9.296	0.099	0.94		0.792	0.489	9.866	0.095	0.91	
320	0.919	0.461	14.93	0.081	0.85		0.922	0.446	15.82	0.077	0.82	
340	1.115	0.419	22.75	0.063	0.77		1.120	0.412	24.04	0.060	0.73	
360	---	0.351	41.52	0.043	0.67		---	0.345	35.08	0.042	0.66	

TABLE V

Certified Analyses of RP-1 and JP-7 Fuels

	<u>RP-1</u>	<u>JP-7</u>	<u>RP-1</u>	<u>JP-7</u>
Distillation, °K				
Initial boiling point	459	473	<.05	<.05
10% evaporated	469	479	<.05	<.05
20% evaporated	473	483	0.52	0.60
50% evaporated	484	485	0.2	0
90% evaporated	508	502	337	343
Final boiling point	527	519	<235	224
Residue, vol%	1.38	1.0	11.3 @ 239K	5.4 @ 253K
Loss, vol%	0.62	1.0	10384	10396
Gravity, °API	43.9	44.9	--	76.6
Aromatics, vol%	1.26	3.9	--	137
Olefins, vol%	0.48	2.02	--	2275
Naphthalenes, vol%	0.05	0.05	--	633
Total sulfur, wt%	0.014	.006	--	0
Mercaptan sulfur, wt%	--	.005	--	6
Nitrogen, wt%	<.001	0.037	1A	1B
Total water, ppm by wt	30.5	19.	--	.128
Iron, ppm by wt	0.4	0.8	--	3.8
Copper, ppm by wt	<.01	<.01	--	
Lead, ppm by wt	<.03	<.03	--	
Cobalt, ppm by wt	<.03	<.03	--	225
Cadmium, ppm by wt	<.03	<.03	--	1.4
Nickel, ppm by wt				
Vanadium, ppm by wt				
Existent gum, mg/100 ml				
Particulate matter, mg/l				
Flash point, °K				
Freezing point, °K				
Viscosity, cs				
Net heating value, cal/gm				
Luminometer no.				
Vapor pressure, mm Hg @ 422K				
Vapor pressure, mm Hg @ 533K				
JFTOT thermal stability				
Temperature, °K				
Pressure drop, mmHg in 5 hrs				
Preheater deposit, TDR				
Copper strip corrosion				
Additives				
Fuel system icing inhibitor, % vol				
2,6-ditertiary-butyl-4-methyl phenol, kg/1000 bb1s				
PWA 536, ppm				
Total potential residue, mg/100 ml				

TABLE VI

Typical Chemical Properties of Propane

Typical Analysis, Vol %	Commercial	Chemically Pure
Propane	> 90.0	99.39
Propylene	< 5.0	0.01
Ethane	} < 5.0	0.05
N-Butane		0.05
I-Butane		0.50
Sulfur, Wt %	< .015	<.005

TABLE VII

Summary of Test Conditions for Kerosene Fuels

Pressure = 136 atm

<u>Run No.</u>	<u>Wall Temp.</u> deg K	<u>Velocity</u> m/sec	<u>Test Duration</u> min
RP-1 Fuel			
1	422	7.2	10
2	589	7.2	10
3	700	7.2	10
4	811	7.2	1
5	589	14.4	10
6	700	14.4	10
7	811	14.4	10
8	811	21.6	9
9	811	7.2	10
10	700	21.6	10
11	589	21.6	10
12	700	28.8	8
13*	Varied	Varied	-
14	811	7.2	10
15	811	24.4	1
16	811	24.4	6
17	589	24.4	8
18	589	30.5	10
19	700	30.1	10
20	811	30.1	10
21	700	24.4	10
22	589	24.4	10
23†	Varied	6.1	-
JP-7 Fuel			
24	700	6.1	9
25	811	6.1	10
26	811	18.3	10
27	700	18.3	20
28	811	30.5	10
29	700	30.5	12
30	811	12.2	7
31	589	18.3	10
32	700	30.5	10

*Calibration Run

†NASA tube

TABLE VIII

Deposit Burnoff Data for RP-1 Fuel

Run-Section	Run Time min	Velocity m/sec	Initial Wall Temperature Deg K	Section Surface Area cm ²	Deposit Weight mg	Deposit Rate $\mu\text{g}/\text{cm}^2\text{-hr}$	Average Wall Temperature Deg K	Average Deposit Rate $\mu\text{g}/\text{cm}^2\text{-hr}$
2 - A B C D	10	7.2	601	2.74	.295	647	572	630
			613	2.68	--	--		
			545	2.68	.292	655		
			530	2.68	.262	588		
3 - A B C D	10	7.2	672	2.60	.287	662	628	446
			661	2.74	--	--		
			605	2.77	.207	393		
			572	2.77	.131	284		
5 - A B C D	10	14.6	573	2.64	.217	493	550	429
			568	2.70	.226	502		
			534	2.64	.121	275		
			526	2.70	.200	446		
6 - A B C D	10	14.6	685	2.70	.109	244	634	523
			633	2.75	.241	526		
			616	2.72	.362	799		
			603	2.77	--	--		
7 - A B C D	10	14.6	800	2.77	.061	130	716	186
			711	2.64	.099	226		
			686	2.72	.070	161		
			666	2.77	.102	225		
10 - A B C D	10	21.6	694	2.70	.162	362	662	314
			661	2.64	.107	244		
			650	2.64	.163	371		
			642	2.64	.122	277		

TABLE VIII
(Continued)

Run-Section	Run Time min	Velocity m/sec	Initial Wall Temperature Deg K	Section Surface Area cm ²	Deposit Weight mg	Deposit Rate µg/cm ² -hr	Average Wall Temperature Deg K	Average Deposit Rate µg/cm ² -hr
12 - A	8	28.8	655	2.70	.057	269	634	320
B			627	2.66	.124	350		
C			623	2.64	.119	339		
D			633	2.72	.117	322		
14 - A	10	7.2	822	2.77	.083	180	726	186
B			744	2.72	.087	193		
C			686	2.66	.094	212		
D			650	2.74	.074	161		
16 - A	6	24.5	801	2.79	.137	502	770	355
B			769	2.70	.080	304		
C			755	2.75	.097	360		
D			753	2.68	.067	255		
18 - A	10	30.5	569	2.79	.099	212	560	188
B			557	2.64	.084	192		
C			561	2.74	.067	147		
D			554	2.74	.091	200		
19 - A	10	30.1	661	2.81	.098	207	634	241
B			630	2.72	.111	246		
C			619	2.77	.112	243		
D			625	2.79	.124	267		
20 - A	10	30.1	766	2.77	.098	191	734	371
B			733	2.82	.266	564		
C			716	2.82	.169	358		
D			722	2.79	--	--		

TABLE VIII
(Continued)

Run-Section	Run Time min	Velocity m/sec	Initial Wall Temperature Deg K	Section Surface Area cm ²	Deposit Weight mg	Deposit Rate μg/cm ² -hr	Average Wall Temperature Deg K	Average Deposit Rate μg/cm ² -hr
21 - A B C D	10	24.4	648	2.83	.192	408	631	474
			633	2.75	.272	592		
			623	2.83	.222	471		
			620	2.74	.194	425		
22 - A B C D	10	24.4	574	2.74	.277	607	557	366
			558	2.70	.091	201		
			550	2.75	.112	243		
			545	2.70	.186	413		

TABLE IX

Results of JFTOT* Evaluation

Fuel	Temperature	Pressure Drop	Deposit Rating	
	Deg K	mm Hg	Visual	TDR
JP-7 Spec.	633	25	< 3	< 12
JP-7	628	0	1	5
JP-7	633	0	1	6
JP-7	638	0	3	12
RP-1	628	0	1	2
RP-1	638	0	1	4
RP-1	648	0	1	6
RP-1	653	0	1	7

*ASTM D3241-27 - Standard Test Method for Thermal Oxidation Stability of Aviation Turbine Fuel (JFTOT Procedure)

TABLE X

Deposit Burnoff Data for
JP-7 Fuel

Run-Section	Run Time min	Velocity m/sec	Initial Wall Temperature Deg K	Section Surface Area cm ²	Deposit Weight mg	Deposit Rate $\mu\text{g}/\text{cm}^2\text{-hr}$	Average Wall Temperature Deg K	Average Deposit Rate $\mu\text{g}/\text{cm}^2\text{-hr}$
24 - A B C D	9	6.1	675	2.60	.152	389	616	470
			609	2.58	.270	698		
			603	2.83	.196	461		
			578	2.62	.130	332		
25 - A B C D	10	6.1	813	2.54	.141	332	719	464
			735	2.79	.129	278		
			676	2.62	.185	424		
			651	2.79	.381	820		
26 - A B C D	10	18.3	769	2.54	.106	251	725	267
			726	2.58	.114	264		
			703	2.54	.099	234		
			702	2.47	.131	319		
27 - A B C D	20	18.3	700	2.56	.099	116	664	172
			666	2.68	.149	171		
			650	2.60	.201	232		
			642	2.60	.144	167		
28 - A B C D	10	30.5	806	2.56	.135	315	771	451
			759	2.71	.288	636		
			759	2.66	.186	419		
			760	2.85	.187	435		
29 - A B C D	12	30.5	665	2.60	.119	233	656	378
			653	2.54	.111	222		
			653	2.54	.304	608		
			655	2.58	.227	447		

TABLE X
(Continued)

Run-Section	Run Time min	Velocity m/sec	Initial Wall Temperature Deg K	Section Surface Area cm ²	Deposit Weight mg	Deposit Rate $\mu\text{g}/\text{cm}^2\text{-hr}$	Average Wall Temperature Deg K	Average Deposit Rate $\mu\text{g}/\text{cm}^2\text{-hr}$
30 - A B C D	7	12.2	794	2.64	.129	420	715	408
			703	2.70	.071	226		
			675	2.70	.175	557		
			686	2.62	.131	429		
31 - A B C D	10	18.3	568	2.56	.177	414	557	345
			552	2.70	.145	322		
			550	2.64	.121	276		
			557	2.64	.162	368		
32 - A B C D	10	30.5	631	2.68	.162	364	620	352
			604	2.60	.167	386		
			606	2.64	.162	367		
			639	2.54	.123	289		

TABLE XI

Summary of Test Conditions for Propane Fuels

Pressure = 136 atm

<u>Run No.</u>	<u>Wall Temp.</u>	<u>Velocity</u>	<u>Test Duration</u>
	deg K	m/sec	min
Commercial-Grade Propane			
33	700	6.1	2
34	700	6.1	5
35	700	18.3	5
36	589	18.3	10
37	589	6.1	10
38	422	6.1	10
39	589	30.5	9
40	700	30.5	10
41	811	30.5	1
42	422	36.6	10
43	422	18.3	10
44	811	18.3	10
45	811	6.1	5
46	700	12.2	10
47	811	12.2	10
48	700	24.4	5
49	589	12.2	10
50	589	24.4	10
51	422	12.2	10
52	422	24.4	10
Chemically-Pure Propane			
53	589	6.1	10
54	422	6.1	10
55	589	18.3	10
56	589	30.5	10
57	422	30.5	10
58	422	18.5	10
59	700	6.1	8
60	580	6.1	3

TABLE XII

Deposit Burnoff Data for Propane
A. Commercial Grade Propane

Run-Section	Run Time min	Velocity m/sec	Initial Wall Temperature Deg K	Section Surface Area cm ²	Deposit Weight mg	Deposit Rate $\mu\text{g}/\text{cm}^2\text{-hr}$	Average Wall Temperature Deg K	Average Deposit Rate $\mu\text{g}/\text{cm}^2\text{-hr}$
33 - A B C D	2	6.1	511	2.60	.114	1755	586	2021
			543	2.68	.106	1581		
			624	2.62	.144	2191		
			666	2.68	.171	2556		
34 - A B C D	5	6.1	596	2.68	.194	850	638	738
			631	2.60	.156	704		
			653	2.60	.142	642		
			673	2.70	.174	758		
35 - A B C D	5	18.3	575	2.64	.115	582	582	661
			571	2.74	.144	700		
			577	2.54	.123	645		
			603	2.74	.147	717		
36 - A B C D	10	18.3	493	2.68	.166	373	530	518
			516	2.68	.212	474		
			541	2.58	.178	414		
			570	2.74	.369	809		
37 - A B C D	10	6.1	513	2.53	.152	361	556	306
			535	2.70	.193	429		
			553	2.64	.090	204		
			623	2.72	.105	231		
38 - A B C D	10	6.1	368	2.64	.181	411	391	450
			383	2.68	.209	468		
			387	2.60	.188	422		
			426	2.72	.226	500		

TABLE XII
(Continued)

Run-Section	Run Time min	Velocity m/sec	Initial Wall Temperature Deg K	Section Surface Area cm ²	Deposit Weight mg	Deposit Rate μg/cm ² -hr	Average Wall Temperature Deg K	Average Deposit Rate μg/cm ² -hr
39 - A B C D	9	30.5	489	2.66	.138	346	514	439
			498	2.74	.156	381		
			523	2.62	.190	482		
			548	2.77	.228	548		
40 - A B C D	10	30.5	593	2.75	.149	324	594	566
			583	2.66	.140	316		
			587	2.72	.279	617		
			612	2.77	.464	1005		
41 - A B C D	1	30.5	506	2.72	.127	2800	539	3462
			518	2.63	.126	2870		
			544	2.72	.175	3870		
			588	2.70	.194	4310		
42 - A B C D	10	36.6	380	2.64	.130	296	392	318
			385	2.66	.160	362		
			397	2.64	.105	238		
			408	2.63	.165	377		
43 - A B C D	10	18.3	379	2.71	.117	260	392	354
			385	2.73	.092	201		
			396	2.60	.062	142		
			408	2.83	.384	814		
44 - A B C D	10	18.3	661	2.70	.100	222	624	340
			600	2.58	.140	324		
			610	2.68	.126	282		
			624	2.71	.240	531		
45 - A B C D	5	6.1	619	2.68	.264	1185	675	920
			620	2.68	.141	630		
			674	2.60	.200	922		
			787	2.70	.213	943		

TABLE XII
(Continued)

Run-Section	Run Time min	Velocity m/sec	Initial Wall Temperature Deg K	Section Surface Area cm ²	Deposit Weight mg	Deposit Rate μg/cm ² -hr	Average Wall Temperature Deg K	Average Deposit Rate μg/cm ² -hr
46 - A B C D	10	12.2	659	2.68	.201	464	650	780
			681	2.70	.349	798		
			609	2.69	.455	1088		
			649	2.66	.330	770		
47 - A B C D	10	12.2	537	2.66	.360	811	569	733
			548	2.68	.263	529		
			565	2.58	.309	742		
			626	2.70	.337	851		
48 - A B C D	5	24.4	588	2.62	.401	1887	592	1272
			581	2.73	.183	826		
			584	2.60	.260	1231		
			615	2.68	.249	1145		
49 - A B C D	10	12.2	501	2.70	.259	576	519	571
			503	2.62	.196	450		
			521	2.64	.324	736		
			550	2.64	.229	522		
50 - A B C D	10	24.4	495	2.66	.263	593	539	616
			530	2.62	.269	617		
			560	2.60	.211	486		
			572	2.77	.356	770		
51 - A B C D	10	12.2	380	2.70	.182	404	393	424
			387	2.75	.186	406		
			396	2.70	.199	442		
			408	2.73	.203	443		
52 - A B C D	10	24.4	376	2.68	.255	572	389	454
			383	2.64	.241	549		
			393	2.71	.158	349		
			405	2.68	.155	348		

TABLE XII
(Continued)

B. Chemically Pure Propane

Run-Section	Run Time min	Velocity m/sec	Initial Wall Temperature Deg K	Section Surface Area cm ²	Deposit Weight mg	Deposit Rate $\mu\text{g}/\text{cm}^2\text{-hr}$	Average Wall Temperature Deg K	Average Deposit Rate $\mu\text{g}/\text{cm}^2\text{-hr}$
53 - A B C D	10	6.1	505	2.68	.147	329	533	352
			510	2.68	.114	255		
			543	2.71	--	--		
			575	2.68	.210	471		
54 - A B C D	10	6.1	384	2.64	.172	391	398	440
			391	2.68	.154	345		
			401	2.62	.234	537		
			416	2.68	.218	488		
55 - A B C D	10	18.3	501	2.64	.170	386	532	491
			511	2.68	.146	327		
			543	2.56	.243	570		
			575	2.75	.308	680		
56 - A B C D	10	30.5	491	2.71	.178	393	522	452
			509	2.68	.151	378		
			530	2.64	--	--		
			558	2.68	.260	584		
57 - A B C D	10	30.5	391	2.62	.178	389	410	381
			411	2.71	.2097	461		
			414	2.60	.113	260		
			422	2.64	.182	414		
58 - A B C D	10	18.3	380	2.75	.154	335	394	381
			385	2.66	.150	338		
			400	2.71	.148	327		
			412	2.71	.236	522		

TABLE XII
(Continued)

Run-Section	Run Time min	Velocity m/sec	Initial Wall Temperature Deg K	Section Surface Area cm ²	Deposit Weight mg	Deposit Rate $\mu\text{g}/\text{cm}^2\text{-hr}$	Average Wall Temperature Deg K	Average Deposit Rate $\mu\text{g}/\text{cm}^2\text{-hr}$
59 - A B C D	8	6.1	554	2.66	.217	613	596	636
			585	2.71	.251	692		
			620	2.62	.268	615		
			624	2.68	.277	622		
60 - A B C D	3	6.1	518	2.64	.097	735	549	918
			529	2.73	.057	417		
			564	2.71	.186	1368		
			584	2.71	.156	1150		

TABLE XIII

Summary of Test Conditions for High Pressure and Nickel-Plated Tubes

RP-1

<u>Run No.</u>	<u>Wall Temp.</u>	<u>Velocity</u>	<u>Pressure</u>	<u>Test Duration</u>
	deg K	m/sec	atm	min
High Pressure Tests				
61	700	18.3	204	10
62	700	18.3	272	10
63	700	18.3	272	6
64	700	18.3	136	10
65	700	18.3	136	10
66	700	18.3	340	9
Nickel-Plated Tubes				
67	700	18.3	136	10
68	811	18.3	136	3
69	589	18.3	136	10
70	700	6.1	136	10
71	589	6.1	136	10

TABLE XIV

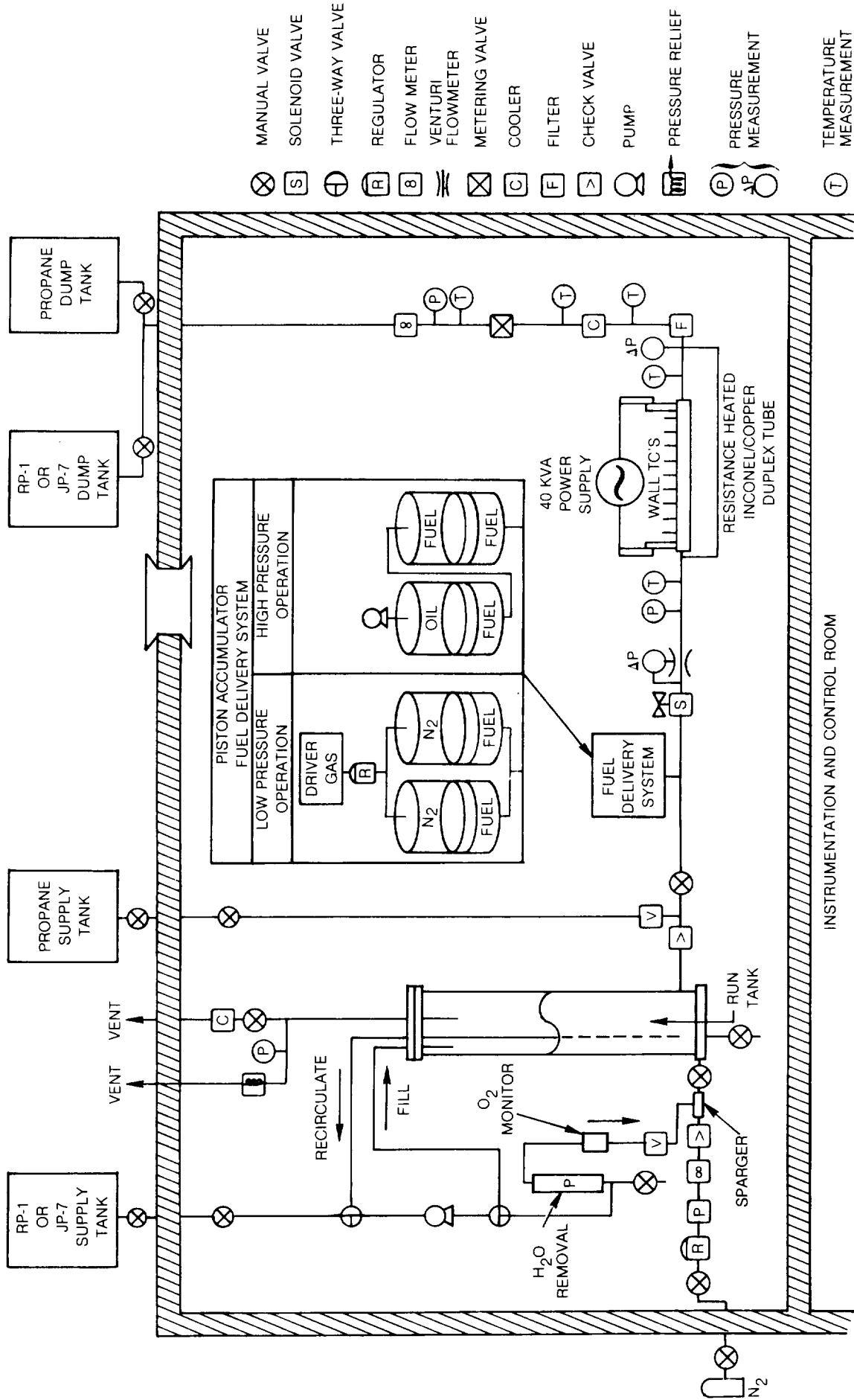
Deposit Burnoff Data for
High Pressure Tests
Velocity = 18.3 m/sec

Run-Section	Run Time min	Pressure atm	Initial Wall Temperature Deg K	Section Surface Area cm ²	Deposit Weight mg	Deposit Rate $\mu\text{g}/\text{cm}^2\text{-hr}$	Average Wall Temperature Deg K	Average Deposit Rate $\mu\text{g}/\text{cm}^2\text{-hr}$
61 - A B C D	10	204	615	2.71	.246	544	616	483
			623	2.68	.293	657		
			615	2.68	--	--		
			609	2.77	.1158	249		
62 - A B C D	10	272	611	2.71	.311	688	480	631
			613	2.70	.310	691		
			647	2.70	--	--		
			598	2.79	.240	516		
63 - A B C D	6	272	626	2.70	.224	830	607	752
			603	2.73	.206	756		
			615	2.68	.218	805		
			584	2.68	.165	615		
64 - A B C D	10	136	645	2.64	.208	473	615	440
			614	2.52	.157	373		
			603	2.70	.192	428		
			598	2.70	.218	484		
65 - A B C D	10	136	676	2.58	.274	638	650	466
			649	2.70	.161	358		
			638	2.64	--	--		
			636	2.64	.177	402		
66 - A B C D	9	340	681	2.77	.173	417	629	533
			626	2.70	.211	517		
			618	2.70	.269	666		
			590	2.73	--	--		

TABLE XV

Deposit Burnoff Data for
Nickel-Plated Tube Tests

Run-Section	Run Time min	Velocity m/sec	Initial Wall Temperature Deg K	Section Surface Area cm ²	Deposit Weight mg	Deposit Rate $\mu\text{g}/\text{cm}^2\text{-hr}$	Average Wall Temperature Deg K	Average Deposit Rate $\mu\text{g}/\text{cm}^2\text{-hr}$
67 - A B C D	10	18.3	661	2.64	.036	82	650	44
			683	2.69	.017	38		
			644	2.69	< .01	< 20		
			614	2.75	< .01	< 20		
69 - A B C D	10	18.3	594	2.62	< .01	< 20	590	77
			583	2.71	< .01	< 20		
			589	2.64	.039	89		
			594	2.67	.079	178		
70 - A B C D	10	6.1	672	2.60	--	--	640	56
			680	2.62	.047	108		
			612	2.60	.017	39		
			497	2.62	< .01	< 20		
71 - A B C D	10	6.1	555	2.54	.044	104	561	41
			605	2.59	< .01	< 20		
			561	2.60	< .01	< 20		
			523	2.58	< .01	< 20		



- MANUAL VALVE
- SOLENOID VALVE
- THREE-WAY VALVE
- REGULATOR
- FLOW METER
- VENTURI FLOWMETER
- METERING VALVE
- COOLER
- FILTER
- CHECK VALVE
- PUMP
- PRESSURE RELIEF
- PRESSURE MEASUREMENT
- TEMPERATURE MEASUREMENT

Figure 1. Deposit Formation of Hydrocarbon Rocket Fuels Test Apparatus

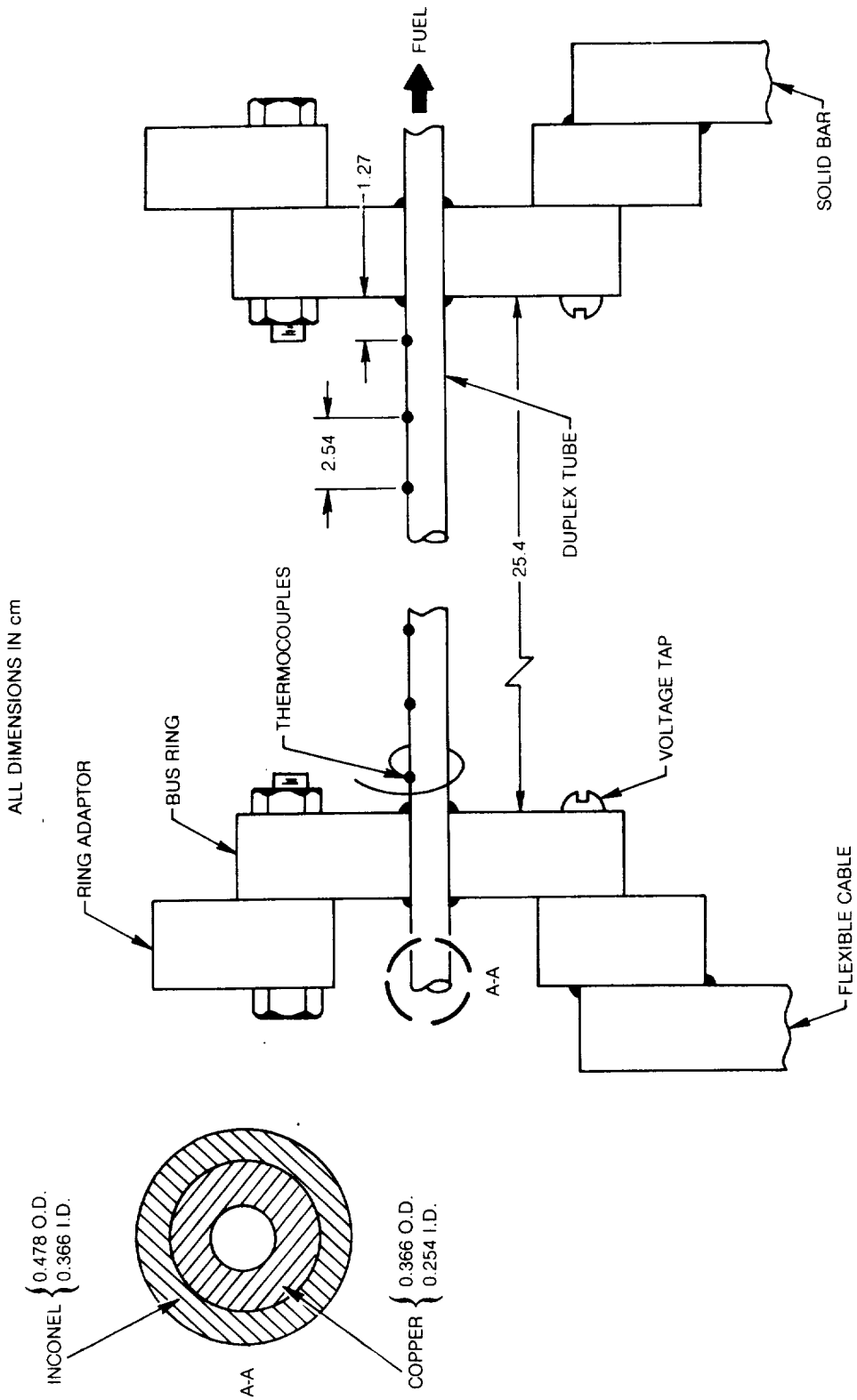


Figure 2. Test Tube Assembly

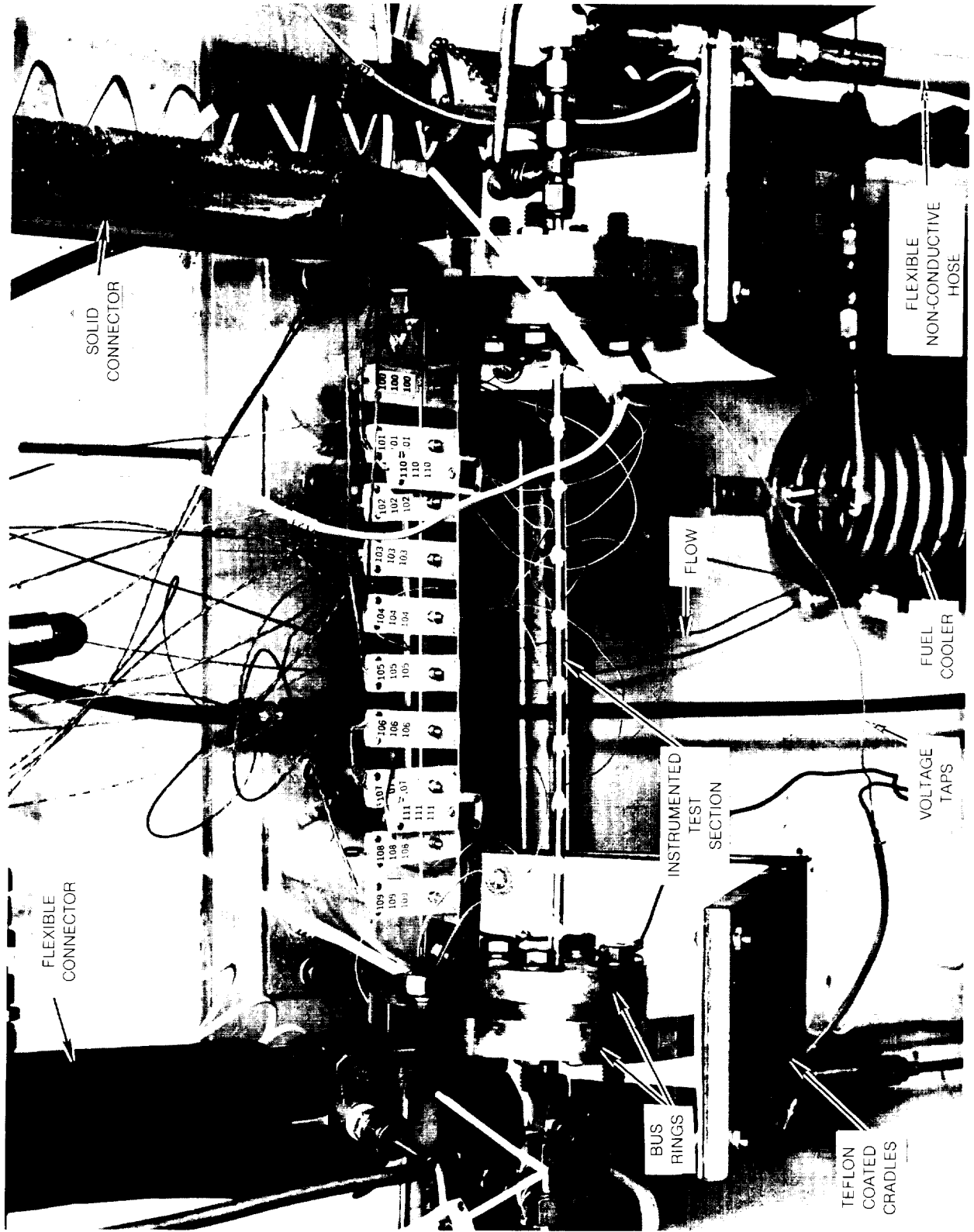


Figure 3. Test Tube Assembly

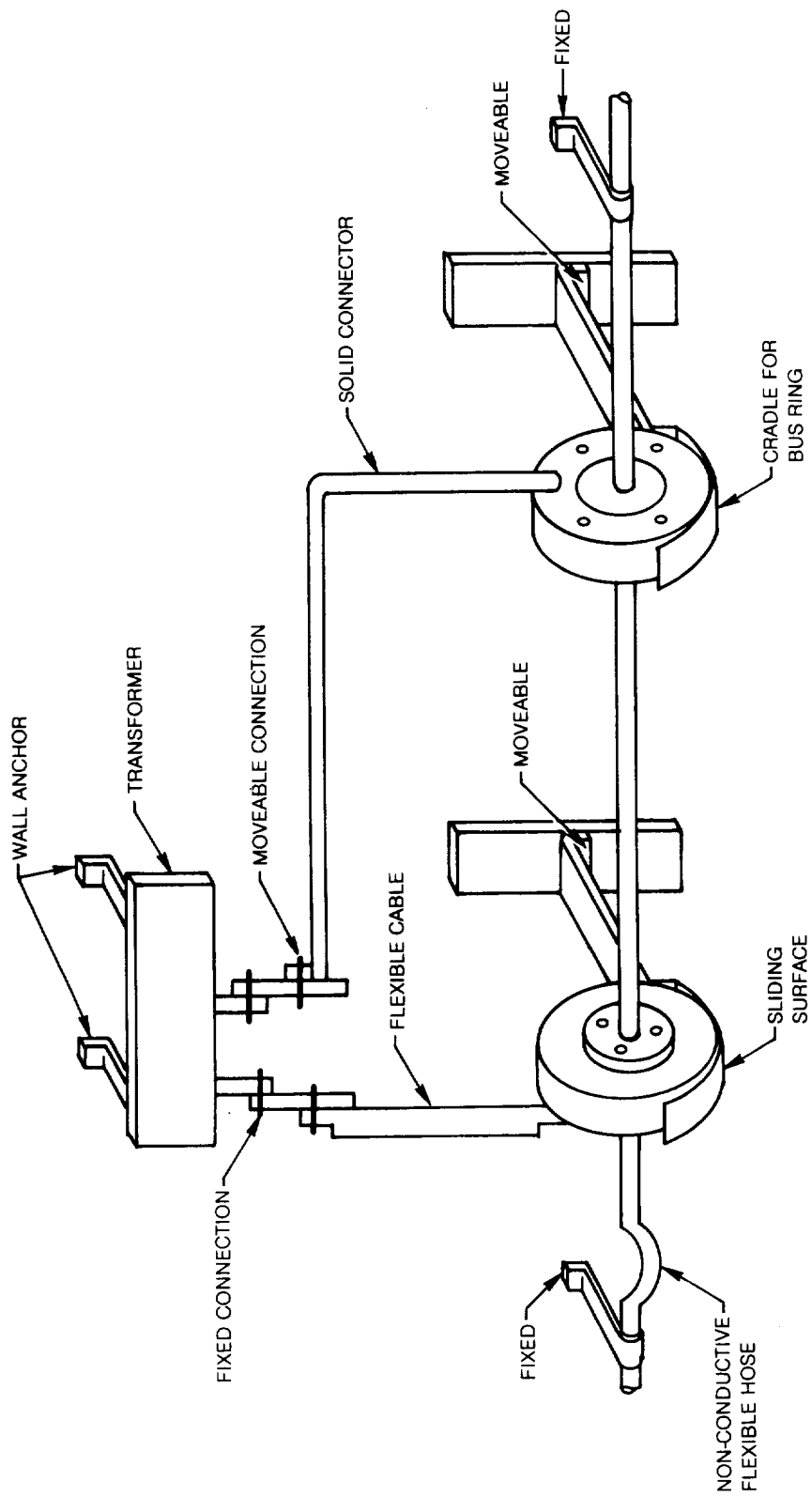


Figure 4. Test Section Mounting

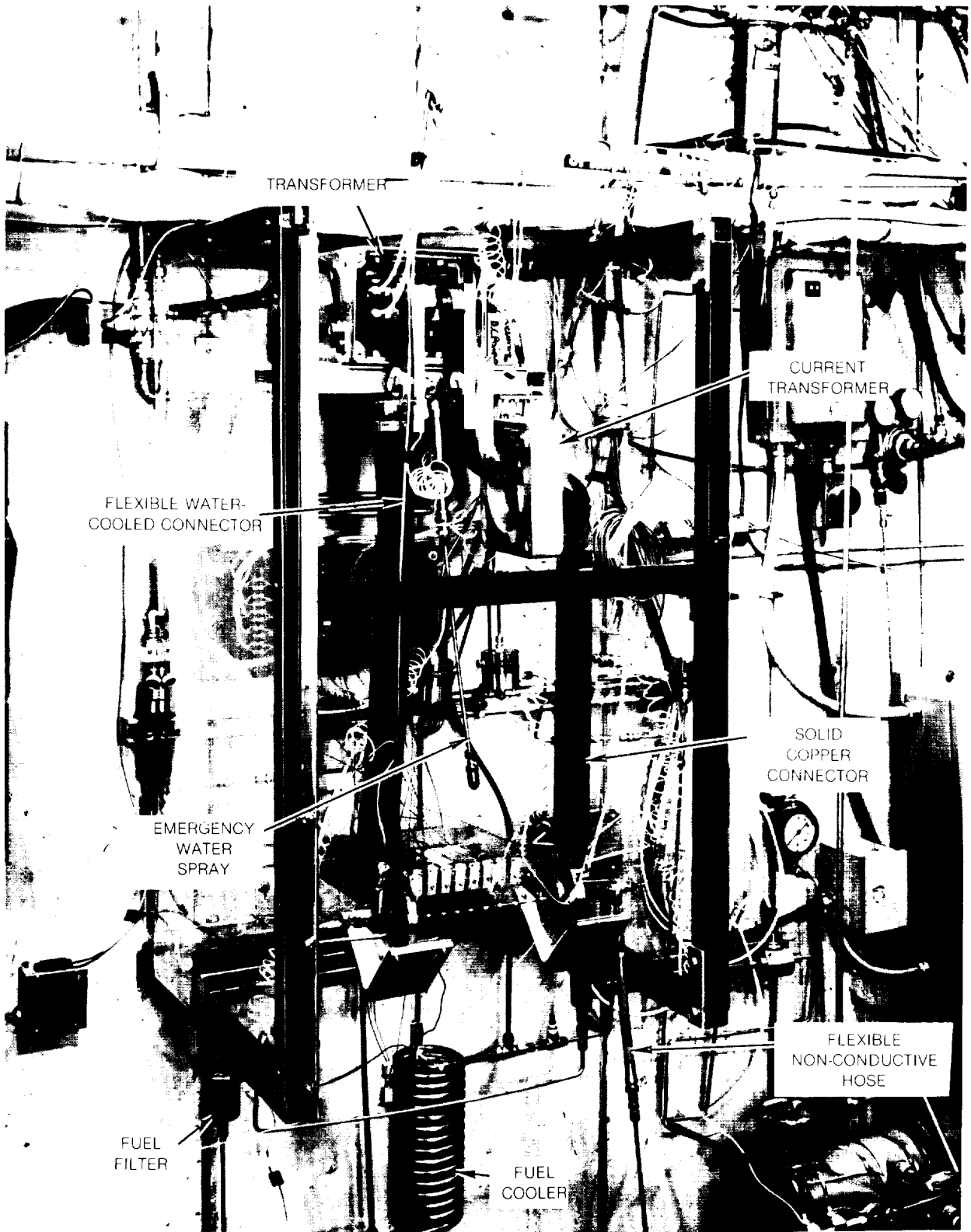


Figure 5. Test Section Installation

RP-1 FUEL
V = 30.5 m/sec
P = 136 atm
 $T_w = 811\text{K}$

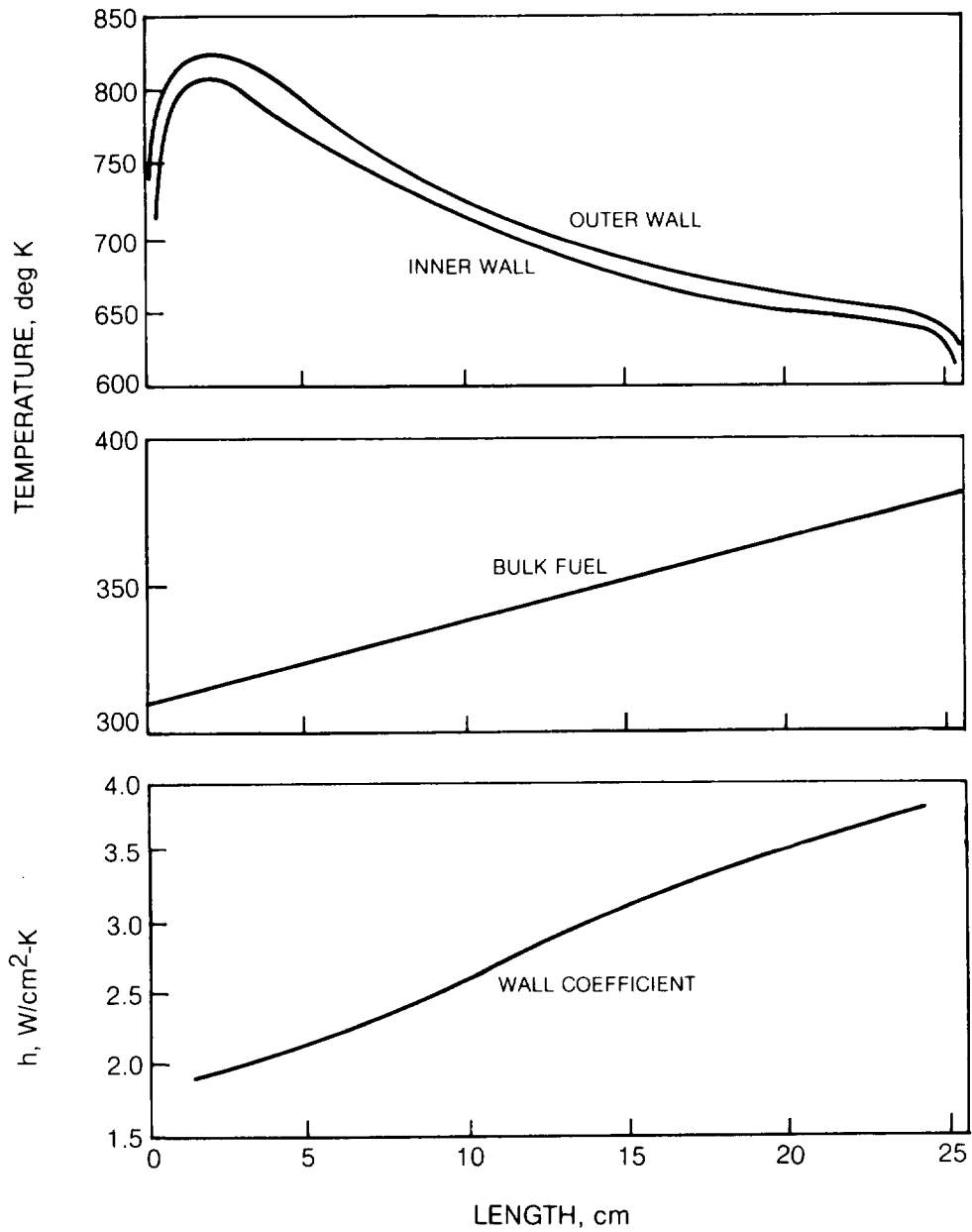


Figure 7. Axial Variation of Temperature and Heat Transfer

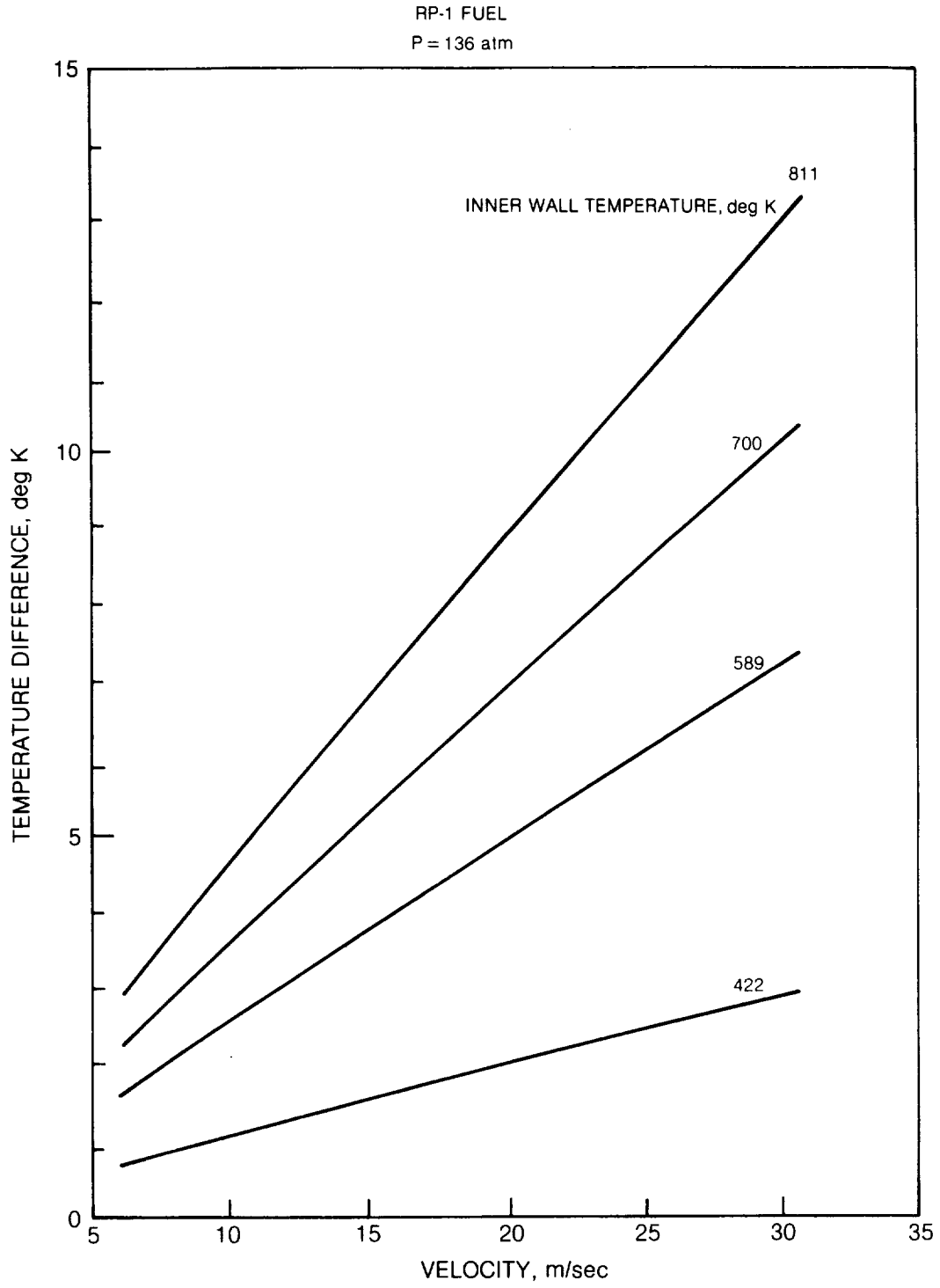


Figure 8. Temperature Difference Between Tube Outer and Inner Walls

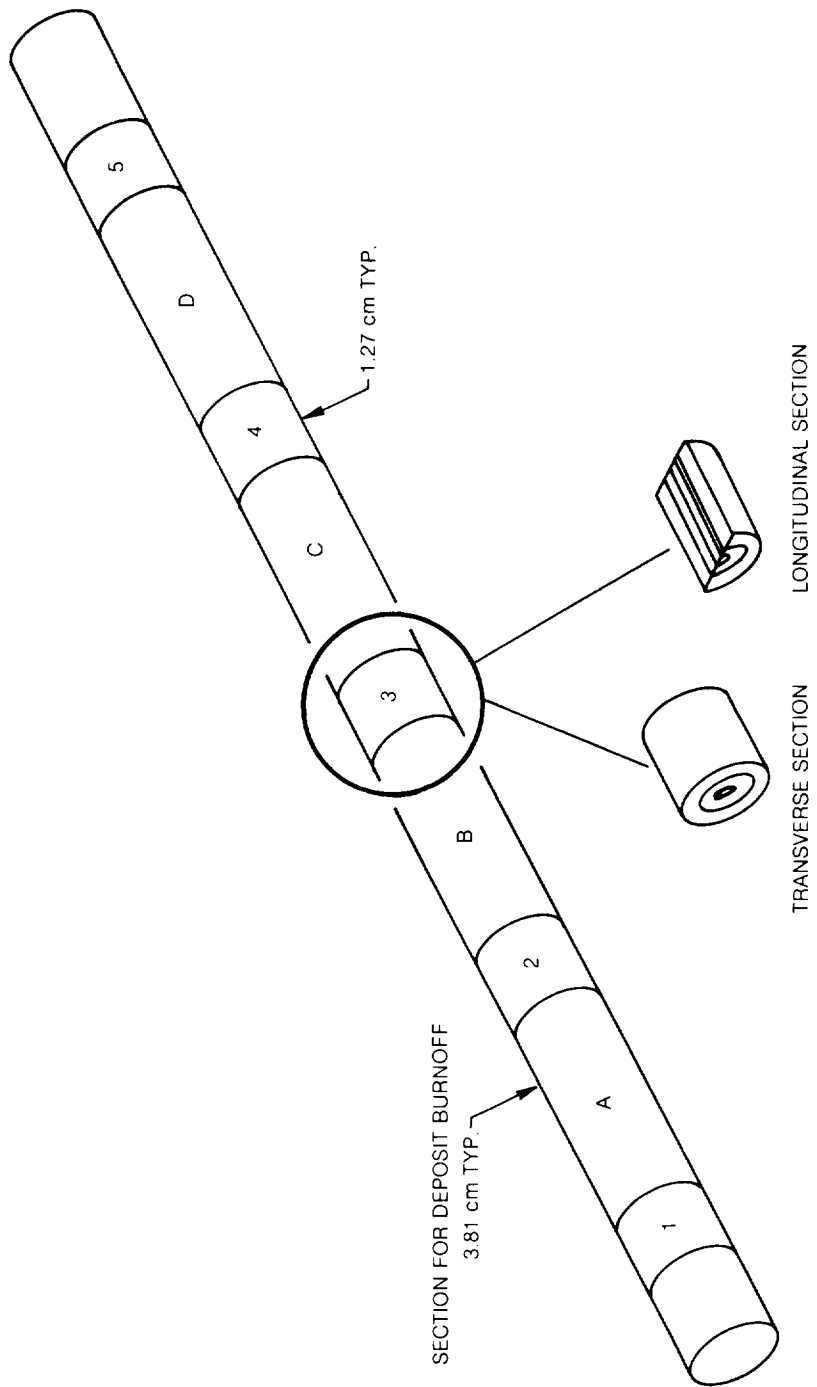


Figure 9. Tube Sectioning

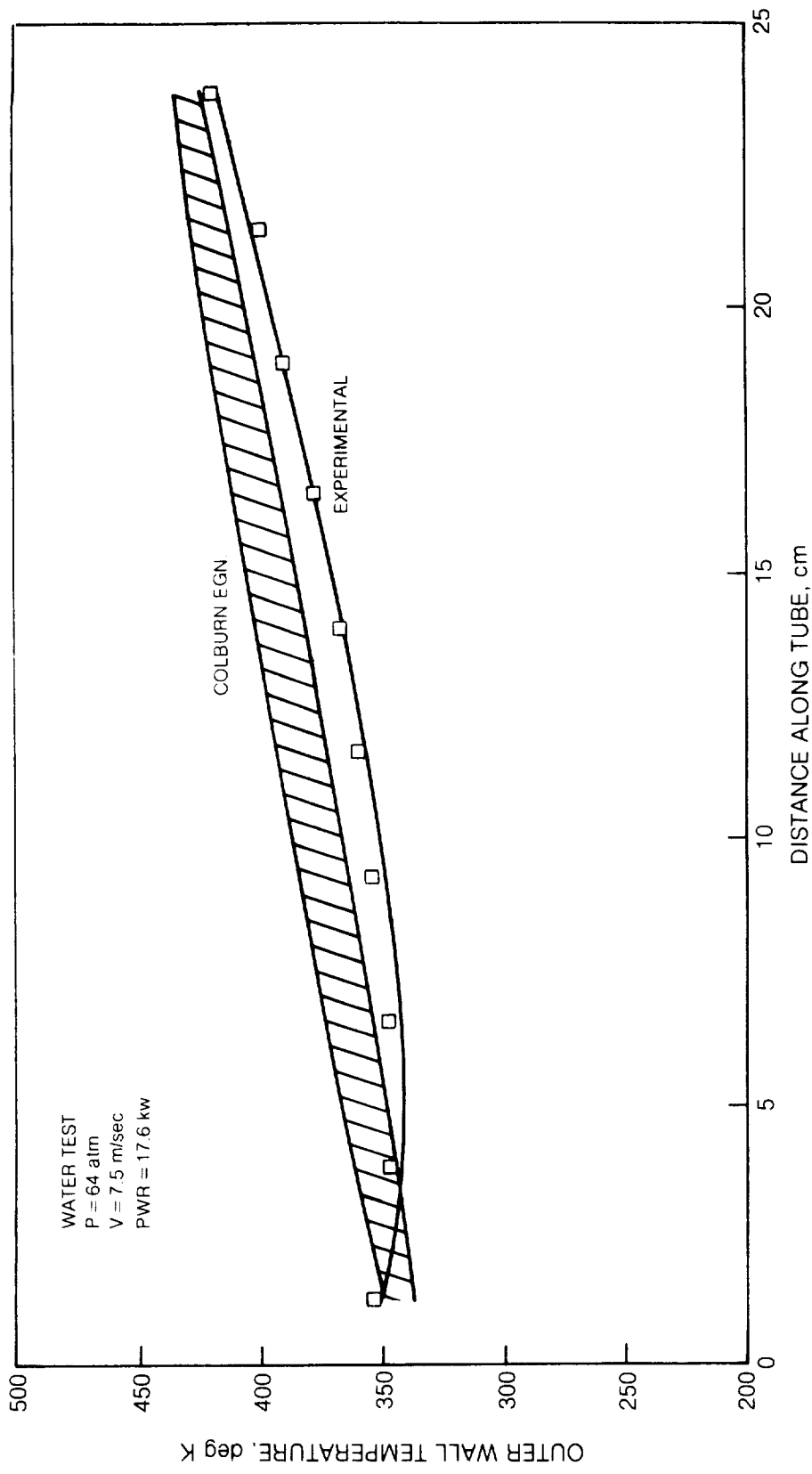


Figure 10. Comparison of TCAL Predictions with Experimental Data

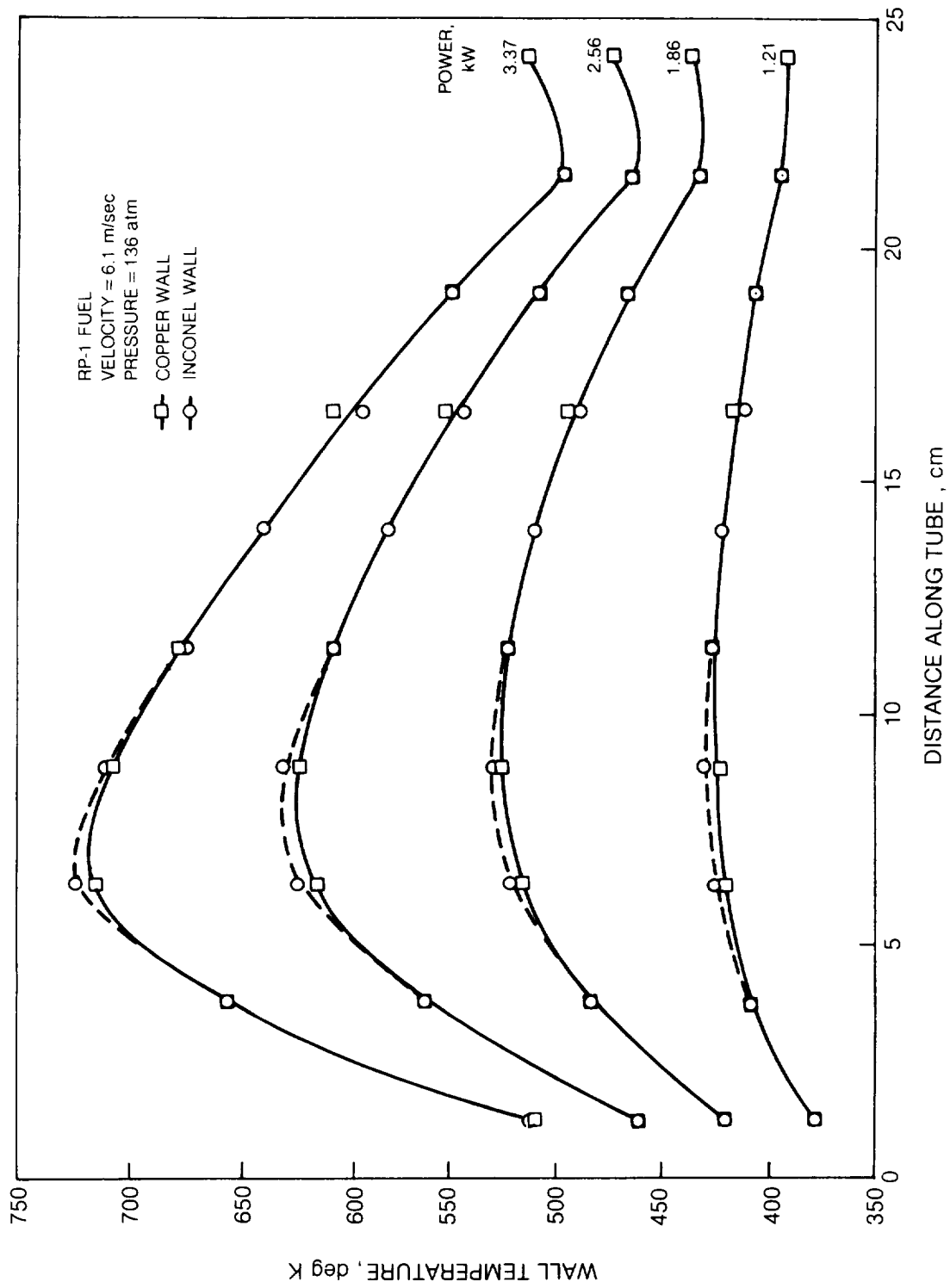


Figure 11. Calibration Tube Temperature Distributions

RP-1 FUEL
P = 136 atm

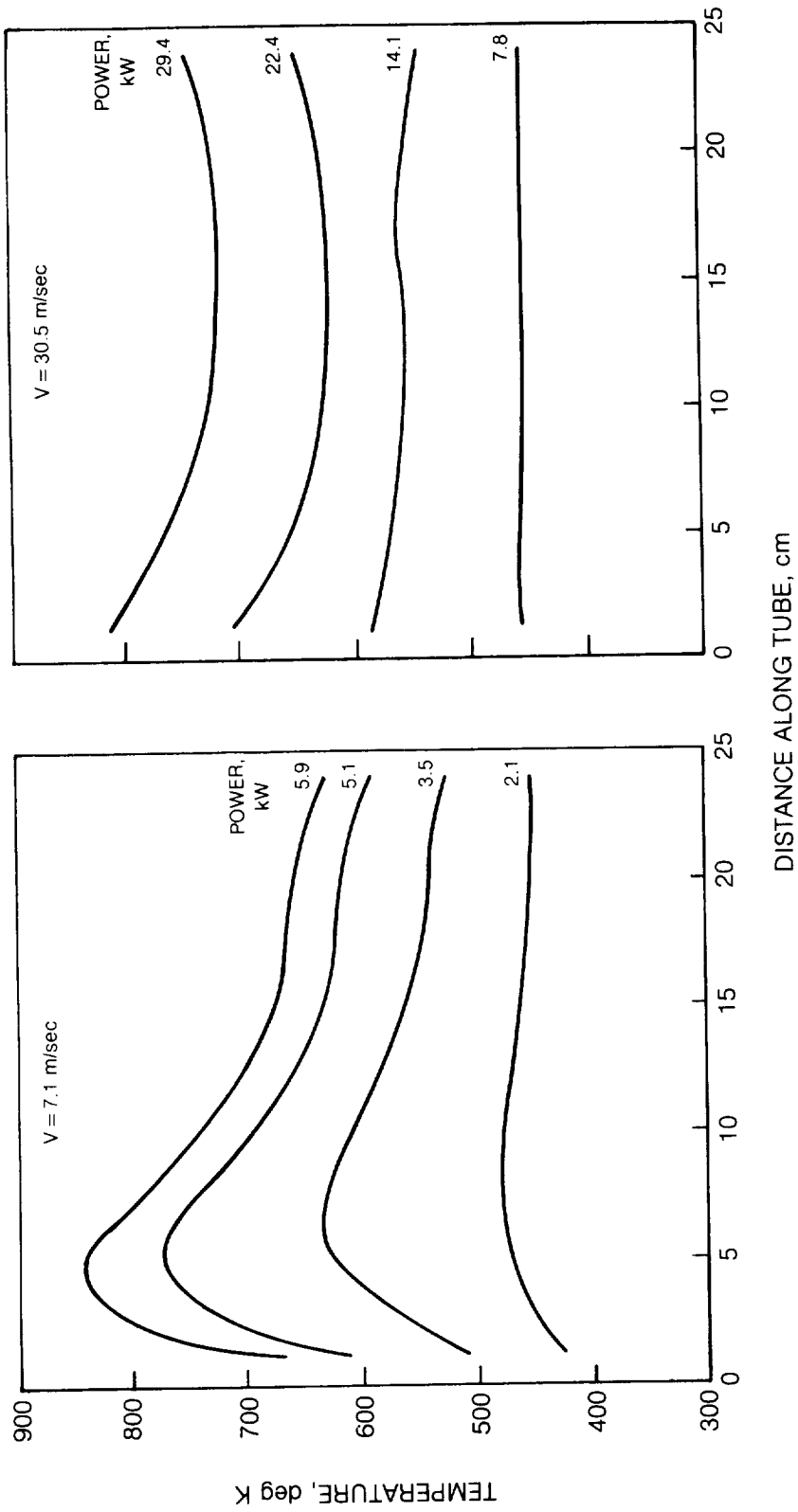


Figure 12. Variation of Axial Wall Temperature with Power

RP-1 FUEL
P = 136 atm
v = 18.3 m/sec

- EXPERIMENTAL DATA (RUN 13)
- - - DITTUS-BOELTER EQN (REF. 45)
- SIEDER-TATE EQN (REF. 45)
- ROCKETDYNE EQN (REF. 47)

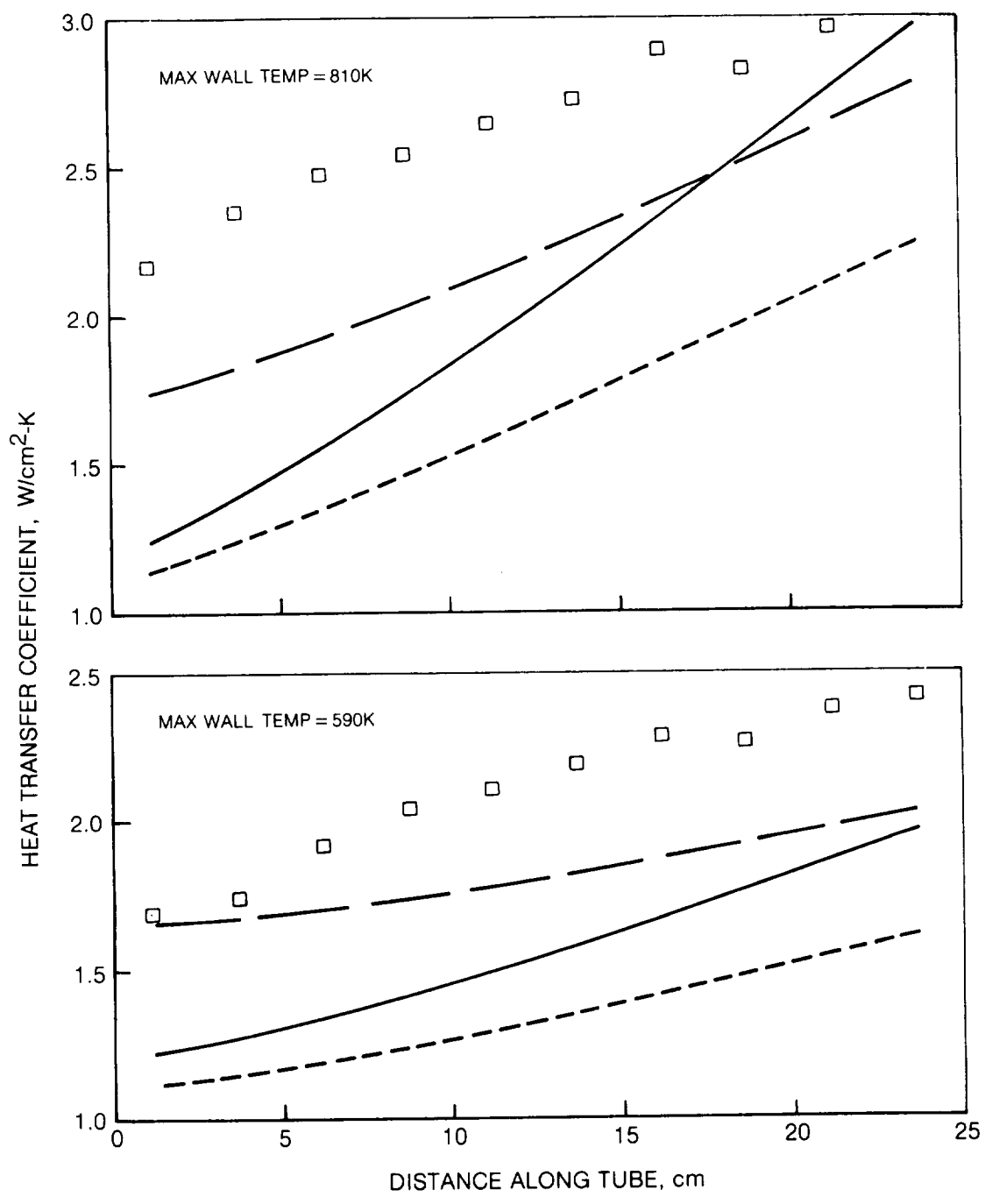


Figure 13. Variation of Heat Transfer Coefficient with Tube Length

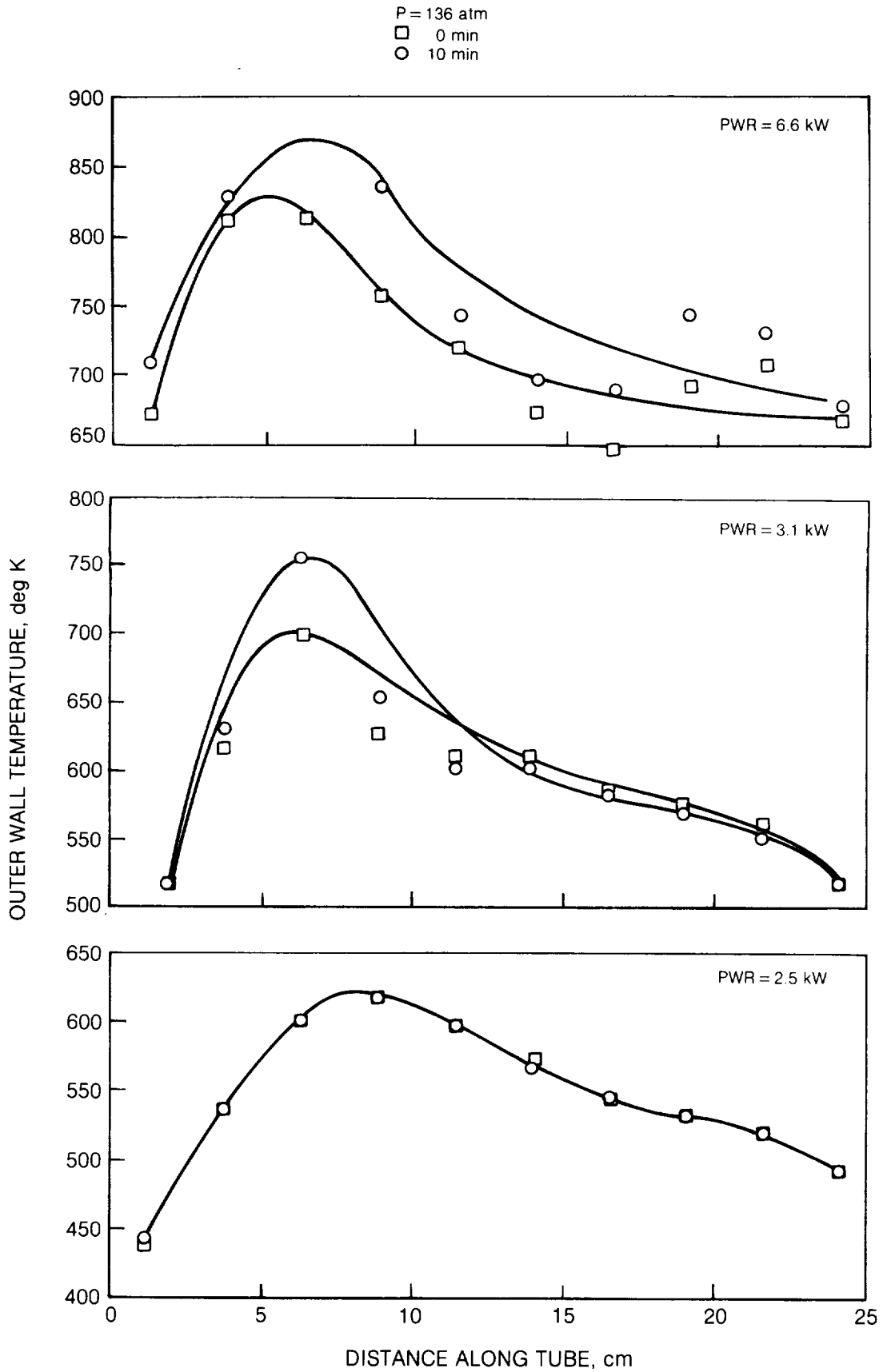


Figure 14. Axial Wall Temperature Variation for RP-1 Fuel, V = 7.3 m/sec

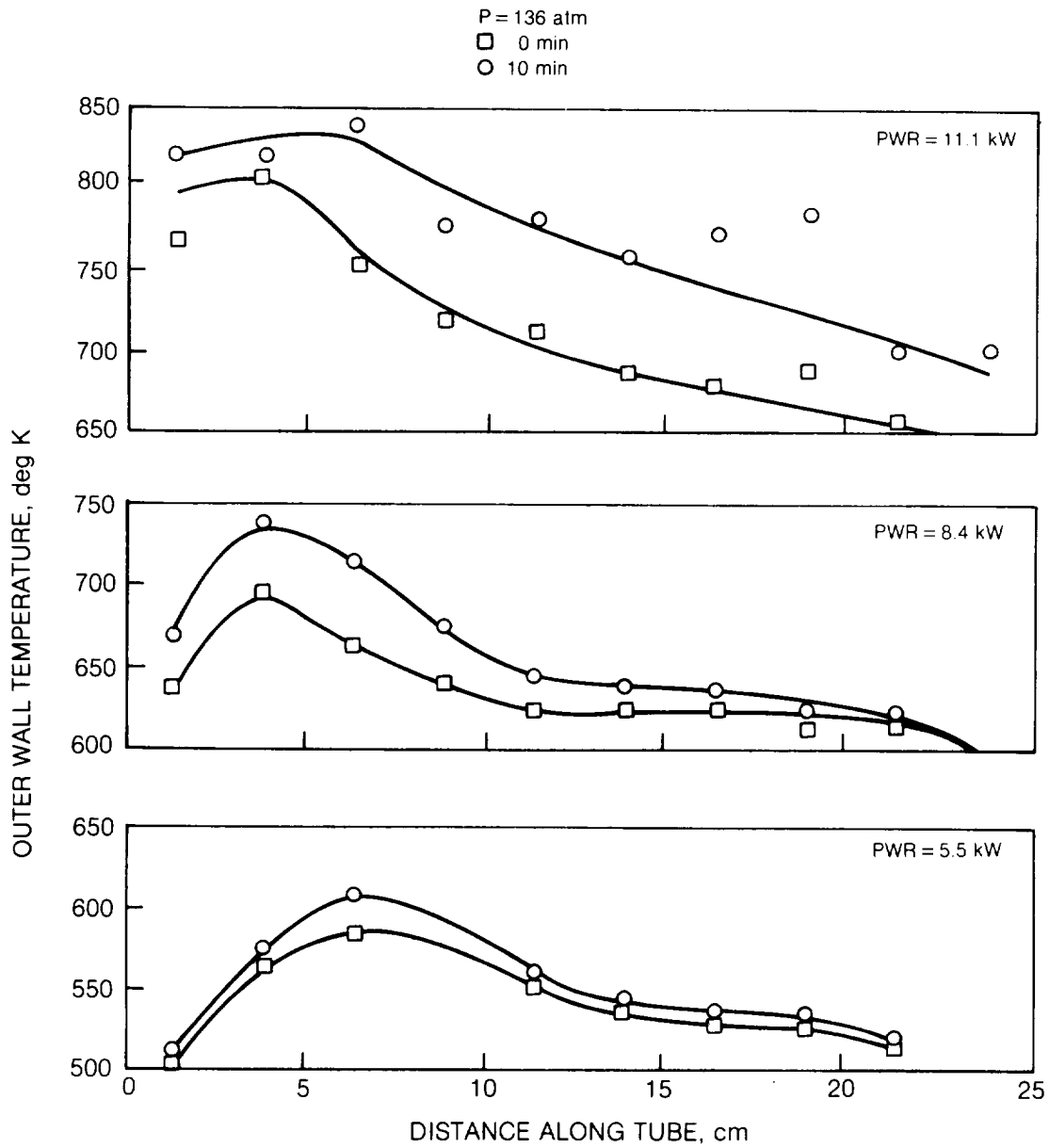


Figure 15. Axial Wall Temperature Distribution for RP-1 Fuel, V = 14.3 m/sec

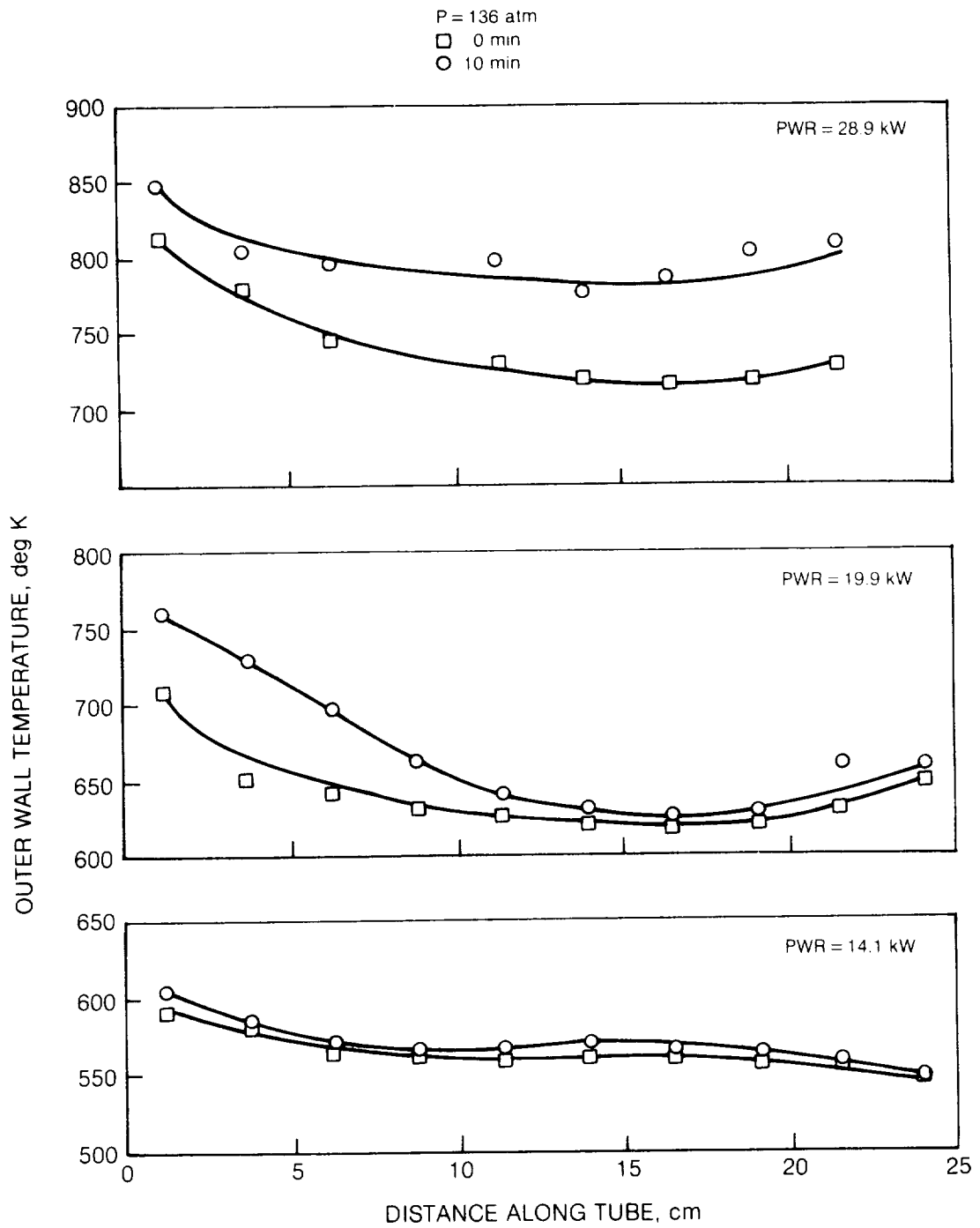


Figure 16. Axial Wall Temperature Distribution for RP-1 Fuel, V = 30.5 m/sec

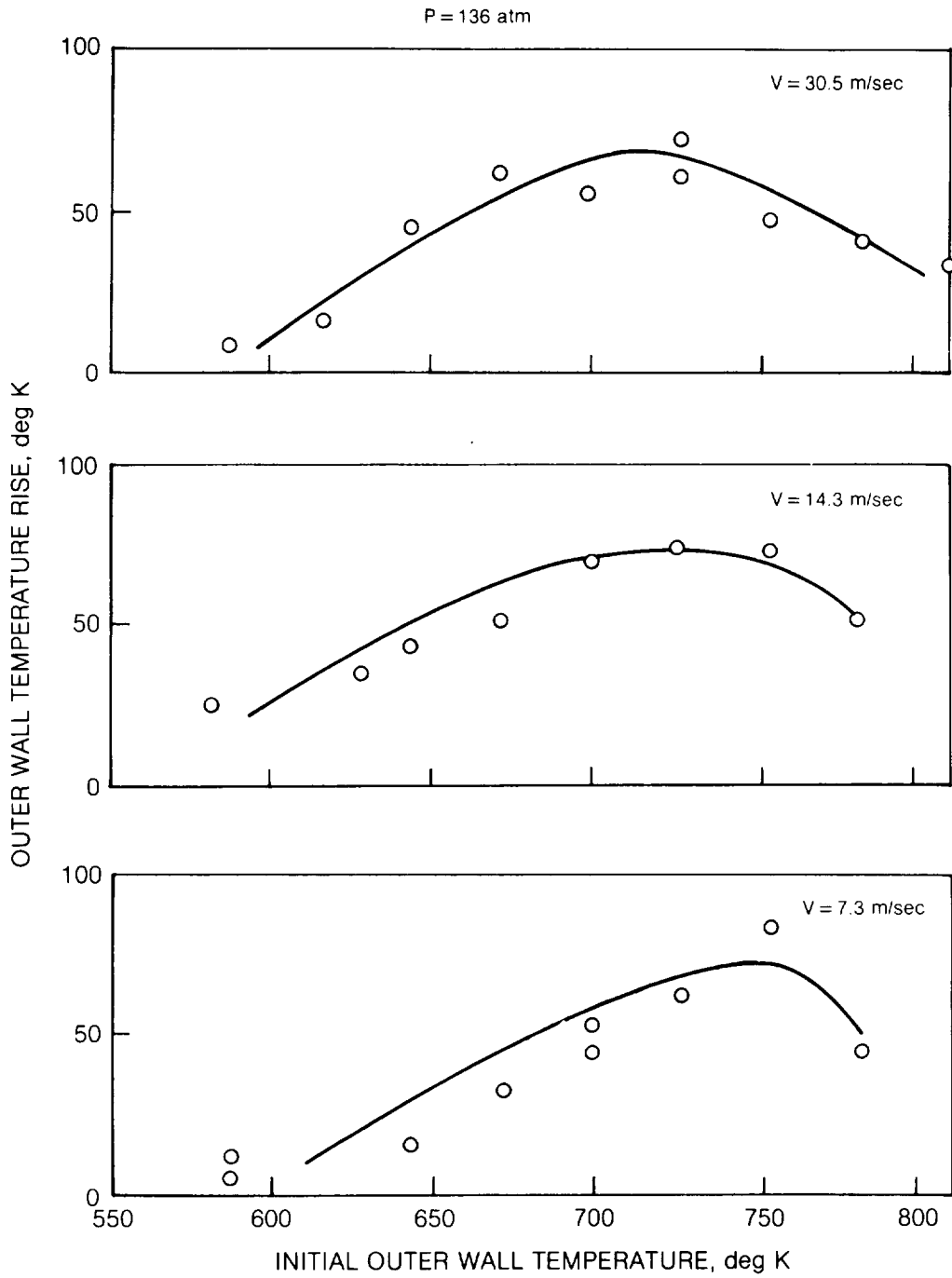
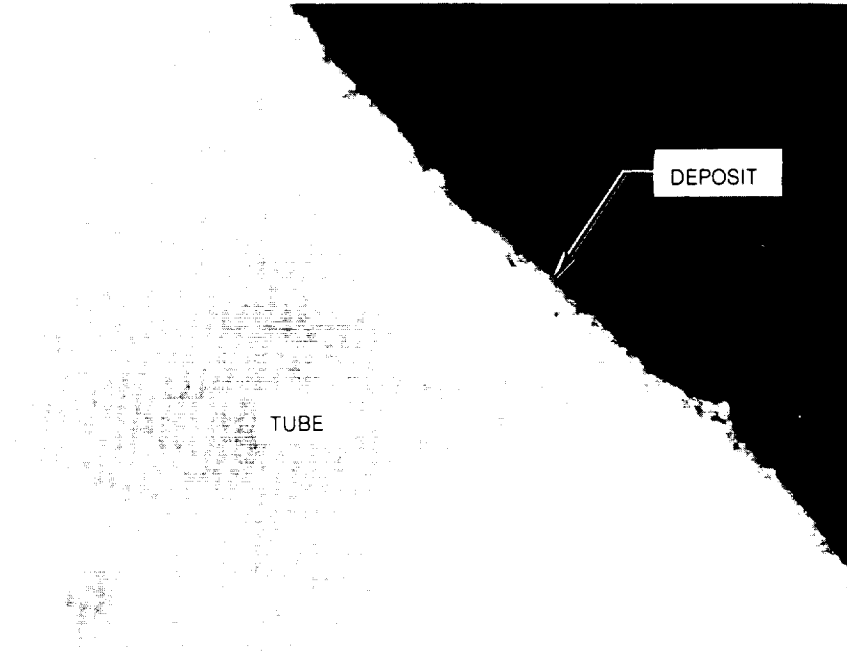
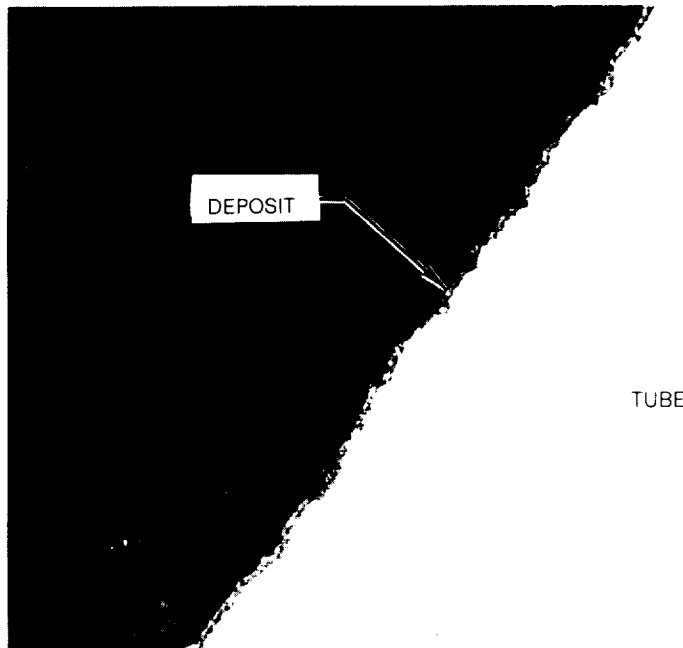


Figure 17. Outer Wall Temperature Rise for RP-1 Fuel

$T_{WALL} = 589 \text{ K}$
500 ×



$V = 7.3 \text{ m/sec}$



$V = 30.5 \text{ m/sec}$

Figure 18. RP-1 Fuel Deposits

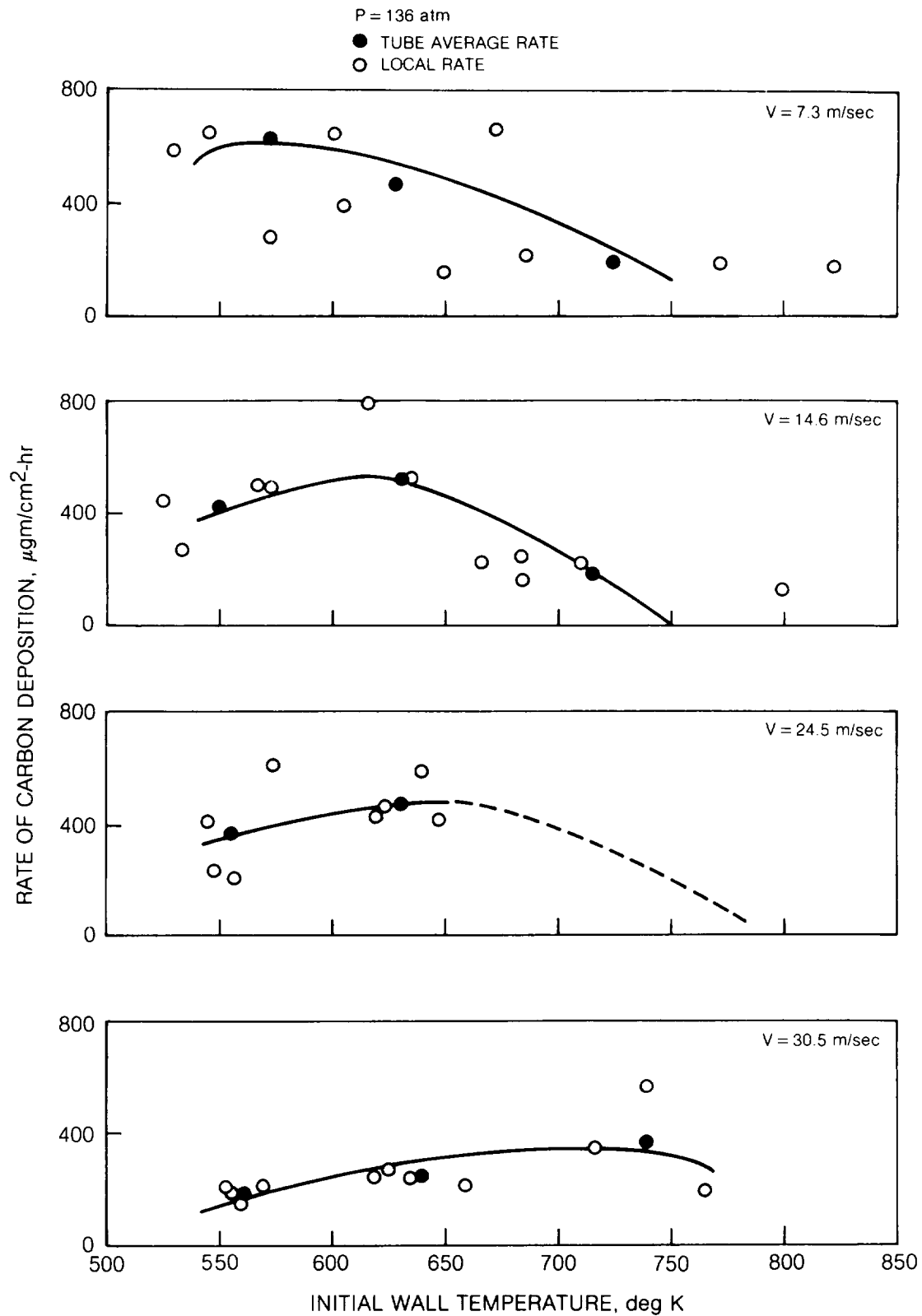


Figure 19. Rate of Carbon Deposition for RP-1 Fuel

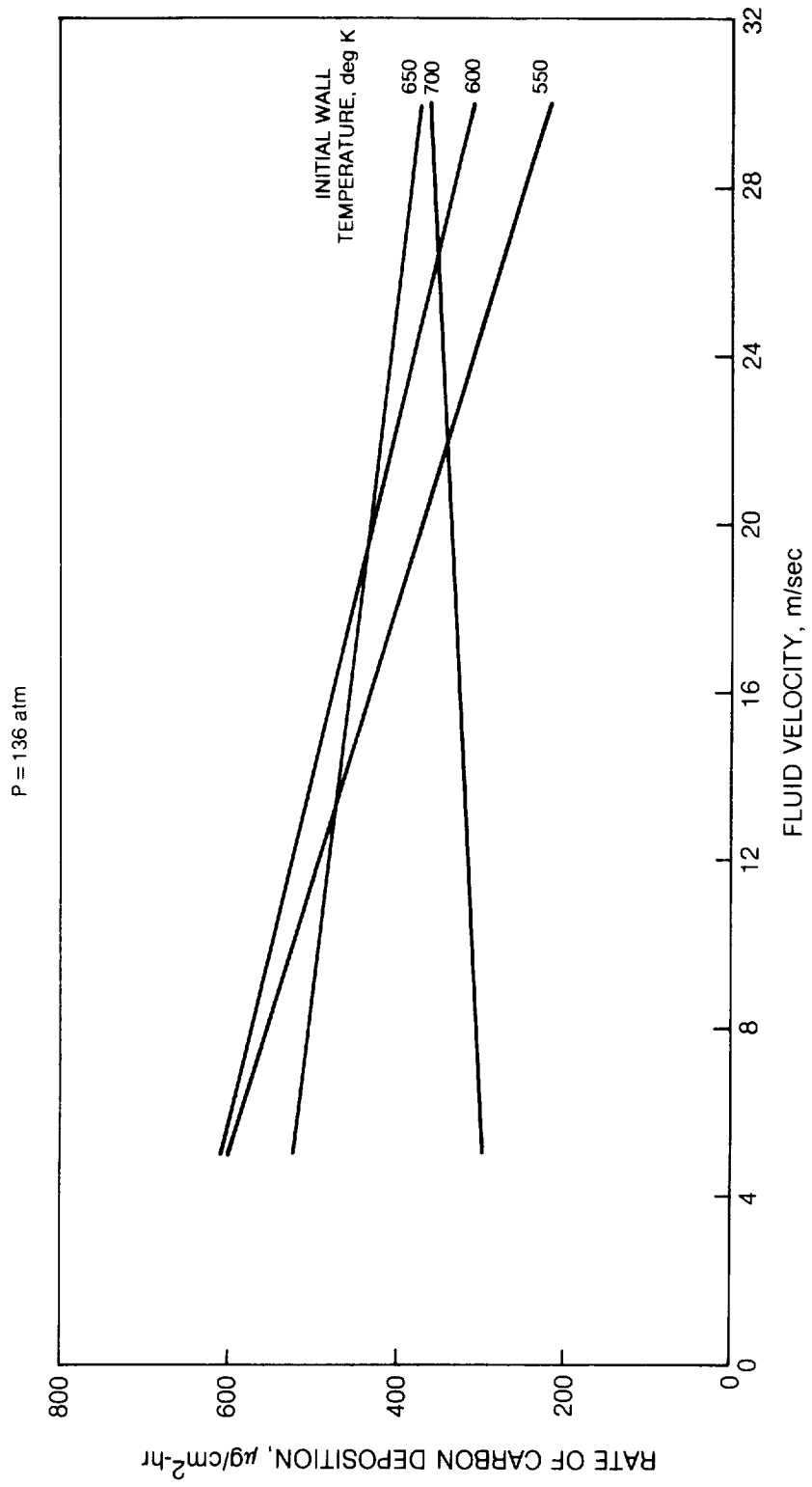


Figure 20. Effect of Velocity on Carbon Deposition Rate for RP-1 Fuel

RP-1 FUEL
P = 1.36 atm

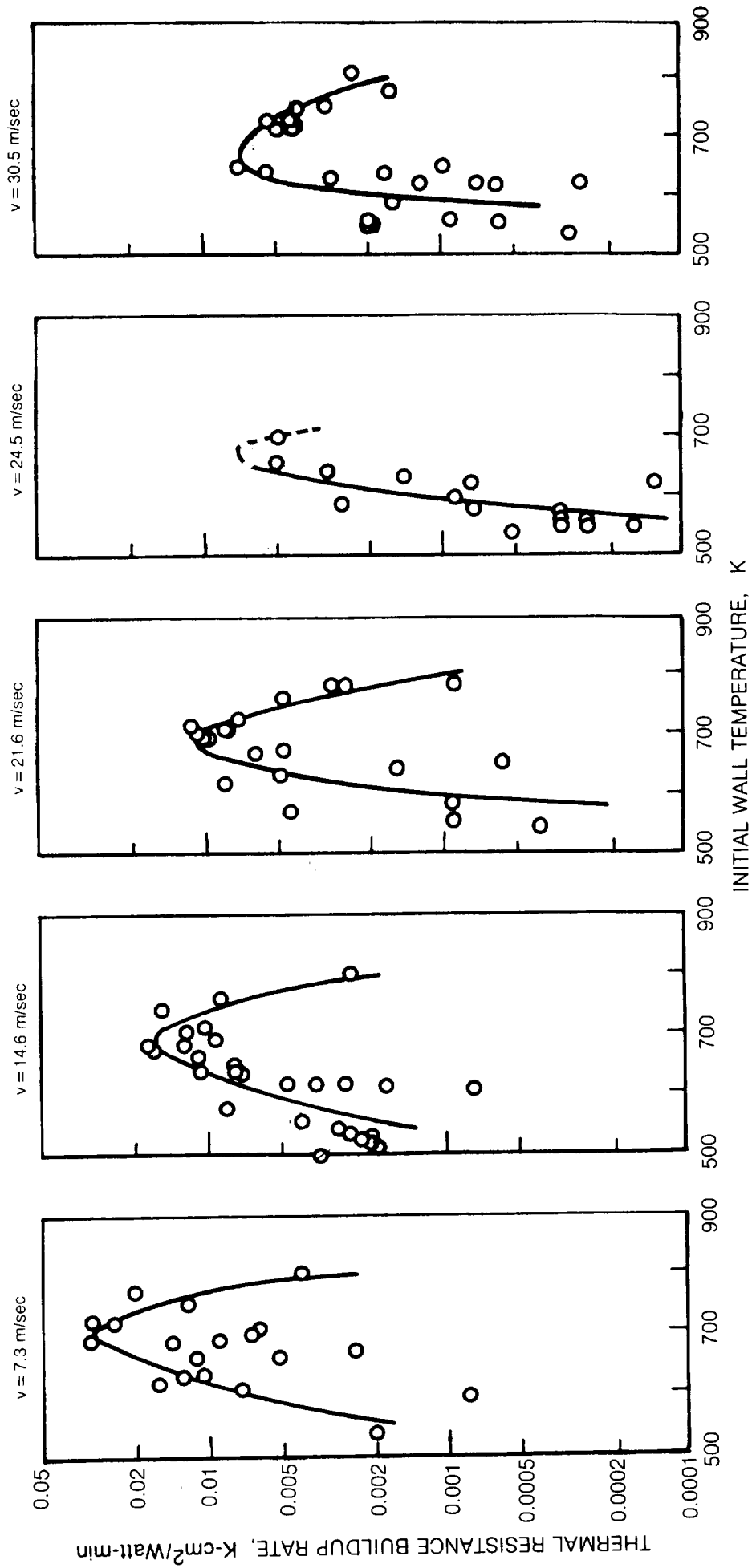


Figure 21. Variation of Thermal Resistance Buildup Rate with Wall Temperature

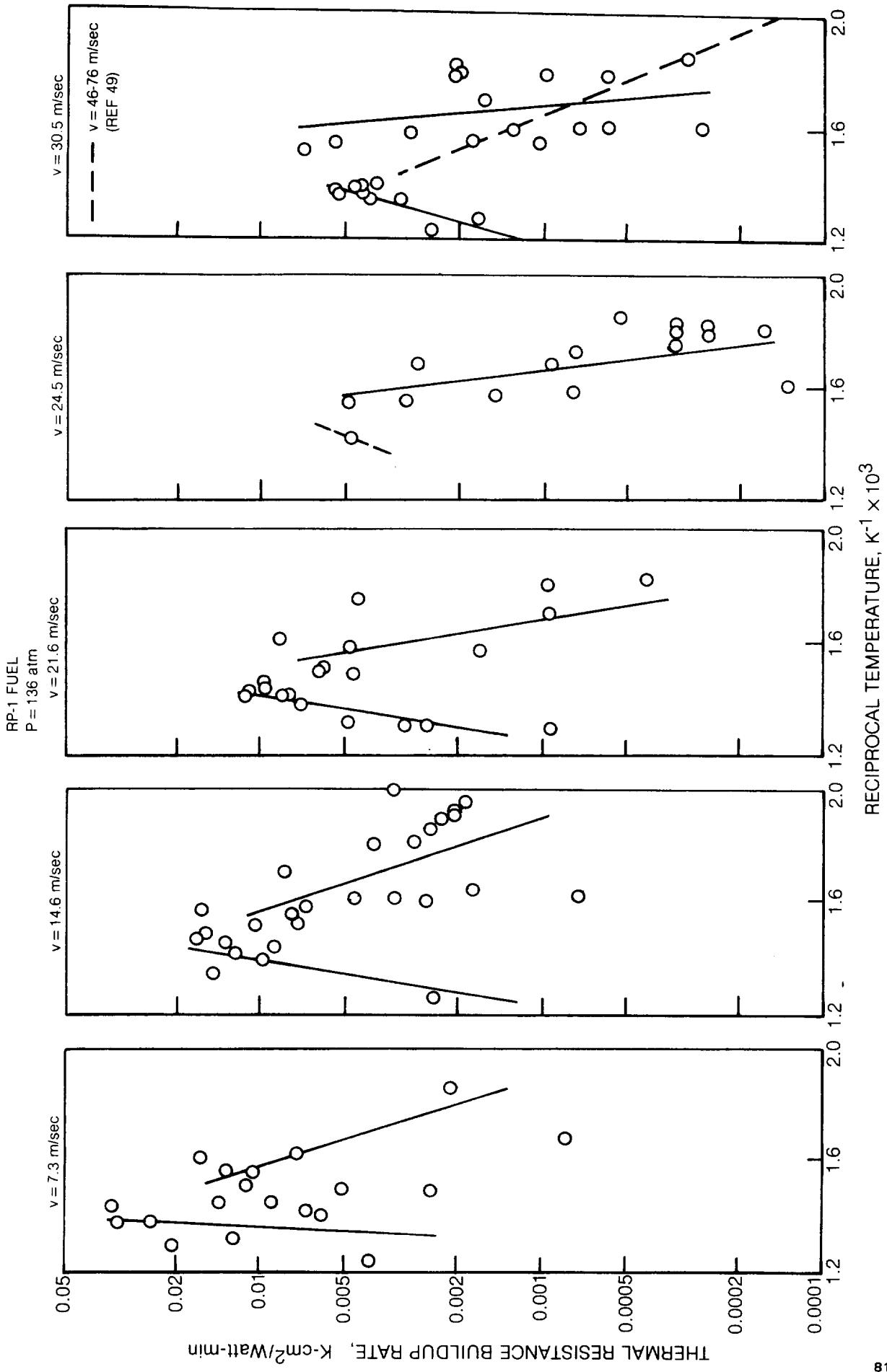


Figure 22. Deposit Thermal Resistance Buildup Rate

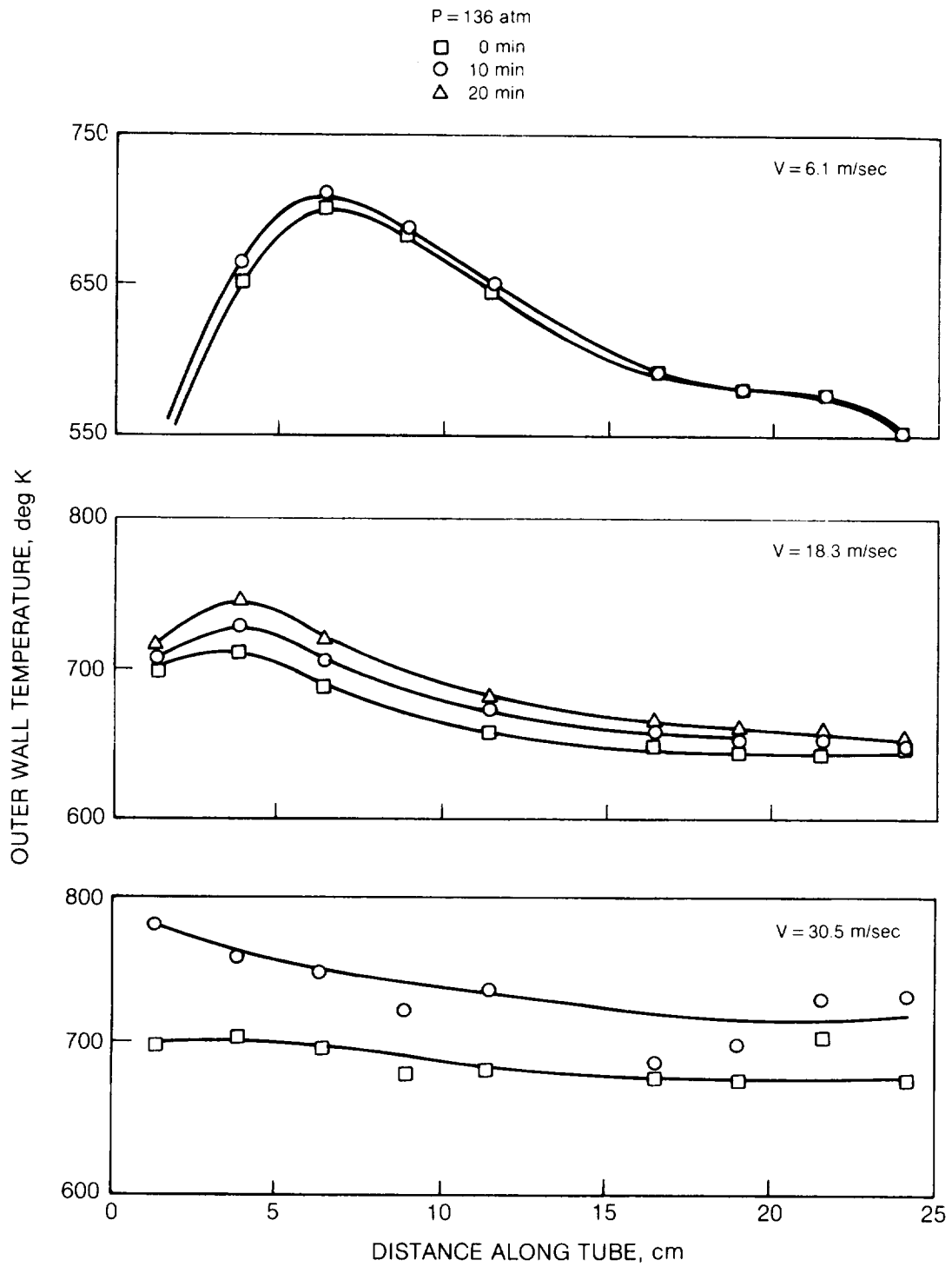


Figure 23. Axial Wall Temperature Distributions for JP-7

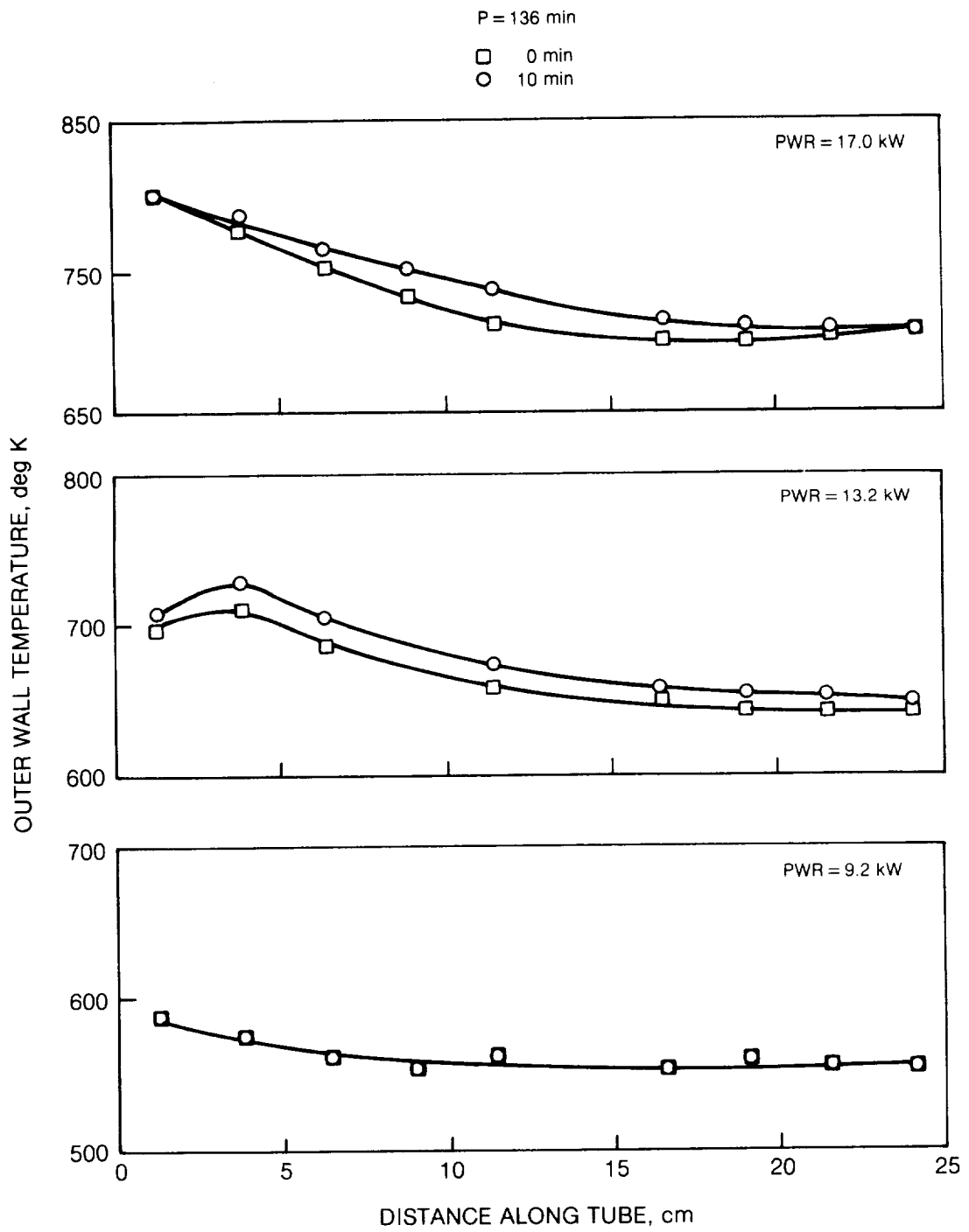


Figure 24. Axial Wall Temperature Distribution for JP-7 Fuel, V = 18.3 m/sec

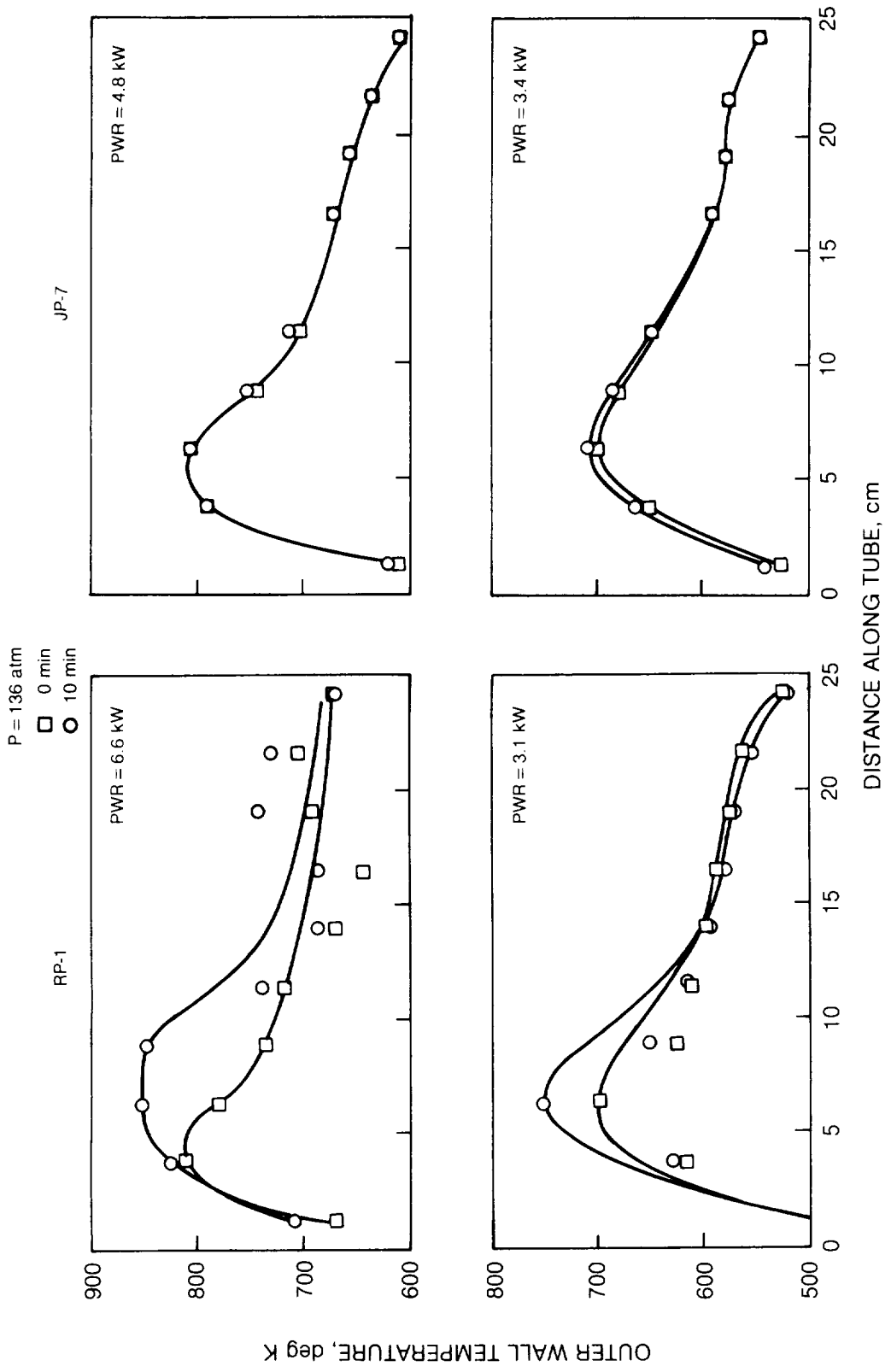


Figure 25. Comparison of Temperature Distribution for RP-1 and JP-7, V = 6.1 m/sec

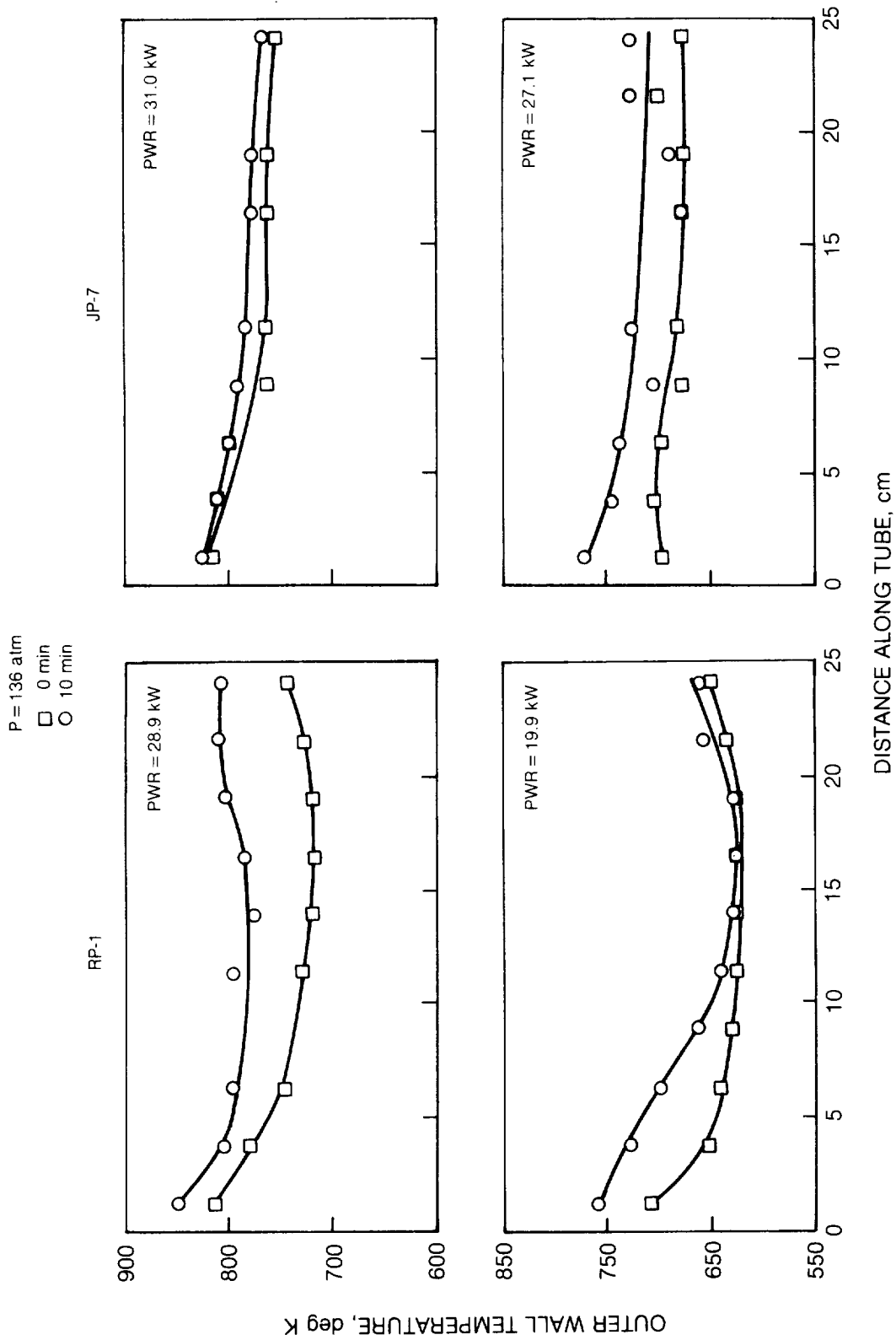
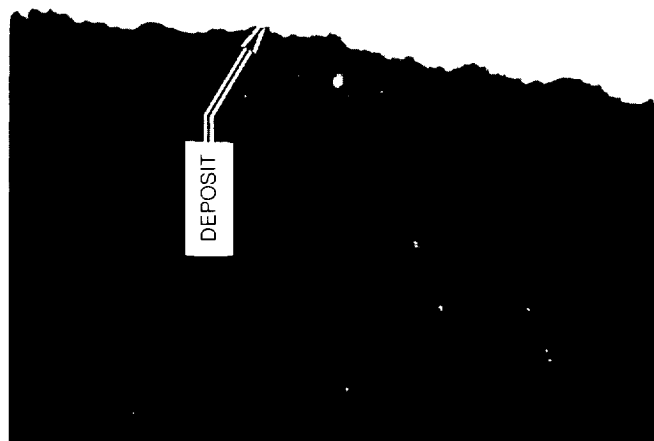
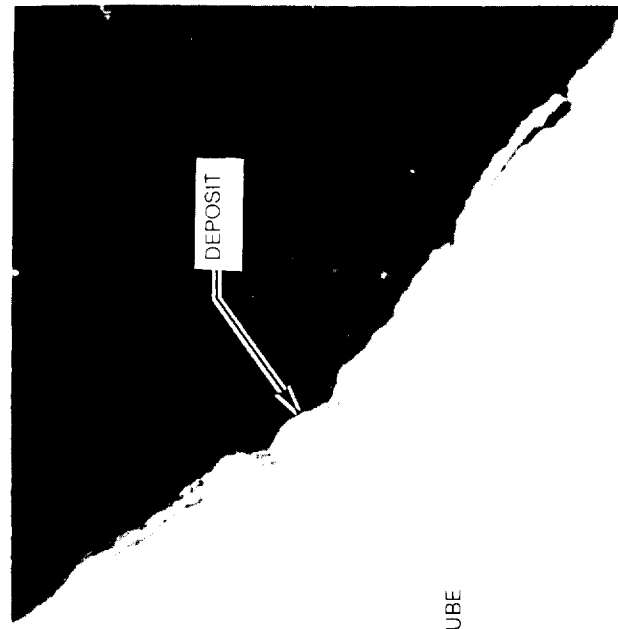


Figure 26. Comparison of Temperature Distributions for RP-1 and JP-7, V = 30.5 m/sec

V = 6.1 m/sec
T_{WALL} = 811 K
500 X



RP-1



JP-7

Figure 27. Kerosene Fuel Deposits

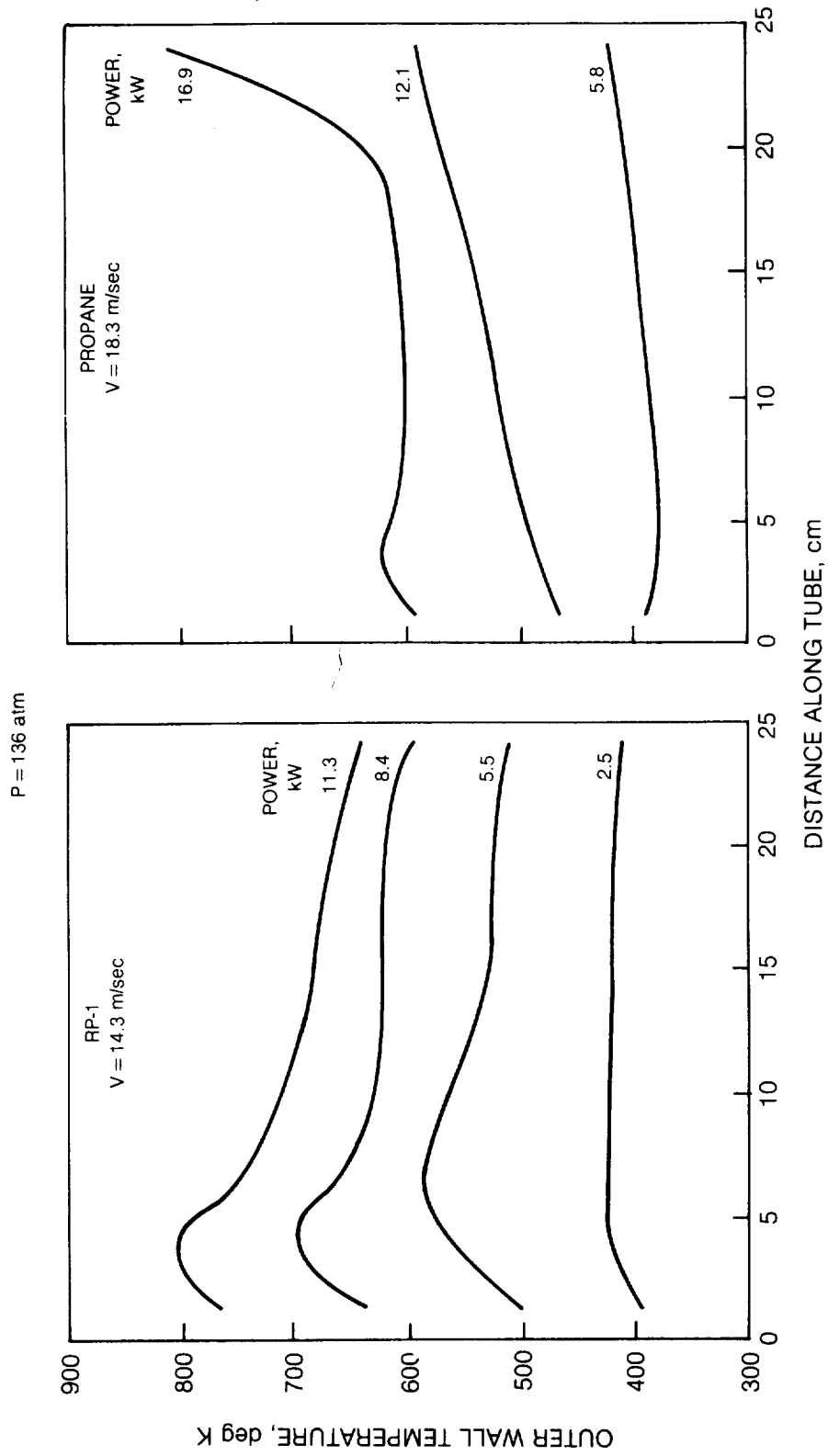


Figure 28. Comparison of RP-1 and Propane Temperature Distributions

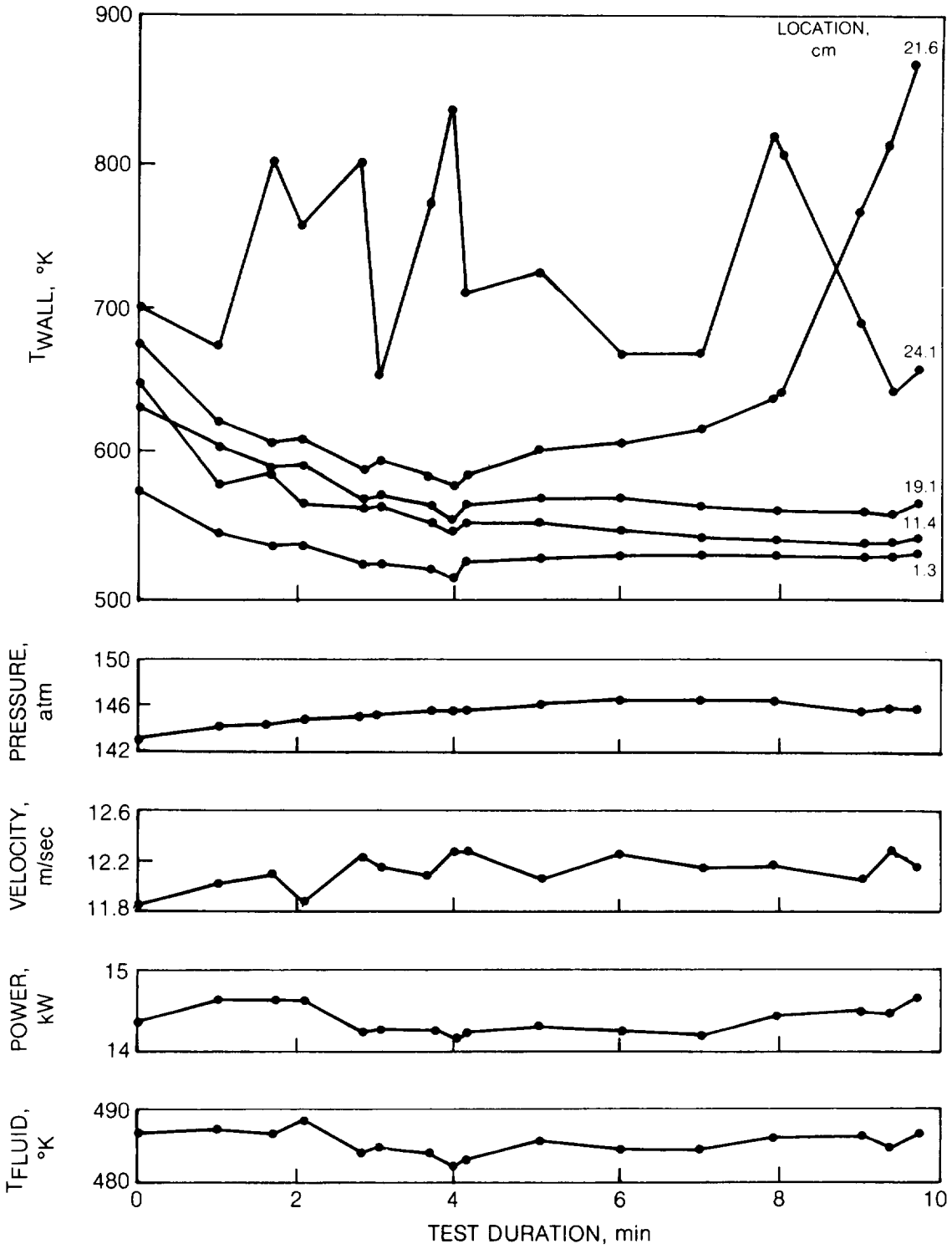


Figure 29. Variation of Propane Test Data with Time

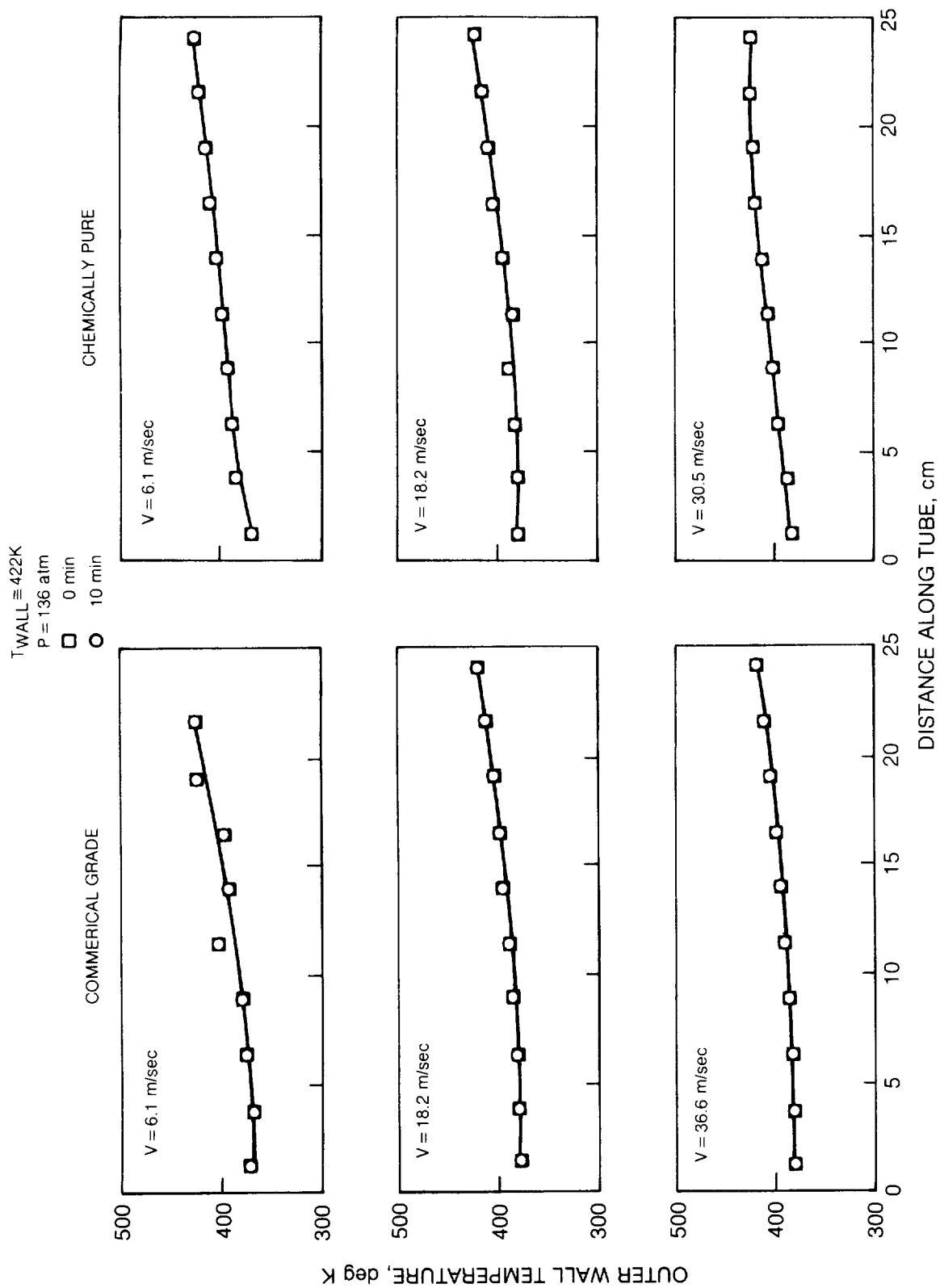


Figure 30. Comparison of Temperature Distributions for Propane

$T_{WALL} \approx 589K$
 $P = 136 \text{ atm}$
 □ 0 min
 ○ 10 min

COMMERCIAL GRADE

CHEMICALLY PURE

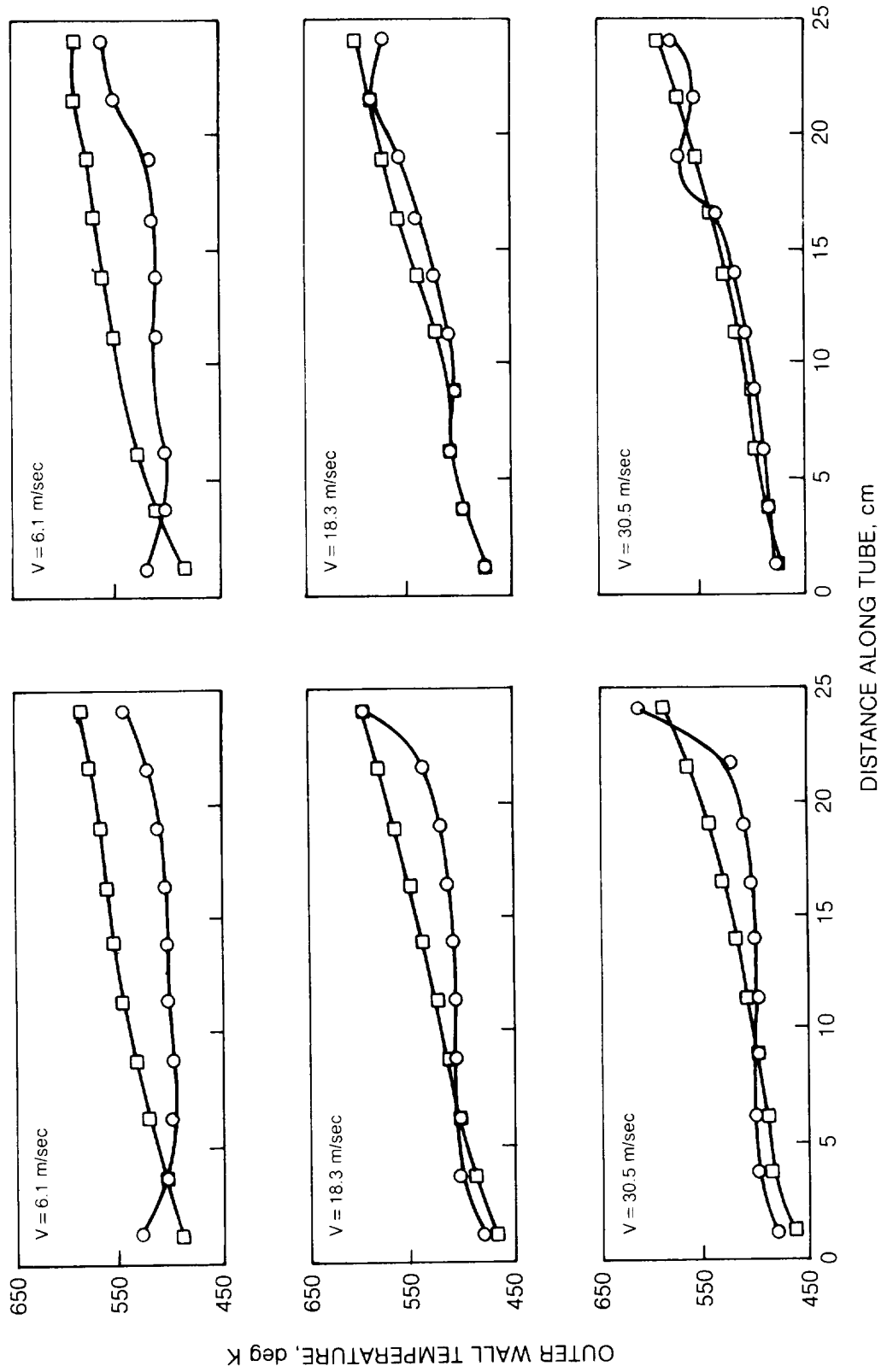


Figure 31. Comparison of Temperature Distributions for Propane

INITIAL WALL TEMPERATURE	
422K	589K
○	□
●	■

COMMERCIAL

CHEMICALLY PURE

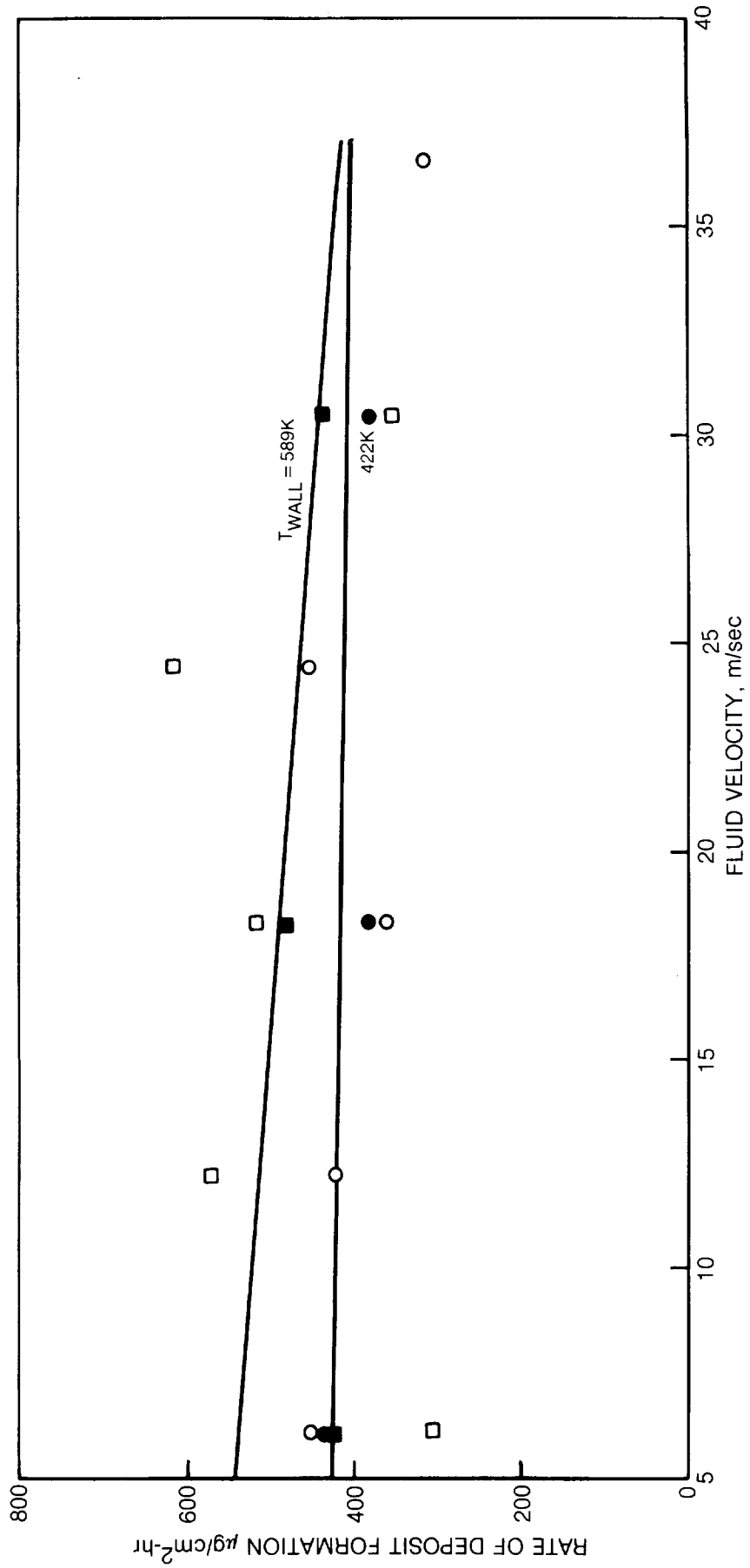


Figure 32. Effect of Velocity on Carbon Deposition Rate for Propane

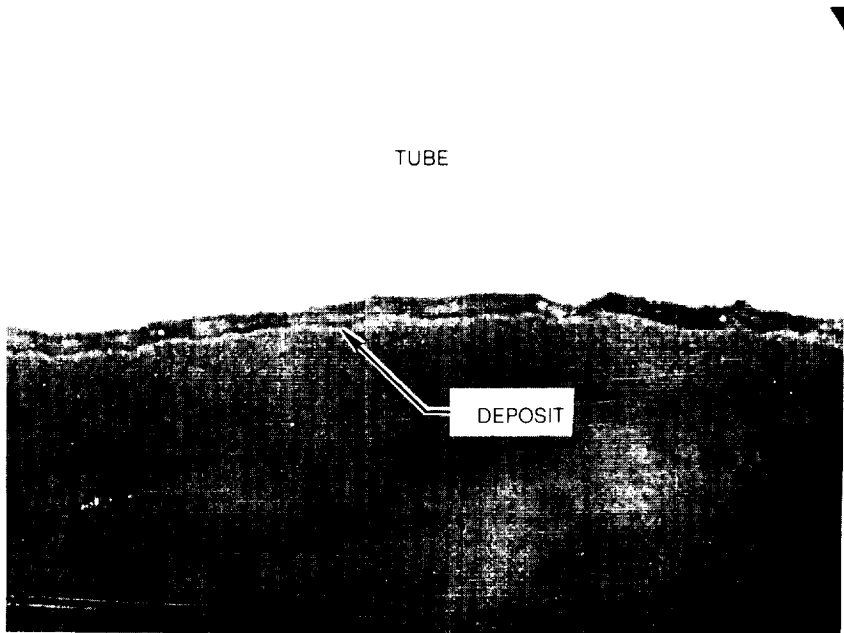
$V = 30.5 \text{ m/sec}$
 $T_{\text{WALL}} \cong 589 \text{ K}$
500x

TUBE



COMMERCIAL

TUBE



CHEMICALLY PURE

Figure 33. Propane Fuel Deposits

ORIGINAL PAGE IS
OF POOR QUALITY

V = 24.4 m/sec
 $T_{WALL} = 700\text{ K}$
500 x

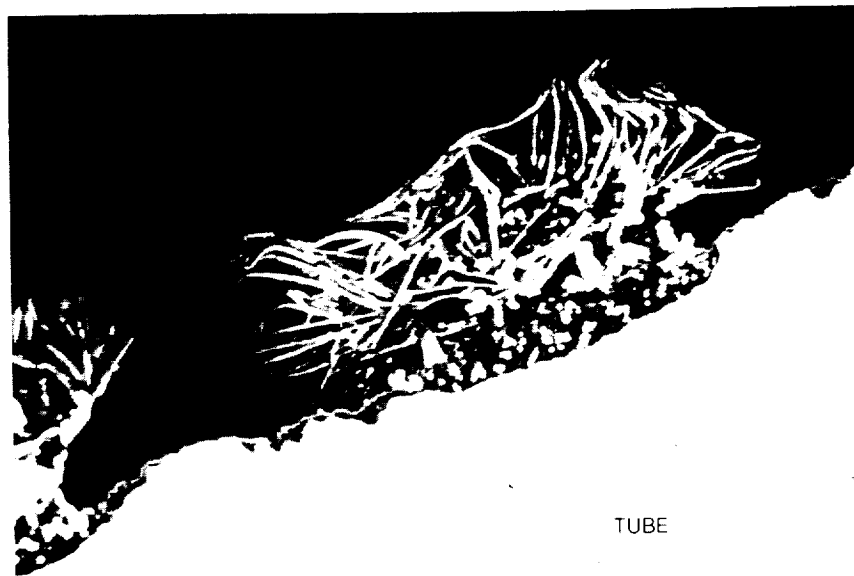
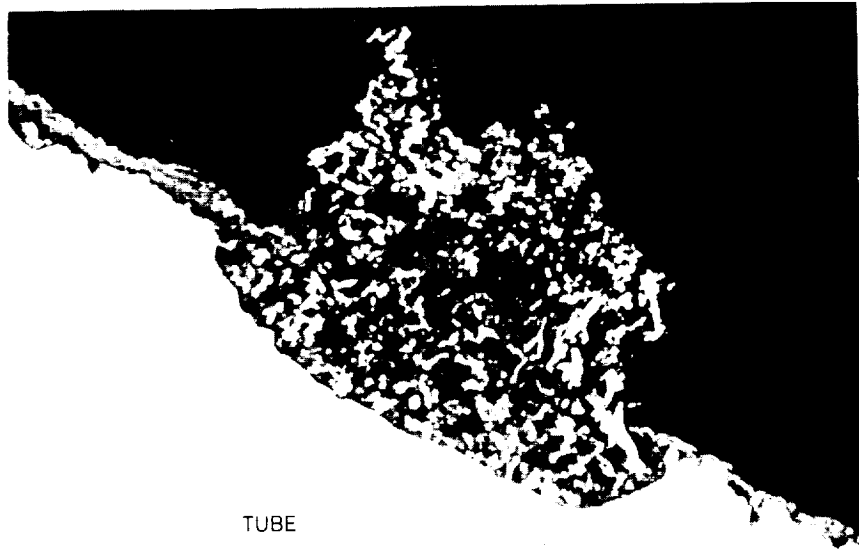


Figure 34. Propane Fuel Deposits

C-2

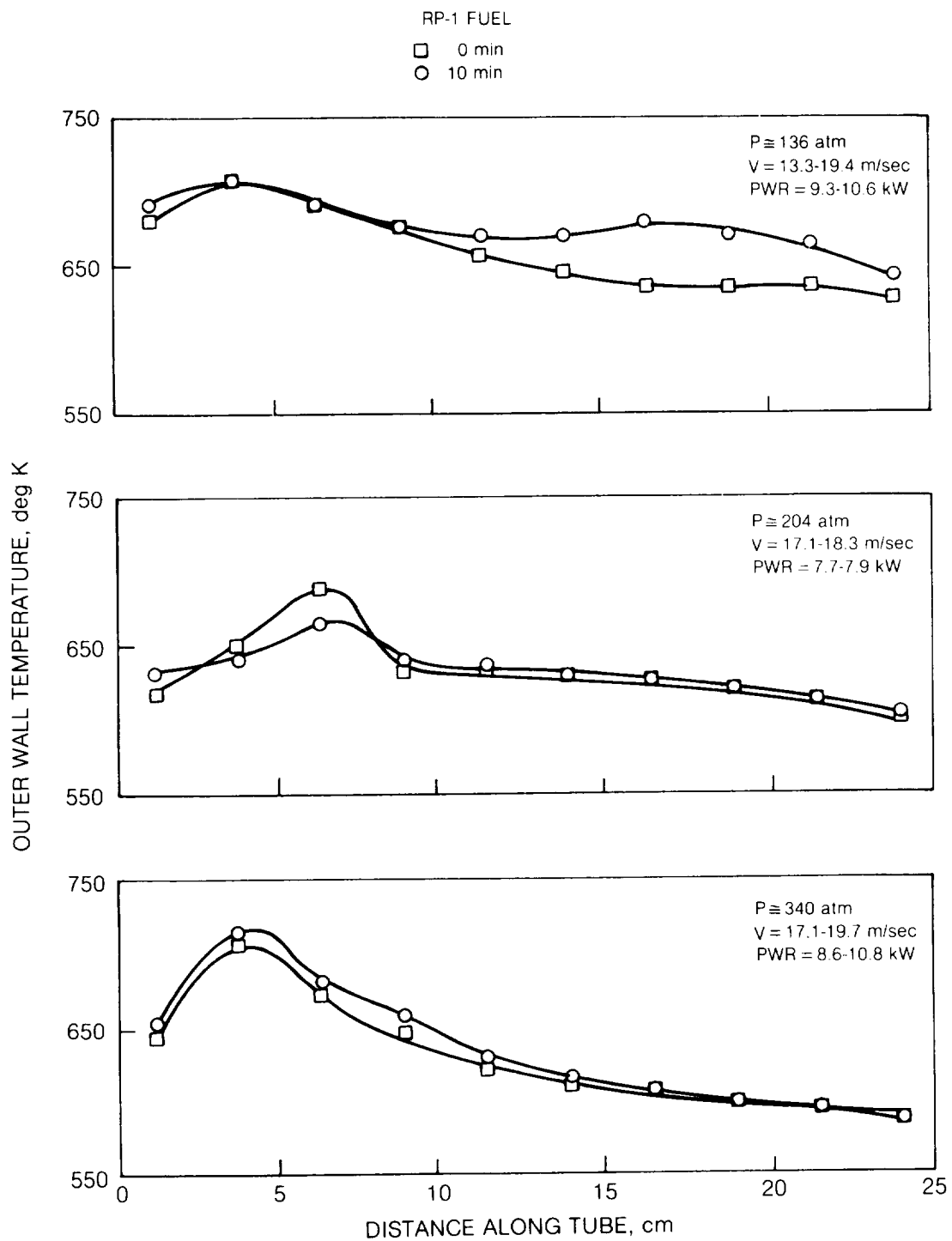


Figure 35. Variation of Wall Temperature with Pressure

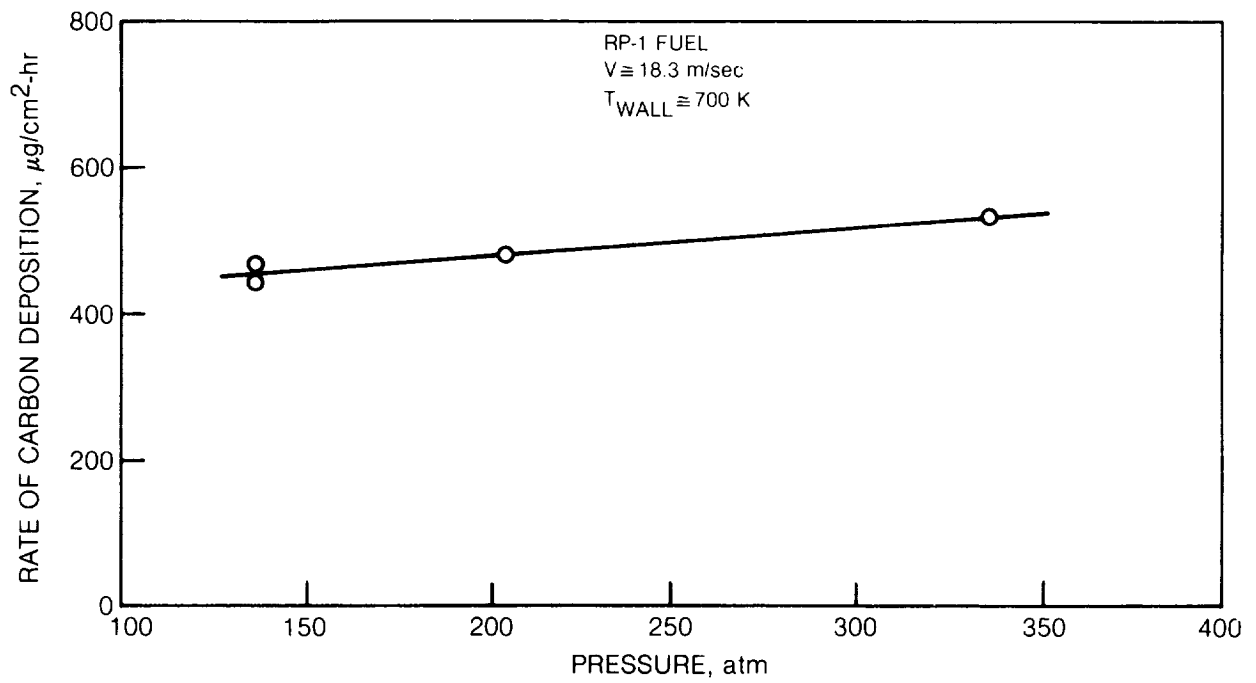


Figure 36. Variation of Deposit Rate with Pressure

RP-1 FUEL

P = 136 atm V = 6.1 m/sec

□ 0 min
○ 10 min

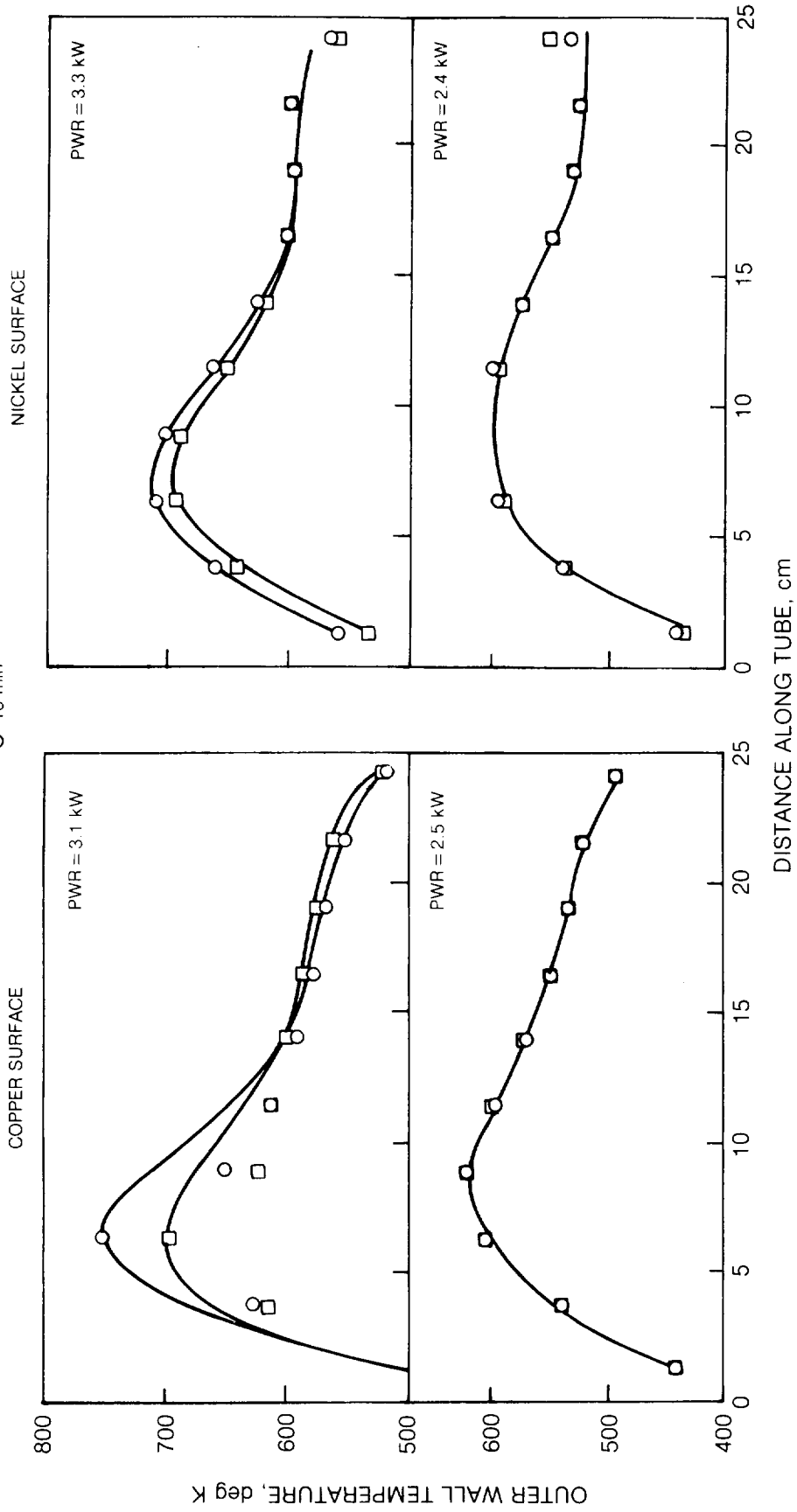


Figure 37. Comparison of Copper and Nickel Temperature Distributions

RP-1 FUEL
V = 6.1 m/sec

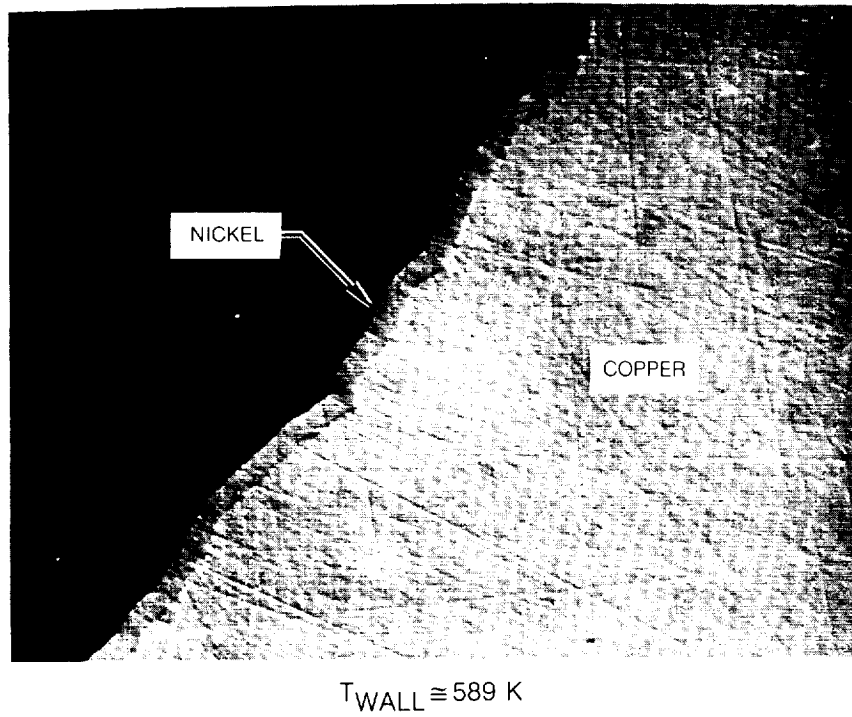
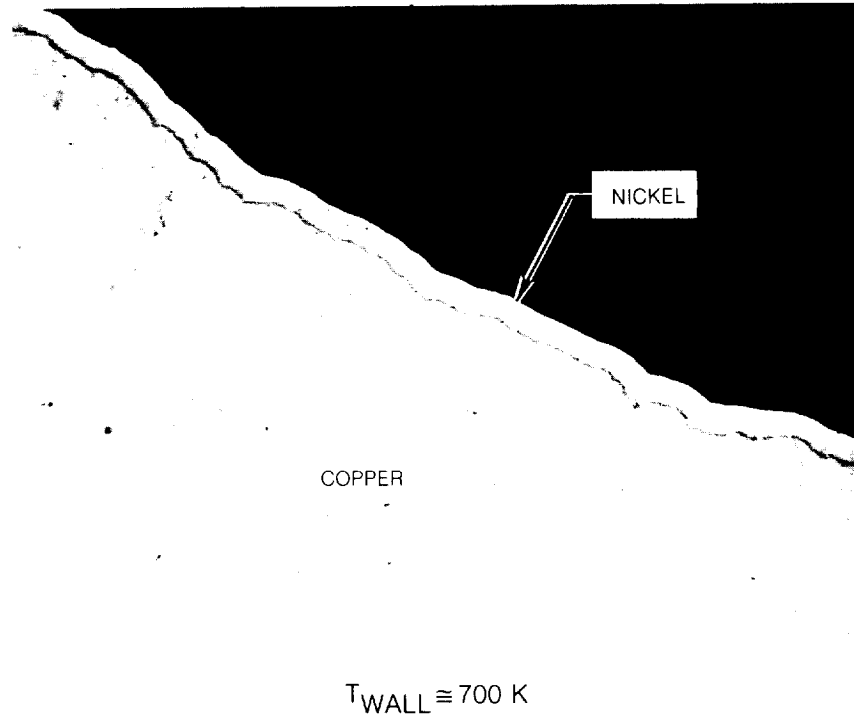


Figure 38. Sectioned Nickel Plated Tubes

P = 136 atm V = 7.2 m/sec T_{WALL} = 700 K

1000 X



UNUSED TUBE



TEST TUBE

5000 X



L = 1.9 cm

L = 12.1 cm

L = 22.2 cm

Figure 39 Microstructure of RP-1 Deposits on Copper

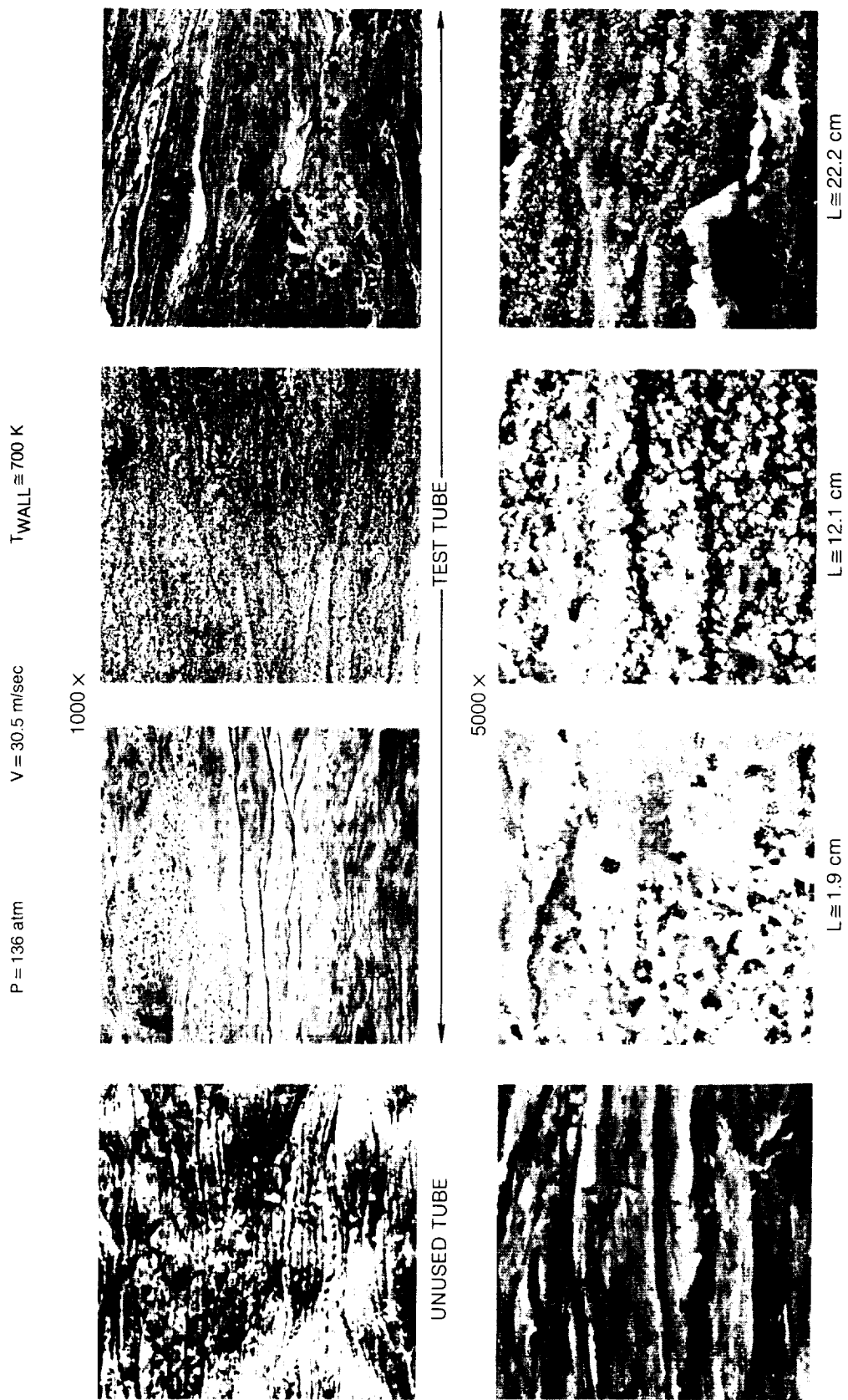
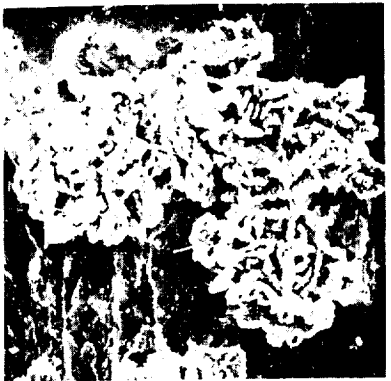
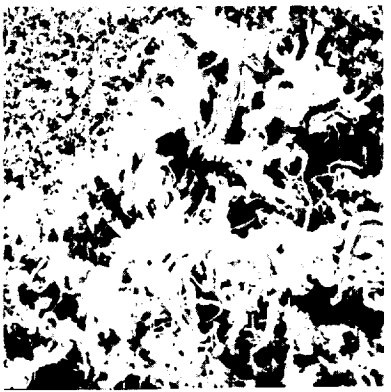


Figure 40. Microstructure of JP-7 Deposits on Copper

P = 136 atm V = 30.5 m/sec T_{WALL} ≈ 644 K

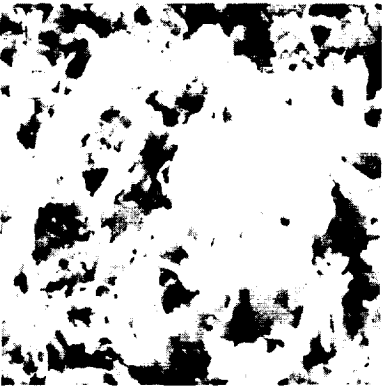
1000 X



TEST TUBE

UNUSED TUBE

5000 X



L ≈ 22.2 cm

L ≈ 12.1 cm

L ≈ 1.9 cm

Figure 41. Microstructure of Commercial Propane Deposits on Copper

$P = 136 \text{ atm}$ $V = 18.3 \text{ m/sec}$ $T_{\text{WALL}} \approx 589 \text{ K}$

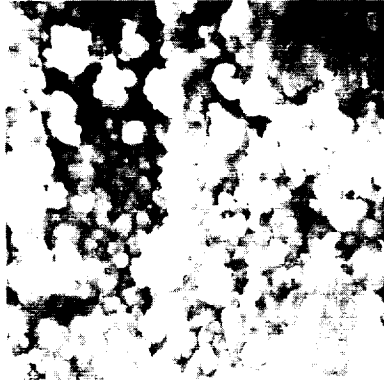
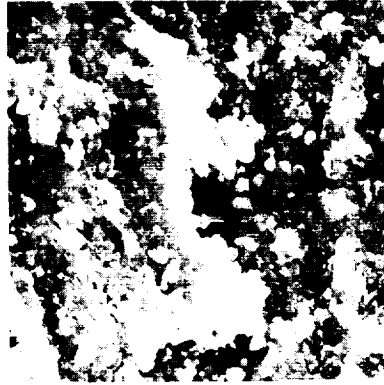
1000 X



UNUSED TUBE

TEST TUBE

5000 X



$L \approx 1.9 \text{ cm}$

$L \approx 12.1 \text{ cm}$

$L \approx 22.2 \text{ cm}$

Figure 42. Microstructure of C.P. Propane Deposits on Copper

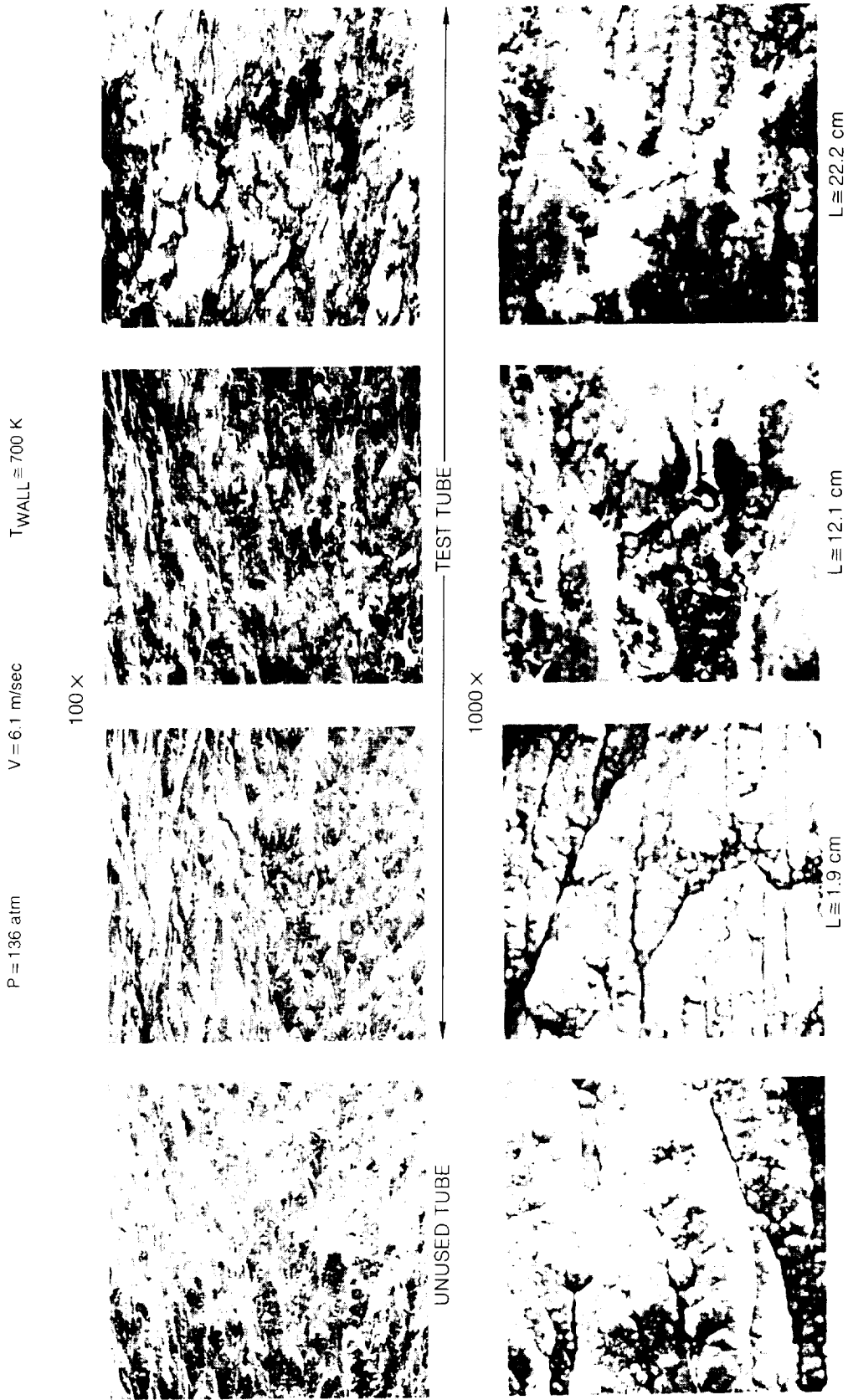


Figure 43. Microstructure of RP-1 Deposits on Nickel

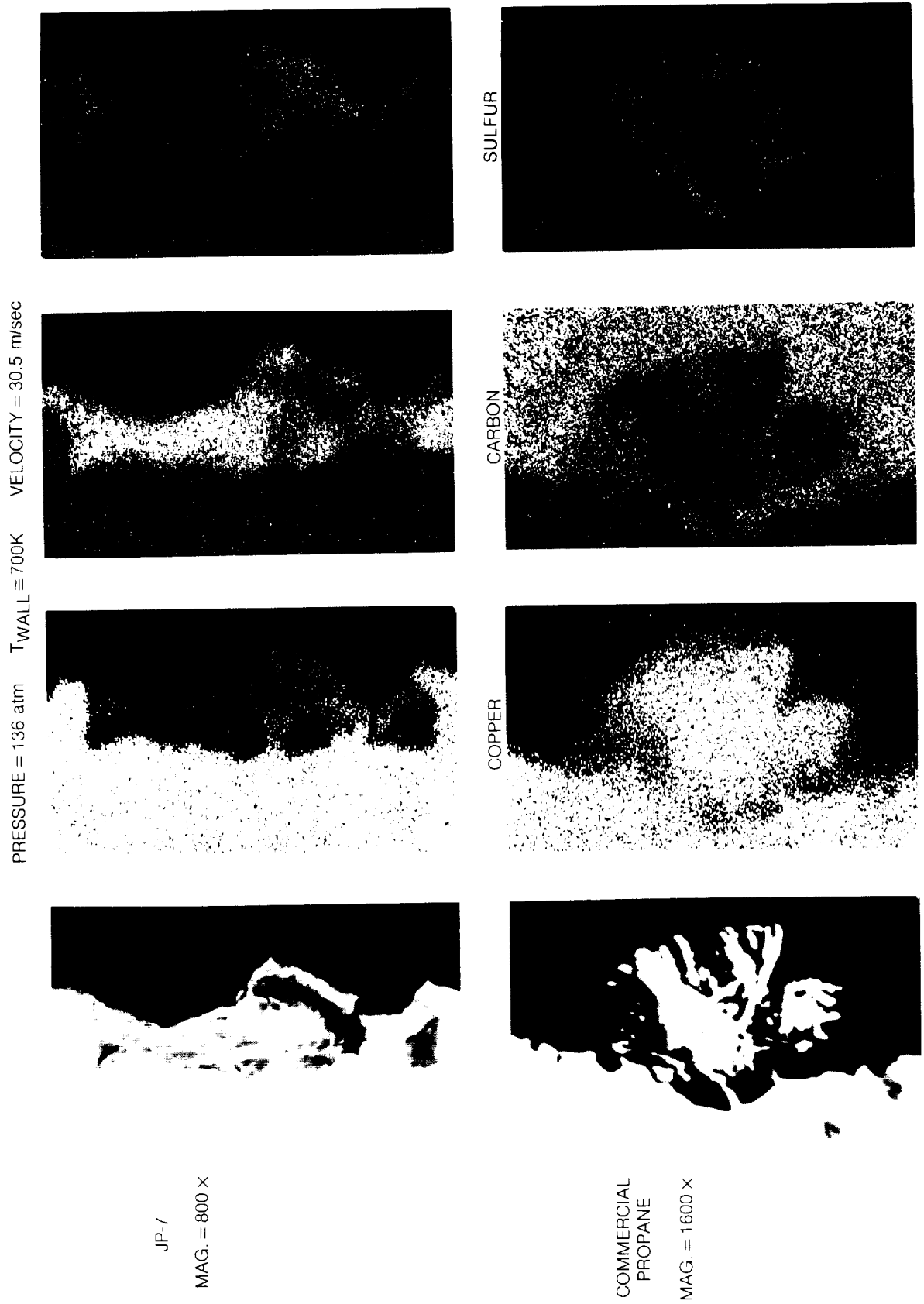


Figure 44. Scanning Electron Microprobe Analysis of Deposits

APPENDIX A
TABULATED TEST DATA

TABLE A-1

TEST DATA FOR RP-1 RUN # 12 JAN 20, 1981

TIC	1.3	DEG K	1.00	2.03	4.00	5.00	6.00	7.02	8.00
TIC	3.8	DEG K	701.	708.	717.	717.	721.	728.	7329.
TIC	6.4	DEG K	663.	667.	676.	676.	681.	688.	6972.
TIC	8.9	DEG K	647.	649.	652.	652.	656.	662.	672.
TIC	11.4	DEG K	632.	631.	639.	629.	630.	634.	641.
TIC	16.5	DEG K	629.	623.	628.	622.	624.	627.	635.
TIC	19.1	DEG K	637.	642.	654.	661.	660.	647.	638.
TIC	24.1	DEG K	643.	647.	656.	663.	672.	673.	663.
TIC	28.8	DEG K	647.	670.	689.	706.	728.	709.	753.
TIC	36.9	DEG K	288.	288.	288.	288.	288.	288.	288.
TIC	81.	DEG K	370.	369.	368.	368.	367.	367.	367.
TIC	10.94	DEG K	82.	81.	80.	79.	79.	79.	79.
TIC	17.60	DEG K	131.	130.	129.	127.	127.	126.	125.
TIC	28.91	DEG K	10.92	10.88	10.87	10.88	10.96	11.06	11.10
TIC	32.51	DEG K	28.81	28.74	28.57	28.55	28.57	28.86	28.99
TIC	35.81	DEG K	3232.	3204.	3156.	3125.	3108.	3106.	3099.
TIC	100.2	DEG K	5.83	5.83	5.85	5.83	5.84	5.87	5.87
TIC	-6.35	DEG K	18.99	18.91	18.79	18.66	18.64	18.67	18.65
TIC	5.64	DEG K	-5.70	-5.62	-6.02	-5.62	-5.88	-5.96	-6.08
TIC	53920.	DEG K	53955.	53823.	53237.	52916.	52825.	52943.	52792.
TIC	0.0000	DEG K	0.00222	0.00441	0.00468	0.00379	0.00384	0.00434	0.00424
TIC	0.0000	DEG K	0.00056	0.00165	0.00269	0.00264	0.00307	0.00369	0.00460
TIC	0.0000	DEG K	0.00000	0.00110	0.00128	0.00115	0.00154	0.00229	0.00331
TIC	0.0000	DEG K	0.00000	0.00000	0.00000	0.00000	0.00000	0.00008	0.00094
TIC	0.0000	DEG K	0.00000	0.00000	0.00000	0.00000	0.00016	0.00016	0.00065
TIC	0.0000	DEG K	0.00222	0.00110	0.00043	0.0011	0.00048	0.00295	0.0137
TIC	0.0000	DEG K	0.01001	0.00745	0.00695	0.00690	0.00567	0.00598	0.0144
TIC	0.0000	DEG K	0.00667	0.00552	0.00581	0.00621	0.00673	0.00598	0.01396
TIC	0.0000	DEG K	0.01112	0.01241	0.01461	0.01552	0.01662	0.01638	0.01568
TIC	0.0000	DEG K	0.01279	0.01324	0.01503	0.01483	0.01355	0.01114	0.00827

TABLE A-1

TEST DATA FOR RP-1 RUN # 15 FEB 11, 1981

TIC	1.3	MIN	CM	DEG	K	504.	00	35	806.	72
TIC	3.8	1.8	CM	DEG	K	517.	04.	791.	763.	791.
TIC	6.9	3.4	CM	DEG	K	517.	04.	752.	758.	752.
TIC	8.4	4.0	CM	DEG	K	517.	04.	740.	771.	740.
TIC	11.0	11.0	CM	DEG	K	522.	04.	834.	841.	834.
TIC	14.5	16.5	CM	DEG	K	517.	04.	753.	766.	753.
TIC	19.1	19.1	CM	DEG	K	507.	04.	741.	745.	741.
TIC	21.6	21.6	CM	DEG	K	489.	04.	694.	713.	694.
TIC	24.1	24.1	CM	DEG	K	510.	04.	749.	759.	749.
TIC	24.1	24.1	CM	DEG	K	510.	04.	749.	761.	749.
TIC	29.2	29.2	CM	DEG	K	292.	04.	292.	292.	292.
TIC	33.8	33.8	CM	DEG	K	411.	04.	411.	412.	411.
TIC	46.	46.	CM	DEG	K	338.	04.	119.	119.	338.
TIC	134.	134.	CM	DEG	K	46.	04.	134.	134.	46.
TIC	137.4	137.4	CM	DEG	K	46.	04.	134.	134.	46.
TIC	6.42	6.42	CM	DEG	K	6.42	04.	6.52	6.43	6.42
TIC	24.41	24.41	CM	DEG	K	24.41	04.	24.78	24.44	24.41
TIC	246.8	246.8	CM	DEG	K	3.63	04.	3421.	3382.	3421.
TIC	3.63	3.63	CM	DEG	K	8.96	04.	7.21	7.24	7.21
TIC	475.	475.	CM	DEG	K	8.96	04.	24.66	24.50	24.66
TIC	-8.15	-8.15	CM	DEG	K	475.	04.	1308.	1300.	475.
TIC	379.39	379.39	CM	DEG	K	-8.15	04.	-6.52	-6.52	-8.15
TIC	0.0000	0.0000	CM	DEG	K	379.39	04.	64331.	63707.	379.39
TIC	0.0000	0.0000	CM	DEG	K	0.0000	04.	62595.	62384.	0.0000
TIC	0.0000	0.0000	CM	DEG	K	0.0000	04.	51434.	52642.	0.0000
TIC	0.0000	0.0000	CM	DEG	K	0.0000	04.	48766.	25883.	0.0000
TIC	0.0000	0.0000	CM	DEG	K	0.0000	04.	52162.	27195.	0.0000
TIC	0.0000	0.0000	CM	DEG	K	0.0000	04.	68175.	34173.	0.0000
TIC	0.0000	0.0000	CM	DEG	K	0.0000	04.	53133.	27493.	0.0000
TIC	0.0000	0.0000	CM	DEG	K	0.0000	04.	50949.	25525.	0.0000
TIC	0.0000	0.0000	CM	DEG	K	0.0000	04.	44762.	24094.	0.0000
TIC	0.0000	0.0000	CM	DEG	K	0.0000	04.	52283.	26718.	0.0000
TIC	0.0000	0.0000	CM	DEG	K	0.0000	04.	52283.	26897.	0.0000

TABLE A-1
TEST DATA FOR RP-1 RUN# 20 JAN 20, 1981

TIC	1.3	812	1.00	2.02	3.00	4.00	5.00	6.00	7.00	8.00	9.00	10.00
TTC	3.8	779	833	814	817	825	831	837	836	838	846	849
TTC	6.4	746	759	764	762	761	764	771	773	778	787	795
TTC	8.9	730	744	754	756	756	759	767	769	775	785	796
TTC	11.0	717	732	743	745	743	747	753	754	758	767	777
TTC	16.5	717	731	742	745	744	749	756	758	763	773	784
TTC	19.1	719	734	746	749	750	756	766	768	776	789	803
TTC	24.6	728	741	748	749	750	757	766	771	779	793	808
TTC	24.1	743	754	777	788	791	792	787	789	792	801	807
FLUID ID	INLET	288	288	288	288	288	288	287	287	283	287	287
FLUID TEMP	DEG K	407	407	407	407	405	405	406	407	403	402	402
FLUID PRESSURE	DEG K	119	119	119	119	117	117	118	117	116	115	115
TUBE INLET	DEG K	139	139	138	138	137	137	137	136	135	133	133
TUBE TEST	ATM	12.93	13.61	13.96	14.16	14.23	14.40	14.43	14.37	14.56	14.61	14.61
DEL P RATE	M/SEC	29.88	30.61	30.96	30.95	30.94	30.98	30.95	30.93	30.98	30.98	30.98
FLOW RATE	MPS	29.97	30.16	30.27	30.23	30.18	30.36	30.22	30.17	30.34	30.34	30.34
VOLUME	LITERS	3645	3610	3593	3570	3544	3539	3528	3496	3473	3449	3449
VOLTAGE	VOLTS	8.07	8.12	8.17	8.14	8.10	8.14	8.22	8.15	8.16	8.21	8.21
POWER	W/SQ.CM	1560	1554	1558	1542	1523	1528	1533	1512	1503	1497	1488
ENERGY	CM	543	533	528	523	521	521	518	518	518	517	517
FLUX	CM	744	740	743	735	729	733	730	720	718	710	707
BALANCE	COEFFICIENT	0.0000	0.0394	0.0088	0.0120	0.0219	0.0254	0.0272	0.0231	0.0222	0.0256	0.0250
CHARGE	CM	0.0000	0.0608	0.0195	0.0048	0.0027	0.0080	0.0139	0.0121	0.0125	0.0157	0.0168
NO	CM	0.0000	0.0822	0.0566	0.0348	0.0237	0.0233	0.0272	0.0252	0.0263	0.0301	0.0320
3	CM	0.0000	0.0000	0.0000	0.0000	0.0000	0.0000	0.0000	0.0000	0.0000	0.0000	0.0000
8	CM	0.0000	0.0000	0.0000	0.0000	0.0000	0.0000	0.0000	0.0000	0.0000	0.0000	0.0000
9	CM	0.0000	0.0029	0.0078	0.0056	0.0029	0.0085	0.0044	0.0067	0.0074	0.0037	0.0044
14	CM	0.0000	0.0965	0.0831	0.0601	0.0429	0.0385	0.0386	0.0346	0.0342	0.0371	0.0399
16	CM	0.0000	0.0929	0.0814	0.0613	0.0456	0.0422	0.0422	0.0388	0.0388	0.0421	0.0455
19	CM	0.0000	0.1001	0.0867	0.0649	0.0511	0.0487	0.0501	0.0467	0.0476	0.0520	0.0564
21	CM	0.0000	0.0822	0.0637	0.0468	0.0365	0.0378	0.0416	0.0409	0.0430	0.0487	0.0541
24	CM	0.0000	0.0679	0.0107	0.0096	0.0078	0.0064	0.0537	0.0430	0.0407	0.0429	0.0425

TABLE A-1

TEST DATA FOR JP-7 RUN # 26 FEB 20, 1981

TIME	MIN	CM	DEG K	1.00	2.00	3.00	4.00	5.00	6.03	7.02	8.00	9.00	10.00
TC	1.3	801.	804.	804.	804.	804.	804.	804.	804.	804.	804.	803.	803.
TC	3.8	781.	786.	786.	786.	786.	786.	786.	786.	786.	787.	786.	787.
TC	6.4	748.	755.	760.	762.	763.	763.	763.	763.	764.	764.	764.	765.
TC	8.9	733.	740.	744.	746.	747.	748.	748.	748.	748.	749.	749.	751.
TC	11.0	714.	723.	729.	732.	733.	734.	734.	734.	735.	737.	737.	739.
TC	14.5	702.	710.	713.	715.	716.	717.	717.	717.	717.	718.	718.	719.
TC	16.5	702.	709.	710.	711.	712.	712.	712.	712.	712.	713.	713.	714.
TC	19.1	706.	708.	709.	710.	711.	711.	711.	711.	711.	712.	712.	713.
TC	21.6	706.	707.	707.	708.	708.	707.	707.	707.	707.	708.	709.	711.
TC	24.1	291.	289.	289.	289.	289.	289.	289.	289.	289.	289.	289.	289.
FLUID INLET TEMP.	DEG K	401.	401.	401.	401.	401.	401.	401.	401.	401.	401.	400.	400.
FLUID EXIT TEMP.	DEG K	111.	112.	112.	112.	112.	111.	111.	111.	111.	111.	111.	111.
FLUID INLET PRESSURE	DEG K ATM	132.	132.	132.	132.	132.	132.	132.	132.	132.	132.	132.	132.
TUBE INLET TUBE	ATM	7.87	7.70	7.67	7.67	7.66	7.67	7.66	7.69	7.67	7.67	7.70	7.70
DELTA T	DEG K	4.87	4.81	4.81	4.81	4.80	4.81	4.80	4.81	4.80	4.80	4.82	4.81
VELOCITY	M/SEC	18.51	18.28	18.29	18.28	18.27	18.28	18.27	18.30	18.24	18.26	18.32	18.31
CURRENT	AMPS	2841.	2820.	2806.	2798.	2791.	2798.	2791.	2785.	2777.	2771.	2767.	2761.
VOLTAGE	VOLTS	5.99	6.00	6.01	6.02	6.02	6.04	6.02	6.03	6.02	6.03	6.03	6.04
POWER	KW	17.01	16.91	16.85	16.84	16.81	16.84	16.81	16.78	16.72	16.70	16.68	16.68
HEAT FLUX	W/SQ.CM	903.	897.	894.	893.	892.	893.	892.	890.	887.	886.	885.	885.
BALANCE	COEFFICIENT	-5.18	-4.75	-4.45	-4.44	-4.30	-4.44	-4.30	-4.52	-4.51	-4.29	-4.41	-4.46
ENERGY CHARGE	NUMBER	429.	429.	430.	430.	430.	430.	430.	429.	429.	429.	430.	429.
REYNOLDS	NUMBER	42058.	41334.	41313.	41295.	41274.	41295.	41274.	41183.	41053.	41108.	41087.	41059.

ORIGINAL PAGE IS OF POOR QUALITY

TIC	1.3	1.00	1.98	3.15	4.00	5.00	6.98	7.98	9.03	9.98	11.00
TTC	3.8	705.	706.	706.	704.	704.	708.	708.	709.	707.	710.
TTC	6.4	693.	696.	721.	699.	722.	704.	728.	729.	705.	731.
TTC	8.9	686.	699.	699.	699.	699.	704.	705.	706.	708.	708.
TTC	11.4	659.	667.	668.	667.	668.	673.	673.	674.	673.	675.
TTC	14.0	650.	656.	657.	656.	656.	660.	660.	661.	659.	662.
TTC	16.5	643.	647.	648.	648.	648.	653.	653.	654.	653.	655.
TTC	19.1	644.	649.	649.	648.	648.	653.	653.	653.	652.	654.
TTC	21.6	644.	649.	649.	648.	648.	646.	647.	648.	647.	649.
TTC	24.1	622.	292.	292.	642.	292.	646.	647.	648.	647.	649.
TTC	26.6	381.	383.	382.	382.	382.	382.	382.	382.	381.	382.
TTC	29.1	89.	91.	91.	91.	90.	91.	91.	91.	89.	90.
TTC	31.6	134.4	134.4	134.3	133.	133.	133.	133.	133.	133.	133.
TTC	34.1	7.54	7.52	7.53	7.51	7.51	7.47	7.49	7.49	7.54	7.52
TTC	36.6	4.80	4.80	4.81	4.80	4.80	4.79	4.80	4.80	4.81	4.81
TTC	39.1	18.25	18.25	18.27	18.26	18.25	18.20	18.26	18.24	18.30	18.29
TTC	41.6	2635.	2644.	2639.	2632.	2627.	2623.	2620	2618.	2611.	2612.
TTC	44.1	5.01	5.08	5.08	5.06	5.05	5.09	5.08	5.08	5.06	5.08
TTC	46.6	13.20	13.45	13.41	13.32	13.27	13.34	13.32	13.30	13.21	13.27
TTC	49.1	701.3	711.3	711.8	707.	704.7	708.	707.	706.	701.	704.
TTC	51.6	-5.03	-4.83	-4.43	-3.92	-4.27	-4.35	-3.95	-3.85	-4.26	-4.05
TTC	54.1	429.	430	431	431	430	431	431	431	431	431
TTC	56.6	36895.	37286.	37094.	37063.	36923.	36952.	37057.	37032.	36881.	37003.

TEST DATA FOR JP-7 RUN # 27 FEB 23, 1981

TIC	11.97	12.97	14.00	15.00	16.00	17.00	18.00	19.00	20.03		
TTC	712.	712.	712.	712.	712.	716.	716.	718.	716.		
TTC	733.	734.	736.	737.	738.	742.	743.	746.	746.		
TTC	709.	710.	711.	712.	713.	716.	717.	720.	719.		
TTC	676.	676.	676.	677.	677.	679.	679.	682.	680.		
TTC	662.	663.	663.	663.	663.	666.	666.	667.	666.		
TTC	656.	657.	657.	657.	658.	660.	661.	662.	661.		
TTC	654.	655.	656.	656.	656.	658.	659.	661.	661.		
TTC	650.	650.	651.	650.	650.	652.	652.	653.	651.		
TTC	292.	292.	291.	291.	291.	291.	291.	291.	291.		
TTC	382.	381.	381.	380.	380.	381.	380.	380.	379.		
TTC	90.	89.	90.	89.	89.	89.	89.	89.	88.		
TTC	133.	133.	131.	131.	130.	130.	130.	130.	130.		
TTC	7.51	7.56	7.57	7.50	7.56	7.53	7.57	7.52	7.61		
TTC	4.81	4.82	4.82	4.79	4.81	4.81	4.81	4.79	4.82		
TTC	18.27	18.33	18.33	18.22	18.28	18.29	18.28	18.23	18.31		
TTC	2609.	2607.	2604.	2592.	2589.	2589.	2585.	2580.	2574.		
TTC	5.08	5.08	5.09	5.06	5.05	5.08	5.08	5.08	5.05		
TTC	13.26	13.25	13.24	13.12	13.09	13.15	13.12	13.10	13.01		
TTC	703.	703.	702.	696.	694.	698.	696.	695.	690.		
TTC	-4.04	-4.34	-3.67	-4.62	-4.09	-3.85	-4.34	-3.90	-4.01		
TTC	.431	.431	.431	.430	.430	.431	.430	.430	.431		
TTC	36966.	36949.	36848.	36376.	36497.	36642.	36493.	36284.	36428.		

ORIGINAL PAGE IS OF POOR QUALITY

TABLE A-1

TEST DATA FOR JP-7 RUN # 30 FEB 24, 1981

TIME	MIN	CM	DEG K	2.00	3.00	4.00	5.00	6.00	7.00
TTC	1.3	DEG K	756.	753.	750.	754.	753.	753.	753.
TTC	3.8	CM	806.	806.	805.	805.	803.	803.	801.
TTC	6.4	DEG K	767.	763.	759.	761.	757.	755.	755.
TTC	8.9	CM	711.	728.	726.	728.	727.	725.	725.
TTC	11.4	DEG K	659.	686.	689.	696.	701.	701.	701.
TTC	14.0	CM	671.	671.	666.	663.	650.	642.	642.
TTC	16.5	DEG K	699.	689.	684.	684.	681.	678.	678.
TTC	19.1	CM	701.	696.	689.	690.	688.	686.	686.
TTC	21.6	DEG K	727.	719.	714.	713.	709.	707.	707.
TTC	24.1	CM	288.	287.	287.	287.	287.	287.	287.
FLUID ID	INLET TEMP	DEG K	392.	391.	389.	390.	389.	389.	389.
FLUID ID	EXIT TEMP	DEG K	104.	104.	103.	103.	102.	102.	102.
FLUID ID	RISE	DEG K	139.	139.	139.	139.	133.	138.	138.
TUBE P	INLET PRESSURE	ATM	3.70	3.64	3.65	3.62	3.60	3.62	3.62
DEL W	INLET TUBE	ATM	3.21	3.21	3.21	3.21	3.20	3.22	3.22
FLOW	INLET RATE	LITER/MIN	12.21	12.45	12.40	12.38	12.32	12.31	12.31
VELOC	INLET RATE	M/SEC	2265.	2245	2240	2238	2232	2231	2231
CURR	INLET RATE	AMPS	10.61	10.50	10.43	10.37	10.32	10.29	10.29
PWR	INLET RATE	W/SQ.CM	563.	554	550	551	548	546	546
HEAT	FLUX BALANCE	COEFFICIENT	-6.413	-5.71	-6.10	-6.00	-5.60	-5.68	-5.68
DISCH	FLUX BALANCE	NUMBER	454	415	416	417	416	415	415
REYN	FLUX BALANCE	NUMBER	25768.	25585.	25510.	25422.	25372.	25322.	25322.

TEST DATA FOR JP-7 RUN # 31 FEB 26, 1981

TIME	MIN	CM	DEG K	3.00	4.00	5.00	6.00	7.00	8.00
TTC	1.3	DEG K	587.	586.	589.	591.	588.	586.	586.
TTC	3.8	CM	576.	573.	577.	576.	576.	572.	572.
TTC	6.4	DEG K	557.	556.	559.	561.	556.	557.	557.
TTC	8.9	CM	552.	551.	556.	556.	555.	552.	552.
TTC	11.4	DEG K	561.	558.	563.	563.	563.	560.	560.
TTC	14.0	CM	553.	552.	555.	555.	555.	551.	551.
TTC	16.5	DEG K	558.	556.	559.	559.	556.	556.	556.
TTC	19.1	CM	553.	552.	557.	557.	557.	554.	554.
TTC	21.6	DEG K	291.	291.	291.	291.	291.	291.	291.
TTC	24.1	CM	353.	353.	354.	354.	354.	353.	353.
FLUID ID	INLET TEMP	DEG K	62.	62.	62.	62.	62.	62.	62.
FLUID ID	EXIT TEMP	DEG K	139.	139.	138.	137.	137.	137.	137.
FLUID ID	RISE	DEG K	62.	62.	63.	63.	62.	62.	62.
TUBE P	INLET PRESSURE	ATM	10.83	10.87	10.82	10.83	10.81	10.83	10.83
DEL W	INLET TUBE	ATM	18.38	18.54	18.32	18.38	18.30	18.38	18.38
FLOW	INLET RATE	LITER/MIN	2351.	2359.	2358.	2363.	2362.	2352.	2352.
VELOC	INLET RATE	M/SEC	9.16	9.12	9.20	9.19	9.23	9.10	9.10
CURR	INLET RATE	AMPS	486.	484	488.	488.	490.	483.	483.
PWR	INLET RATE	W/SQ.CM	-6.13	-5.76	-5.94	-5.87	-6.35	-5.76	-5.76
HEAT	FLUX BALANCE	COEFFICIENT	370	369	370	371	370	369	369
DISCH	FLUX BALANCE	NUMBER	31121.	31281.	30935.	31217.	31088.	30919.	30919.
REYN	FLUX BALANCE	NUMBER	5572.	5566.	5559.	5559.	5559.	5559.	5559.

TABLE A-1

TEST DATA FOR C3H8 RUN # 48 MAR 16, 1981

TIME	MIN	00	95	197	297	383
TTC	1.3	618	612	1603	296	583
TTC	3.8	559	546	533	525	521
TTC	6.9	551	539	532	526	518
TTC	11.4	557	541	534	528	521
TTC	16.5	563	559	558	554	545
TTC	19.1	584	580	576	569	558
TTC	21.6	612	609	608	608	608
TTC	24.1	684	703	731	743	876
FLUID INLET TEMP	DEG K	260	294	294	294	294
FLUID EXIT TEMP	DEG K	460	461	461	466	458
TUBE INLET TEMP	DEG K	166	167	167	166	164
TUBE P RISE	DEG, ATM	138	138	138	138	137
DELTA P	ATM	12	13	14	15	15
FLOW RATE	M/SEC	12.38	16.39	16.37	15.42	15.42
VELOCITY	M/SEC	24.26	34.31	34.24	24.38	24.43
CURRENT	AMPS	38.40	38.75	38.75	38.75	38.43
VOLTAGE	VOLTS	6.61	6.77	6.79	6.49	6.44
POWER	KW	24.40	24.79	24.79	24.79	24.64
HEAT FLUX	W/SQ.CM	1305	1314	1315	1315	1307
ENERGY BALANCE	COEFFICIENT	18.19	18.57	18.10	17.89	17.92
DISECHARGE	NUMBER	---	---	---	---	---
REYNOLDS	NUMBER	---	---	---	---	---

TEST DATA FOR C3H8 RUN # 49 MAR 16, 1981

TIME	MIN	00	13	200	300	400	500	600	700	800	900	1000
TTC	1.3	518	135	239	342	443	543	641	740	840	936	1035
TTC	3.8	466	496	506	508	526	535	544	544	546	554	554
TTC	6.9	502	488	485	486	489	489	487	488	493	492	493
TTC	11.4	489	488	489	488	489	489	489	491	493	492	493
TTC	16.5	551	555	556	556	556	557	557	557	558	556	556
TTC	19.1	549	541	541	538	538	535	535	534	535	532	532
TTC	21.6	581	574	573	571	570	569	568	568	569	567	567
TTC	24.1	391	292	292	292	292	292	292	292	292	292	292
FLUID INLET TEMP	DEG K	291	292	292	292	292	292	292	292	292	292	292
FLUID EXIT TEMP	DEG K	100	101	101	101	101	101	101	101	102	101	101
TUBE INLET TEMP	DEG, ATM	133	133	133	133	133	133	133	133	133	133	133
DELTA P	ATM	13	13	13	13	13	13	13	13	13	13	13
FLOW RATE	M/SEC	3.30	3.22	3.21	3.21	3.21	3.21	3.21	3.21	3.21	3.21	3.21
VELOCITY	M/SEC	2188	2172	2175	2177	2177	2183	2187	2188	2185	2183	2184
CURRENT	AMPS	3.27	3.28	3.29	3.30	3.30	3.30	3.30	3.30	3.30	3.30	3.30
VOLTAGE	VOLTS	380	378	380	381	382	382	382	382	382	381	381
POWER	KW	12.74	13.38	13.21	13.11	13.04	12.70	12.70	12.69	12.50	12.47	12.54
HEAT FLUX	W/SQ.CM	---	---	---	---	---	---	---	---	---	---	---
ENERGY BALANCE	COEFFICIENT	---	---	---	---	---	---	---	---	---	---	---
DISECHARGE	NUMBER	---	---	---	---	---	---	---	---	---	---	---
REYNOLDS	NUMBER	---	---	---	---	---	---	---	---	---	---	---

TABLE A-1

TEST DATA FOR C3H8 RUN # 50 MAR 16, 1981

TIME		00	1.00	2.00	3.00	4.00	5.00	6.05	7.00	8.00	9.00	10.00
TTC	@	474	478	479	484	485	486	487	489	491	491	492
TTC	@	511	513	514	516	517	518	519	521	523	525	526
TTC	@	540	541	543	547	548	549	551	554	556	558	560
TTC	@	558	551	554	558	561	564	569	572	575	578	581
TTC	@	540	533	526	522	518	515	513	512	511	510	508
TTC	@	560	557	552	549	548	544	542	542	541	540	537
TTC	@	593	591	589	589	589	589	589	589	589	589	587
FLUID	INLET	99	99	99	99	99	99	99	99	99	98	98
FLUID	EXIT	133	133	133	132	131	131	130	130	129	129	129
FLUID	INLET	134	133	133	133	134	135	136	137	138	139	140
DELTA	TEMP.	15.8	15.8	16.2	16.4	16.3	16.4	16.4	16.4	16.4	16.4	16.4
TUBE	P	6.3	6.4	6.4	6.4	6.4	6.4	6.4	6.4	6.4	6.4	6.4
FLOW	CIT	24.0	24.0	24.0	24.0	24.0	24.0	24.0	24.0	24.0	24.0	24.0
VOLTAGE		297.2	299.6	300.5	301.0	300.8	301.6	301.8	301.5	302.0	301.3	300.9
POWER	KW	4.5	4.5	4.5	4.5	4.5	4.5	4.5	4.5	4.5	4.5	4.5
HEAT	FLUX	17.1	17.2	17.2	17.2	17.2	17.2	17.2	17.2	17.2	17.1	17.1
ENERGY	BALANCE	16.8	16.2	16.2	16.2	16.2	16.2	16.2	16.2	16.2	16.2	16.2
DISCHARGE		16.8	16.2	16.2	16.2	16.2	16.2	16.2	16.2	16.2	16.2	16.2
REYNOLDS	NUMBER											

TEST DATA FOR C3H8 RUN # 51 MAR 17, 1981

TIME		00	1.07	2.08	3.07	4.00	5.00	6.32	7.05	8.00	9.00	10.00
TTC	@	371	370	371	371	371	371	371	371	371	371	371
TTC	@	378	377	377	378	378	378	378	378	378	378	378
TTC	@	383	382	382	382	382	382	382	382	382	382	382
TTC	@	387	386	386	386	386	386	386	386	386	386	386
TTC	@	391	391	391	391	391	391	391	391	391	391	391
TTC	@	397	396	396	396	396	396	396	396	396	396	396
TTC	@	402	402	402	402	402	402	402	402	402	402	402
TTC	@	408	407	407	407	407	407	407	407	407	407	407
TTC	@	414	413	413	413	413	413	413	413	413	413	413
TTC	@	422	421	421	421	421	421	421	421	421	421	421
FLUID	INLET	338	338	339	339	339	339	339	339	339	339	339
FLUID	EXIT	48	48	48	48	48	48	48	48	48	48	48
FLUID	INLET	135	135	135	135	135	135	135	135	135	135	135
DELTA	TEMP.	1.4	1.4	1.4	1.4	1.4	1.4	1.4	1.4	1.4	1.4	1.4
TUBE	P	1.4	1.4	1.4	1.4	1.4	1.4	1.4	1.4	1.4	1.4	1.4
FLOW	CIT	12.1	12.1	12.1	12.1	12.1	12.1	12.1	12.1	12.1	12.1	12.1
VOLTAGE		169.5	169.5	169.5	169.5	169.5	169.5	169.5	169.5	169.5	169.5	169.5
POWER	KW	1.9	1.9	1.9	1.9	1.9	1.9	1.9	1.9	1.9	1.9	1.9
HEAT	FLUX	17.3	17.3	17.3	17.3	17.3	17.3	17.3	17.3	17.3	17.3	17.3
ENERGY	BALANCE	17.3	17.3	17.3	17.3	17.3	17.3	17.3	17.3	17.3	17.3	17.3
DISCHARGE		17.3	17.3	17.3	17.3	17.3	17.3	17.3	17.3	17.3	17.3	17.3
REYNOLDS	NUMBER											

TABLE A-1
TEST DATA FOR RP-1 RUN # 62 APR 07, 1981

TIME	MIN		1.00	2.03	3.00	10.23	11.23	12.32	13.23	14.45	15.23	16.23
TTC	1.3	CM	6.23	6.10	6.01	6.44	6.36	6.41	6.51	6.68	6.73	6.82
TTC	3.8	DEG K	6.07	5.94	5.84	6.29	6.22	6.31	6.43	6.65	6.71	6.76
TTC	6.4	CM	7.06	6.93	6.84	7.01	6.92	6.94	7.01	7.09	7.09	7.08
TTC	8.9	CM	6.34	6.19	6.10	6.68	6.58	6.67	6.67	6.88	6.88	6.91
TTC	11.4	CM	6.30	6.18	6.08	6.33	6.24	6.27	6.37	6.53	6.57	6.61
TTC	14.0	CM	6.31	6.17	6.07	6.43	6.35	6.48	6.58	6.74	6.78	6.81
TTC	16.5	CM	6.58	6.47	6.40	6.36	6.29	6.38	6.50	6.67	6.71	6.74
TTC	19.1	CM	5.99	5.86	5.76	6.44	6.37	6.46	6.61	6.74	6.78	6.81
TTC	21.6	CM	5.94	5.86	5.79	6.43	6.38	6.46	6.63	6.77	6.82	6.87
TTC	24.1	CM	2.90	2.89	2.89	2.91	2.91	2.91	2.91	2.91	2.91	2.91
FLUID INLET TEMP.	DEG K		3.62	3.58	3.56	3.72	3.70	3.70	3.74	3.80	3.81	3.82
FLUID EXIT TEMP.	DEG K		7.2	6.9	6.6	8.1	7.9	7.9	8.4	8.9	9.1	9.2
FLUID INLET PRESSURE	ATM		2.69	2.65	2.60	2.74	2.73	2.74	2.75	2.76	2.76	2.76
FLUID INLET TUBE AREA	LITER/MIN		5.31	5.23	5.16	5.27	5.14	5.15	5.12	5.10	5.10	5.10
DEL P RATE	M/SEC		4.78	4.76	4.69	4.89	4.84	4.82	4.82	4.80	4.80	4.80
FLOW RATE	M/SEC		21.02	21.32	21.54	20.75	20.97	20.68	20.53	20.11	20.84	20.01
VELOCITY	M/SEC		3.76	3.73	3.72	3.89	3.88	3.78	3.90	3.94	3.95	3.96
CURRENT	AMPS		7.90	7.96	8.01	8.08	8.14	8.15	8.01	7.92	8.23	8.19
VOLTAGE	VOLTS		4.19	4.22	4.25	4.27	4.32	4.15	4.25	4.20	4.37	4.19
POWER FLUX	W/SQ.CM		25.56	16.83	14.25	23.27	23.85	25.15	24.37	24.51	19.57	24.29
HEAT FLUX	W/SQ.CM		.508	.466	.453	3.1469	3.2295	3.1336	3.0777	2.9595	2.9374	2.9133
ENERGY BALANCE	COEFFICIENT		32631	31282	31526	31469	32295	31336	30777	29595	29374	29133
DISCHARGE	NUMBER											
REYNOLDS	NUMBER											

TIME	MIN		1.02	2.00	3.05	4.00	5.00	6.00	7.00	8.00	9.00	10.00
TTC	1.3	CM	6.86	6.88	7.00	7.24	7.35	7.45	7.58	7.76	7.89	7.99
TTC	3.8	DEG K	6.93	6.94	7.08	7.41	7.58	7.76	7.76	7.76	7.76	7.76
TTC	6.4	CM	6.65	6.67	6.80	7.09	7.24	7.38	7.38	7.38	7.38	7.38
TTC	8.9	CM	6.38	6.39	6.49	6.75	6.88	7.02	7.02	7.02	7.02	7.02
TTC	11.4	CM	6.07	6.23	6.31	6.54	6.66	6.77	6.77	6.77	6.77	6.77
TTC	14.0	CM	6.13	6.12	6.18	6.37	6.47	6.56	6.56	6.56	6.56	6.56
TTC	16.5	CM	6.06	6.05	6.10	6.27	6.35	6.43	6.43	6.43	6.43	6.43
TTC	19.1	CM	6.02	6.00	6.05	6.22	6.28	6.36	6.36	6.36	6.36	6.36
TTC	21.6	CM	5.97	5.94	5.99	6.14	6.20	6.26	6.26	6.26	6.26	6.26
TTC	24.1	CM	5.90	5.89	5.92	6.05	6.10	6.15	6.15	6.15	6.15	6.15
FLUID INLET TEMP.	DEG K		2.93	2.93	2.93	2.93	2.92	2.92	2.92	2.92	2.92	2.92
FLUID EXIT TEMP.	DEG K		3.64	3.68	3.69	3.74	3.77	3.79	3.79	3.79	3.79	3.79
FLUID INLET PRESSURE	ATM		7.1	7.4	7.7	8.2	8.4	8.4	8.4	8.4	8.4	8.4
DEL P RATE	LITER/MIN		3.32	3.30	3.28	3.20	3.10	2.92	2.92	2.92	2.92	2.92
FLOW RATE	M/SEC		4.84	4.73	4.59	4.20	4.05	3.90	3.90	3.90	3.90	3.90
VELOCITY	M/SEC		18.41	17.99	17.46	15.97	15.38	14.83	14.83	14.83	14.83	14.83
CURRENT	AMPS		20.68	20.85	20.69	20.21	19.98	19.76	19.76	19.76	19.76	19.76
VOLTAGE	VOLTS		4.00	4.00	4.02	4.05	4.06	4.07	4.07	4.07	4.07	4.07
POWER FLUX	W/SQ.CM		8.27	8.34	8.31	8.18	8.12	8.05	8.05	8.05	8.05	8.05
HEAT FLUX	W/SQ.CM		4.39	4.42	4.41	4.34	4.31	4.27	4.27	4.27	4.27	4.27
ENERGY BALANCE	COEFFICIENT		18.86	22.58	21.47	20.86	21.63	21.56	21.56	21.56	21.56	21.56
DISCHARGE	NUMBER											
REYNOLDS	NUMBER		34164	34434	33509	31814	31046	30417	30417	30417	30417	30417

TABLE A-1

TEST DATA FOR RP-1 RUN # 64 APR 09, 1981

TIME	MIN	CM	DEG K	3.13	4.00	5.00	7.00	8.00	9.00	10.00
TTC	1.3	703	707	717	713	719	722	724	723	725
TTC	3.8	643	677	674	677	668	663	661	657	648
TTC	6.9	625	644	645	647	642	638	639	637	629
TTC	11.4	621	625	624	626	620	617	618	616	610
TTC	16.5	614	618	619	619	613	610	609	608	602
TTC	19.1	609	604	611	604	604	594	594	592	585
TTC	21.6	608	603	606	603	598	588	588	587	580
TTC	24.1	602	598	599	598	593	590	588	588	581
TTC	27.1	608	601	601	601	594	592	592	592	584
TTC	31.1	292	292	292	292	292	292	292	292	292
TTC	37.6	376	375	375	374	373	373	373	372	372
TTC	83	83	83	82	82	81	81	81	80	80
TTC	139	139	139	140	140	139	139	140	140	140
TTC	4.82	4.83	4.82	4.83	4.82	4.83	4.82	4.82	4.82	4.82
TTC	18.34	18.37	18.34	18.35	18.34	18.35	18.32	18.33	18.34	18.33
TTC	21.93	2181	2152	2152	2154	2103	2108	2121	2092	2059
TTC	4.29	9.42	9.27	9.33	9.29	9.08	9.12	9.23	9.08	8.91
TTC	500	495	492	495	493	482	484	490	482	473
TTC	23.16	23.57	24.28	21.78	23.09	24.19	22.49	21.07	22.25	22.65
TTC	36703	36571	36559	36283	36402	36134	35920	35937	35820	35497

TEST DATA FOR RP-1 RUN # 65 APR 10, 1981

TIME	MIN	CM	DEG K	2.45	3.33	4.02	5.82	6.38	7.45	8.45
TTC	1.3	680	676	697	723	745	681	684	689	691
TTC	3.8	695	697	721	758	791	692	684	698	707
TTC	6.9	684	684	709	742	767	678	684	684	673
TTC	11.4	669	674	694	723	744	666	675	668	673
TTC	14.0	653	657	678	705	724	657	669	666	672
TTC	16.5	641	644	664	692	713	654	668	665	670
TTC	19.1	634	638	656	681	701	657	668	675	679
TTC	21.6	632	633	651	674	693	643	664	664	672
TTC	24.1	623	623	638	657	690	636	653	657	666
TTC	27.1	623	623	638	657	690	636	653	657	666
TTC	31.1	291	291	291	291	291	291	291	291	291
TTC	37.6	377	375	381	388	394	375	377	376	378
TTC	86	84	84	80	88	84	84	84	86	87
TTC	137	137	137	138	138	139	137	137	137	137
TTC	4.51	4.63	4.23	3.50	3.80	3.50	3.01	3.86	4.94	4.81
TTC	17.16	17.61	16.09	13.32	14.44	13.32	19.07	18.47	18.79	18.30
TTC	22.65	2277	2218	2107	2155	2107	2347	2325	2329	2313
TTC	4.31	4.30	4.33	4.42	4.38	4.42	4.51	4.52	4.51	4.52
TTC	9.75	9.78	9.61	9.31	9.44	9.31	10.58	10.51	10.51	10.45
TTC	51.7	51.9	51.0	49.4	50.1	49.4	56.1	55.7	55.7	55.4
TTC	15.12	15.33	14.90	14.96	14.90	14.96	15.49	15.86	16.22	16.26
TTC	34254	34722	34650	33056	31411	30315	37610	37032	37364	36847

TABLE A-1

TEST DATA FOR RP-1 RUN # 66 APR 14, 1981

TIME	MIN	CM	DEG K	1.00	2.00	3.00	4.00	5.00	6.00	7.00	8.00	9.00
TC	1.3	DEG K	699.	713.	713.	644.	644.	646.	647.	649.	650.	650.
TC	3.8	DEG K	736.	758.	758.	706.	704.	707.	709.	712.	714.	714.
TC	6.4	DEG K	704.	718.	718.	671.	670.	673.	675.	678.	680.	681.
TC	8.9	DEG K	677.	689.	689.	644.	645.	648.	651.	653.	656.	657.
TC	11.4	DEG K	651.	660.	660.	618.	618.	621.	622.	624.	627.	627.
TC	14.0	DEG K	643.	651.	651.	608.	608.	609.	611.	613.	614.	614.
TC	16.5	DEG K	636.	642.	642.	601.	600.	603.	603.	604.	605.	604.
TC	19.1	DEG K	631.	636.	636.	595.	594.	597.	598.	598.	598.	598.
TC	21.6	DEG K	626.	629.	629.	589.	588.	589.	589.	591.	592.	591.
TC	24.1	DEG K	624.	627.	627.	584.	583.	584.	584.	585.	586.	585.
FLUID INLET TEMP	292.	DEG K	292.	291.	291.	362.	361.	362.	362.	362.	362.	362.
FLUID EXIT TEMP	374.	DEG K	374.	376.	376.	71.	70.	71.	71.	71.	71.	71.
FLUID INLET PRESSURE	82.	DEG K	82.	84.	84.	336.	336.	336.	336.	335.	335.	335.
FLUID INLET TUBE	335.	ATM	335.	336.	336.	4.56	4.59	4.56	4.54	4.51	4.51	4.49
FLOW RATE	19.74	LITER/MIN	19.74	17.97	17.97	17.34	17.46	17.33	17.28	17.16	17.14	17.09
VELOCITY	2416.	M/SEC	2416.	2355.	2327.	2183.	2183.	2178.	2174.	2170.	2166.	2162.
CURRENT	4.46	AMPS	4.46	4.50	4.51	3.93	3.94	3.94	3.95	3.96	3.97	3.96
VOLTAGE	10.78	VOLTS	10.78	10.60	10.49	8.59	8.59	8.58	8.58	8.60	8.59	8.56
HEAT FLUX	572.	W/SQ.CM	572.	562.	557.	456.	456.	455.	455.	456.	456.	454.
ENERGY BALANCE	5.85	COEFFICIENT	5.85	5.66	6.37	6.68	6.42	6.62	6.39	6.35	6.27	6.37
DISCHARGE	37316.	NUMBER	37316.	35404.	34597.	31079.	31169.	31058.	30976.	30886.	30847.	30754.

TEST DATA FOR RP-1 RUN # 67 APR 21, 1981

TIME	MIN	CM	DEG K	1.00	2.00	3.00	4.00	5.00	6.00	7.00	8.00	9.00
TC	1.3	DEG K	611.	613.	613.	615.	617.	621.	622.	621.	624.	626.
TC	3.8	DEG K	678.	642.	642.	642.	642.	643.	643.	643.	639.	638.
TC	6.4	DEG K	678.	677.	677.	676.	676.	676.	676.	672.	671.	670.
TC	8.9	DEG K	681.	681.	681.	678.	678.	678.	678.	674.	674.	672.
TC	11.4	DEG K	609.	609.	609.	608.	608.	609.	609.	607.	606.	606.
TC	14.0	DEG K	607.	607.	607.	607.	607.	607.	607.	605.	603.	603.
TC	16.5	DEG K	667.	666.	666.	664.	663.	663.	663.	659.	657.	657.
TC	19.1	DEG K	649.	649.	649.	647.	647.	647.	647.	643.	642.	642.
TC	21.6	DEG K	669.	668.	668.	667.	666.	666.	666.	662.	661.	661.
TC	24.1	DEG K	652.	652.	652.	651.	651.	651.	650.	648.	647.	646.
FLUID INLET TEMP	293.	DEG K	293.	293.	293.	293.	293.	293.	293.	293.	293.	293.
FLUID EXIT TEMP	364.	DEG K	364.	364.	364.	364.	364.	364.	364.	364.	364.	364.
FLUID INLET PRESSURE	72.	DEG K	72.	71.	71.	71.	72.	72.	72.	71.	71.	71.
FLUID INLET TUBE	135.	ATM	135.	135.	135.	135.	135.	136.	136.	135.	135.	135.
FLOW RATE	4.72	LITER/MIN	4.72	4.81	4.81	4.81	4.80	4.79	4.77	4.83	4.80	4.81
VELOCITY	17.94	M/SEC	17.94	18.28	18.28	18.28	18.27	18.20	18.13	18.36	18.27	18.28
CURRENT	2211.	AMPS	2211.	2224.	2224.	2224.	2225.	2223.	2221.	2225.	2223.	2222.
VOLTAGE	4.11	VOLTS	4.11	4.11	4.11	4.11	4.12	4.12	4.12	4.12	4.12	4.12
HEAT FLUX	9.08	W/SQ.CM	9.08	9.15	9.15	9.14	9.16	9.16	9.15	9.16	9.16	9.16
ENERGY BALANCE	482.	COEFFICIENT	482.	485.	485.	485.	486.	486.	486.	486.	486.	485.
DISCHARGE	6.26	NUMBER	6.26	6.64	6.64	6.68	7.34	6.91	6.56	6.94	6.36	6.56
REYNOLDS	33177.	NUMBER	33177.	33823.	33929.	33668.	33796.	33661.	33526.	33820.	33651.	33663.

TABLE A-1

TEST DATA FOR RP-1 RUN # 68 APR 21, 1981

TIME	MIN	CM	DEG	42	1.00	2.00	3.00
TTC	1.3	CM	DEG	715.	719.	728.	735.
TTC	3.8	CM	DEG	788.	784.	792.	797.
TTC	6.4	CM	DEG	781.	777.	782.	786.
TTC	8.9	CM	DEG	804.	798.	798.	799.
TTC	11.4	CM	DEG	758.	752.	753.	754.
TTC	14.0	CM	DEG	767.	761.	761.	761.
TTC	16.5	CM	DEG	803.	794.	793.	793.
TTC	19.1	CM	DEG	757.	752.	754.	756.
TTC	21.6	CM	DEG	736.	734.	734.	734.
TTC	24.1	CM	DEG	681.	687.	691.	694.
FLUID ID	INLET	TEMP.	DEG	294.	294.	294.	294.
FLUID ID	EXIT	TEMP.	DEG	395.	395.	397.	398.
FLUID ID	INLET	TEMP.	DEG	101.	101.	103.	104.
TUBE	P	TEST	PRESSURE,	136.	136.	136.	136.
DEL	P	TEST	TUBER,	---	---	---	---
FLOW	RATE	LITER		4.24	4.17	4.10	4.10
VELOCITY	M/SEC			16.11	15.84	15.60	15.60
CURRENT	AMPS			2327.	2333.	2327.	2327.
POWER	KW			4.57	5.09	5.10	5.10
HEAT	FLUX	W/SQ.CM		10.48	11.92	11.88	11.86
ENERGY	BALANCE			556.	633.	629.	629.
DISCHARGE	COEFFICIENT			4.40	6.02	6.21	6.10
REYNOLDS	NUMBER			36447.	37726.	38054.	37436.

TEST DATA FOR RP-1 RUN # 69 APR 22, 1981

TIME	MIN	CM	DEG	07	2.05	3.02	4.00
TTC	1.3	CM	DEG	158.	570.	574.	577.
TTC	3.8	CM	DEG	599.	615.	620.	623.
TTC	6.4	CM	DEG	582.	603.	608.	610.
TTC	8.9	CM	DEG	587.	598.	599.	601.
TTC	11.4	CM	DEG	590.	595.	603.	606.
TTC	14.0	CM	DEG	586.	601.	605.	608.
TTC	16.5	CM	DEG	582.	612.	616.	619.
TTC	19.1	CM	DEG	586.	596.	600.	603.
TTC	21.6	CM	DEG	576.	612.	616.	619.
TTC	24.1	CM	DEG	576.	585.	588.	589.
FLUID ID	INLET	TEMP.	DEG	291.	291.	291.	291.
FLUID ID	EXIT	TEMP.	DEG	358.	362.	363.	364.
TUBE	P	TEST	PRESSURE,	135.	139.	141.	141.
DEL	P	TEST	TUBER,	---	---	---	---
FLOW	RATE	LITER		4.24	4.02	3.94	3.89
VELOCITY	M/SEC			16.13	15.29	14.99	14.81
CURRENT	AMPS			2135.	2113.	2103.	2098.
POWER	KW			---	---	---	---
HEAT	FLUX	W/SQ.CM		---	---	---	---
ENERGY	BALANCE			---	---	---	---
DISCHARGE	COEFFICIENT			---	---	---	---
REYNOLDS	NUMBER			30537.	28202.	27406.	26877.

